



Department of Physics and Astronomy  
Georgia State University  
Atlanta, GA 30303-3083



U.S. DEPARTMENT OF  
**ENERGY**

Support:



# **Nanoplasmonics: Optical Properties of Plasmonic Nanosystems**

## **Mark I. Stockman**

Department of Physics and Astronomy, Georgia State  
University, Atlanta, GA 30303, USA

Lecture 3:

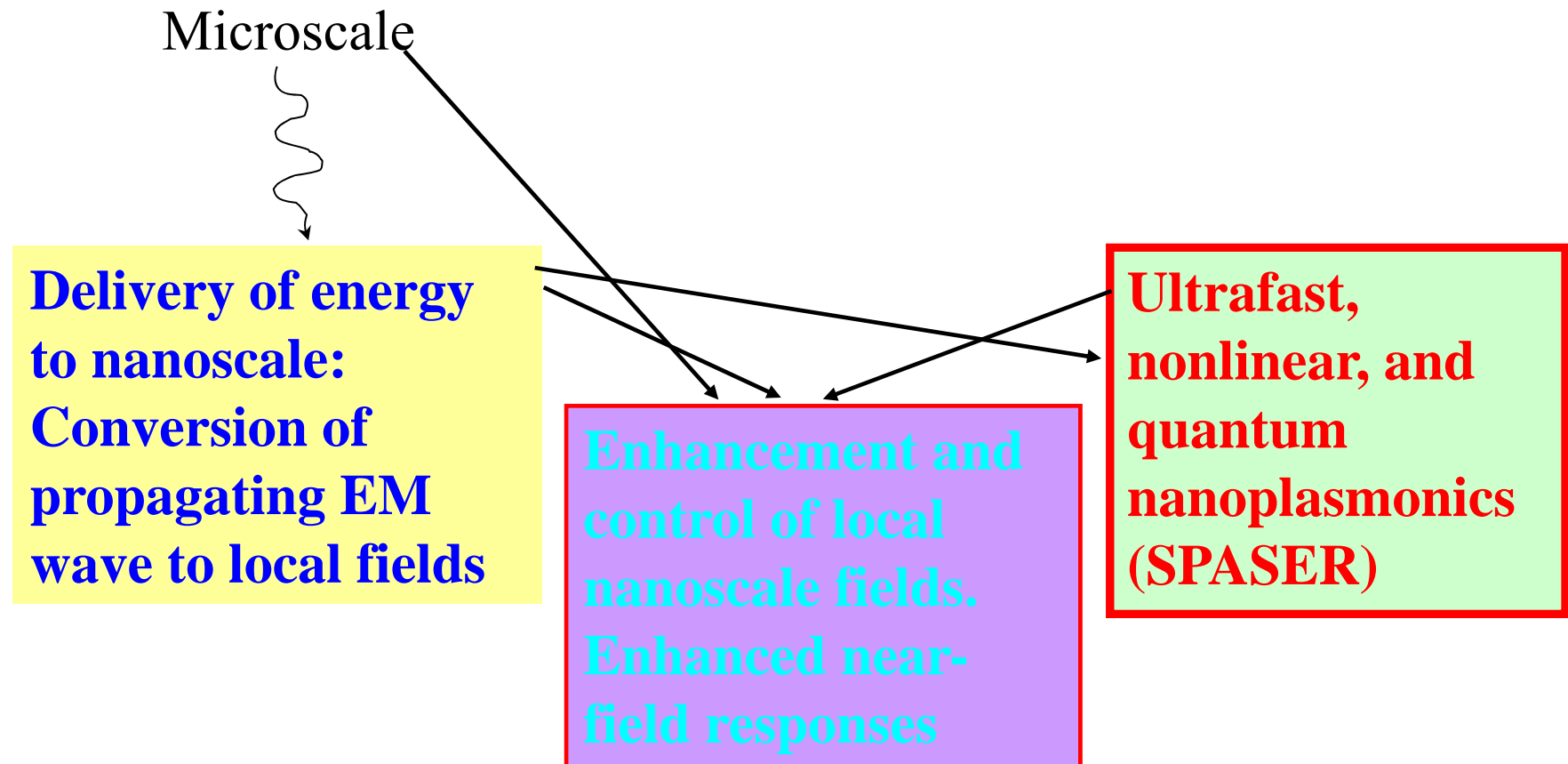
# **Ultrafast, Nonlinear, and Quantum Nanoplasmonics**

## LECTURE 3

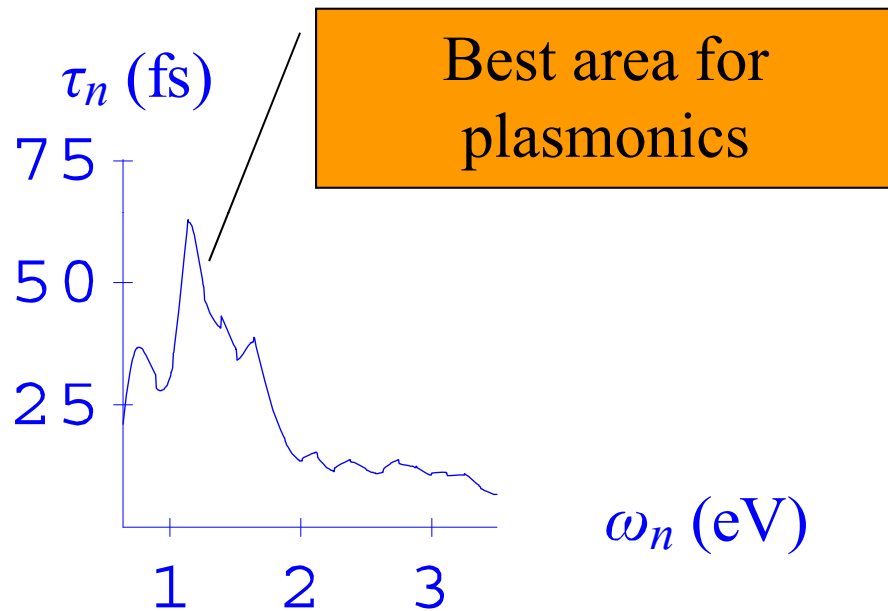
### **Ultrafast, Nonlinear, and Quantum Nanoplasmonics**

1. Introduction: Problem of nanoscale control of local optical fields
2. Coherent control using pulse shaping
3. Two-pulse (interferometric) coherent control and visualization
4. Time-reversal and determination of controlling pulses
5. Attosecond nanoplasmonics: attosecond plasmonic field microscope
6. Generation of high harmonics (EUV and XUV radiation)
7. Surface plasmon amplification by stimulated emission of radiation (SPASER) and nanolasers

## PROBLEMS IN NANOOPTICS



## Nanoplasmonics is intrinsically ultrafast:



Surface plasmon relaxation times are in  
 $\sim 10$ - $100$  fs range

Spectrally, surface plasmon resonances in complex systems occupy a very wide frequency band

$$\Delta\omega \sim \omega_p \sim 10 \text{ eV}$$

Corresponding shortest time of plasmonic responses  
 $\sim 100$  as

# COHERENT CONTROL ON NANOSCALE

**Problem of dynamic spatial control at the nanoscale:** The wavelength of the excitation radiation is orders of magnitude too large to control spatial distribution of local fields on nanoscale by focusing

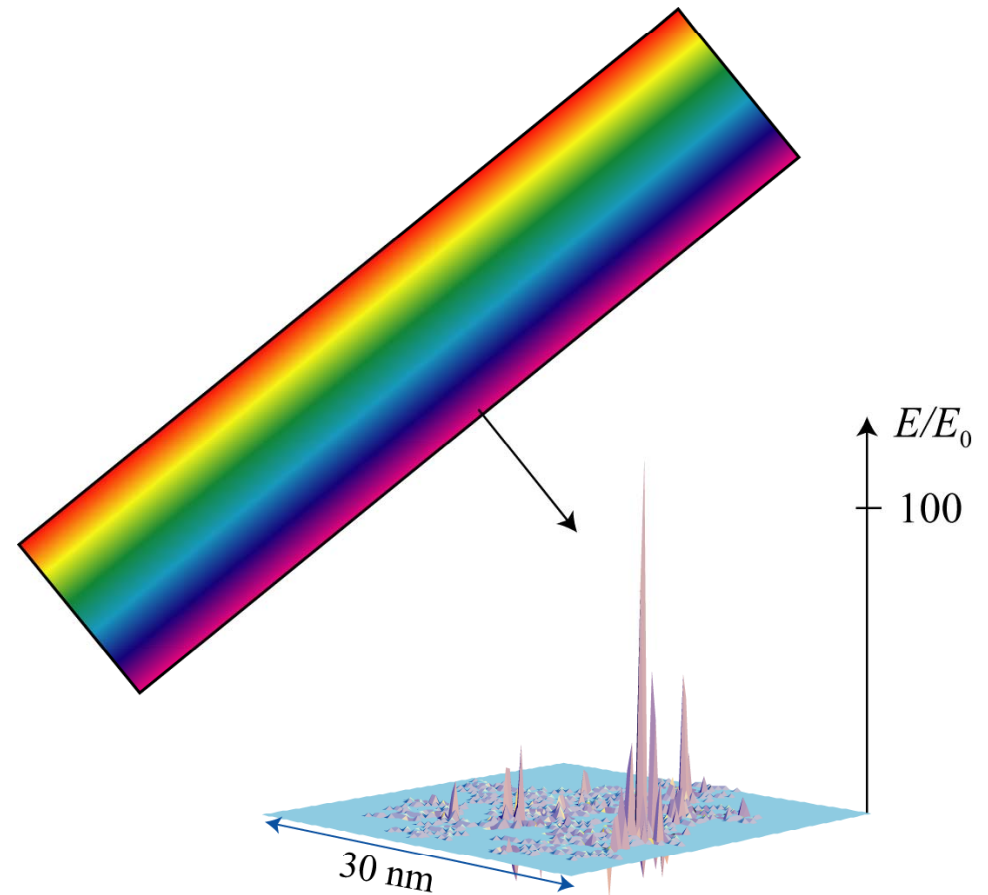
Thus, optical radiation does not have spatial degrees of freedom on the nanoscale

**However, it does possess spectral (phase, or temporal) degrees of freedom and polarization. These can be used to *dynamically* control the optical energy localization at the nanoscale**

Different spectral components of the excitation pulse excite resonant surface plasmon modes.

These excitations dynamically interfere creating time-dependent hot spots of local fields during their coherence time

This interference can be directed by choosing phases and amplitudes of the different frequency components of the excitation pulse (pulse shaping)



# Principles of coherent (quantum) control

D. J. Tannor and S. A. Rice, *Control of Selectivity of Chemical Reaction Via Control of Wave Packet Evolution*, The Journal of Chemical Physics **83**, 5013-5018 (1985); P. Brumer and M. Shapiro, *Principles of the Quantum Control of Molecular Processes* (Wiley, New York, 2003); R. S. Judson and H. Rabitz, *Teaching Lasers to Control Molecules*, Phys. Rev. Lett. **68**, 1500 (1992); A. P. Heberle, J. J. Baumberg, and K. Kohler, *Ultrafast Coherent Control and Destruction of Excitons in Quantum-Wells*, Phys. Rev. Lett. **75**, 2598-2601 (1995).

## REFERENCES ON COHERENT CONTROL OF OPTICAL ENERGY NANOLocalIZATION

- M. I. Stockman, S. V. Faleev, and D. J. Bergman, *Coherent Control of Femtosecond Energy Localization in Nanosystems*, Phys. Rev. Lett. **88**, 67402-1-4 (2002).
- M. I. Stockman, D. J. Bergman, and T. Kobayashi, *Coherent Control of Nanoscale Localization of Ultrafast Optical Excitation in Nanosystems*, Phys. Rev. B **69**, 054202-10 (2004)
- A. Kubo, K. Onda, H. Petek, Z. Sun, Y. S. Jung, and H. K. Kim, *Femtosecond Imaging of Surface Plasmon Dynamics in a Nanostructured Silver Film*, Nano Lett. **5**, 1123-1127 (2005)
- M. I. Stockman and P. Hewageegana, *Nanolocalized Nonlinear Electron Photoemission under Coherent Control*, Nano Lett. **5**, 2325-2329 (2005)
- M. Aeschlimann, M. Bauer, D. Bayer, T. Brixner, F. J. G. d. Abajo, W. Pfeiffer, M. Rohmer, C. Spindler, and F. Steeb, *Adaptive Subwavelength Control of Nano-Optical Fields*, Nature **446**, 301-304 (2007).
- X. Li and M. I. Stockman, *Highly Efficient Spatiotemporal Coherent Control in Nanoplasmonics on a Nanometer-Femtosecond Scale by Time Reversal*, Phys. Rev. B **77**, 195109-1-10 (2008).

- Femtosecond local fields on nanoscale:

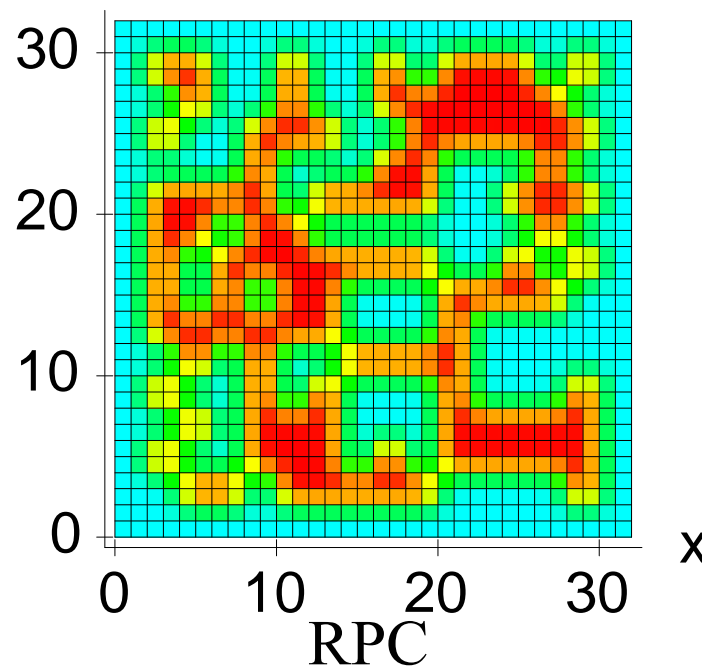
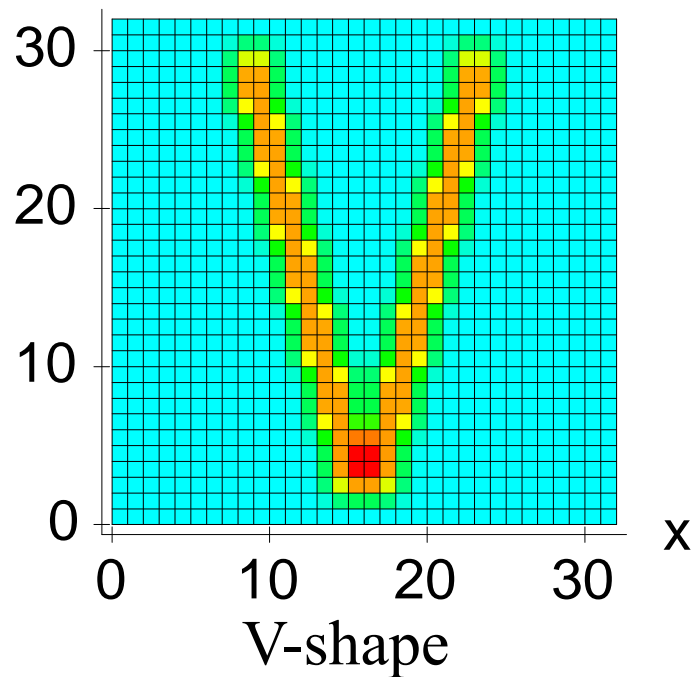
$$\varphi(\mathbf{r}, t) = \varphi_0(\mathbf{r}, t) - \int \varphi_0(\mathbf{r}', t') \nabla_{\mathbf{r}'}^2 G(\mathbf{r}, \mathbf{r}'; t - t') d^3 r' dt'$$

Example to be considered: The exciting pulses are  $z$ -polarized, have Gaussian envelopes, and carry linear chirp,

$$E_z^{(0)}(t) = \exp \left[ i\omega_0 \left( 1 + \alpha \frac{t - T/2}{T} \right) (t - T/2) - \frac{3}{2} \left( \frac{t - T/2}{T} \right)^2 \right] + \text{c.c.}$$

## Possibility Coherent Control on Nanoscale Demonstrated

The nanosystems studied are an “engineered” V-shape and a random planar composite (RPC), positioned in the  $xy$  plane. The material is silver; the spatial scale is 1-3 nm/grid unit.



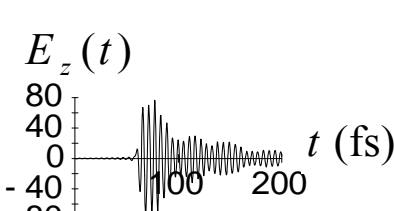
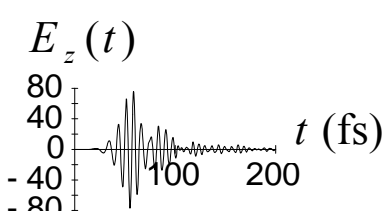
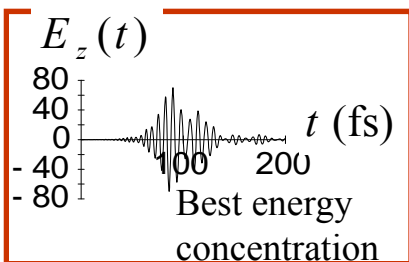
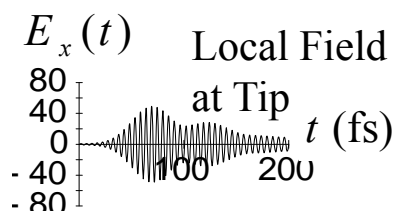
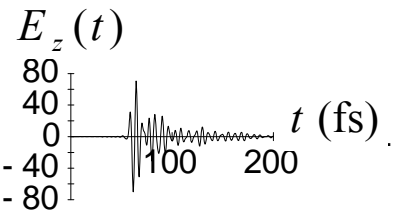
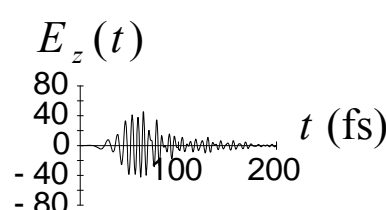
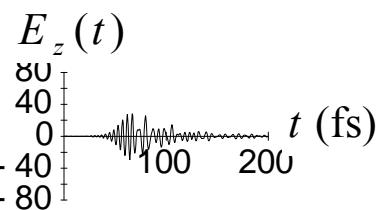
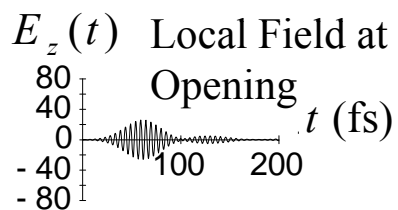
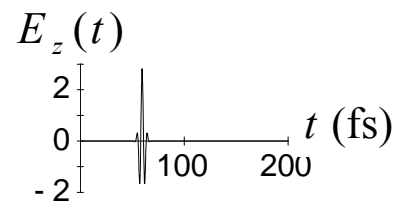
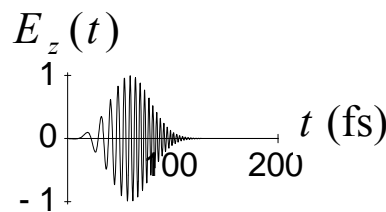
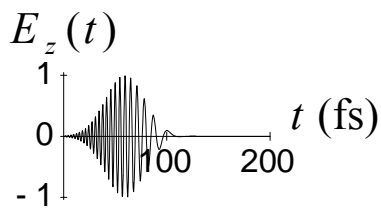
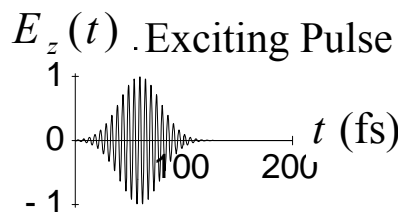
# Linear responses

No Chirp

Negative Chirp

Positive Chirp

Transform-Limited

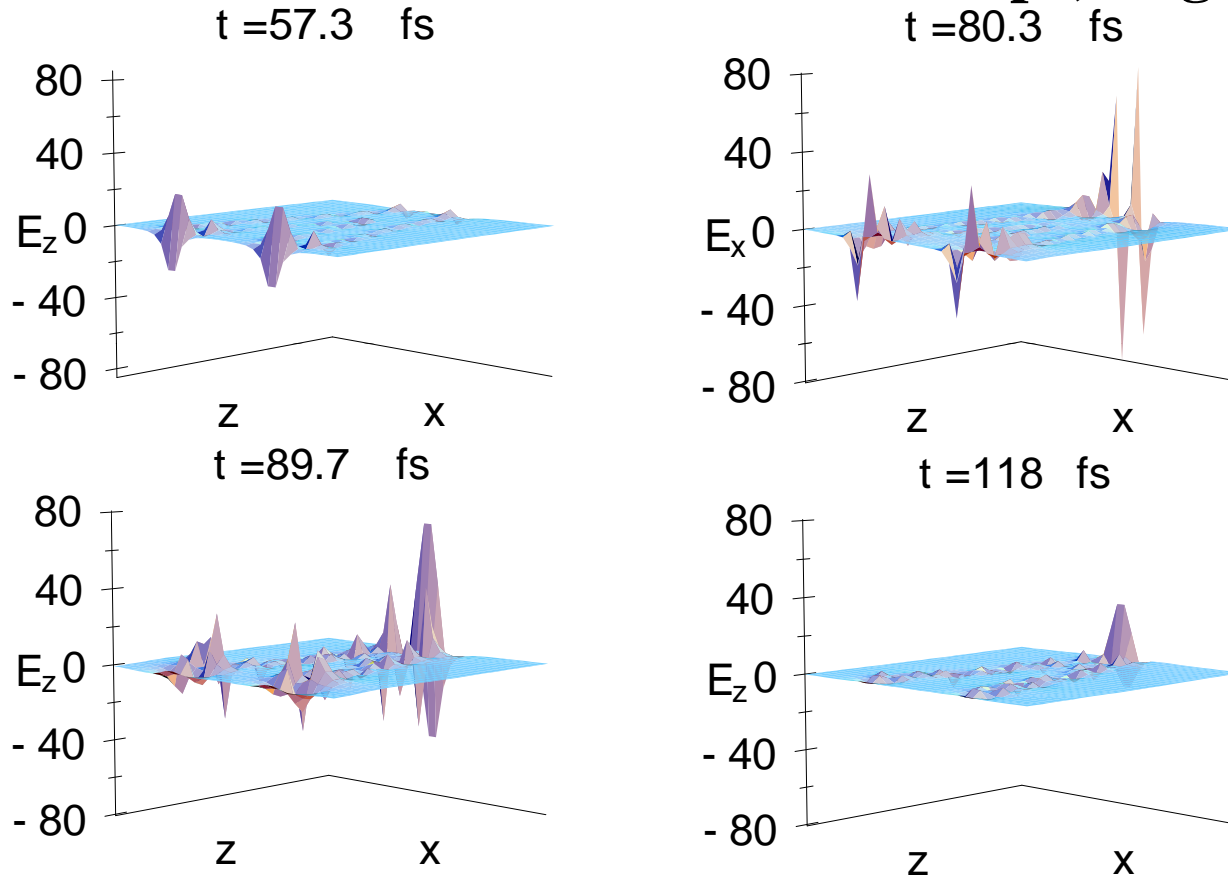


Same spectrum

Same envelope

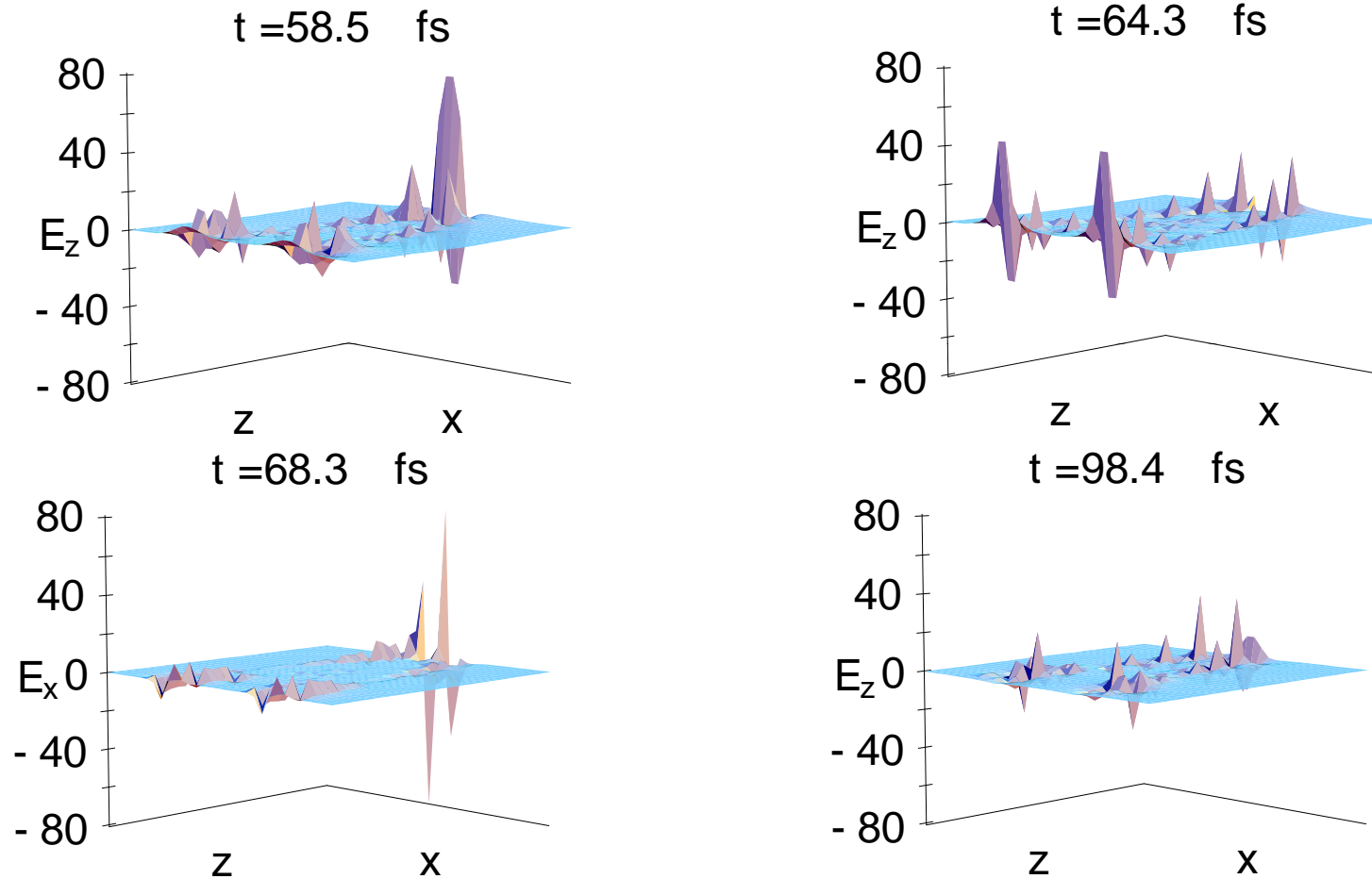
Same average period

## Spatial Distribution: Local Fields in V-shape, Negative Chirp



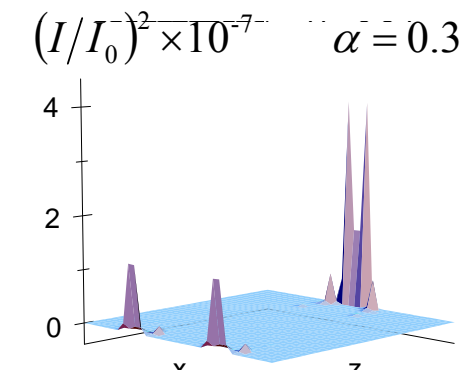
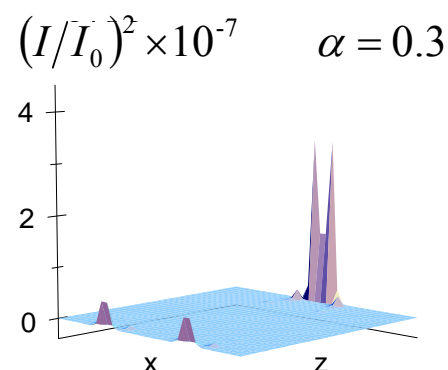
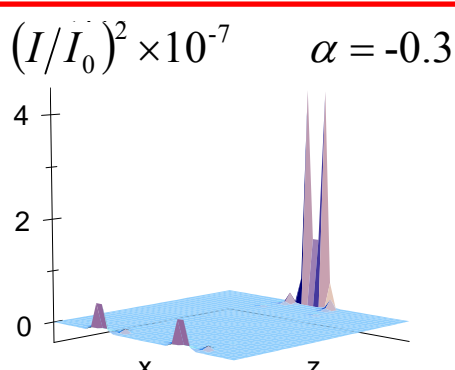
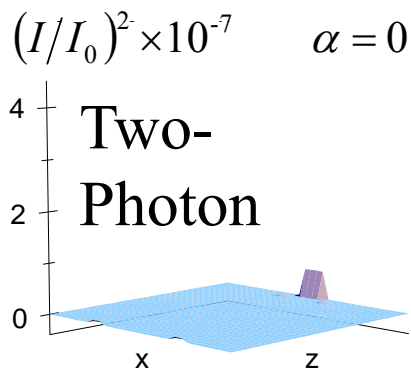
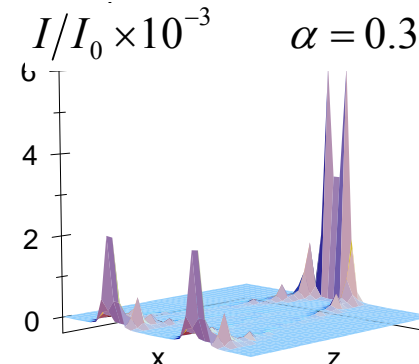
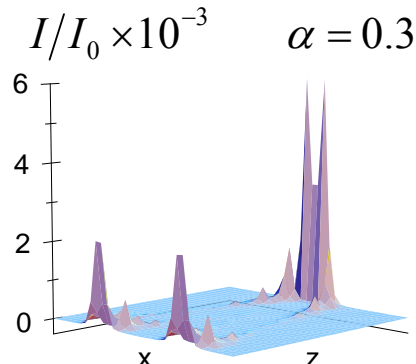
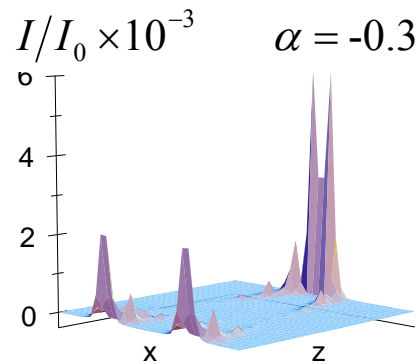
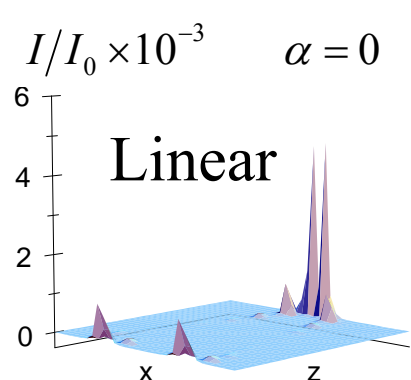
**Conclusion: There is a strong localization of the excitation energy at the tip of the nanostructure during a time interval on order of the pulse length**

## Spatial Distribution: Local Fields in V-shape, Positive Chirp



**Conclusion: Excitation energy is transferred between the tip and the opening of the nanostructure. No spatial concentration of energy takes place.**

## Time-Averaged Responses



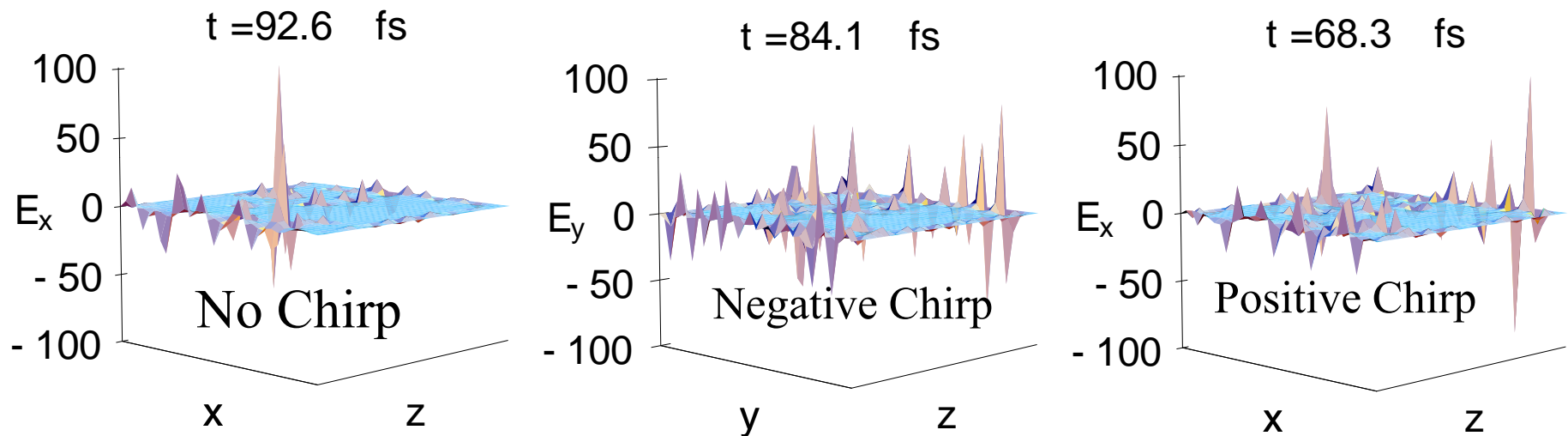
Same spectrum

Same envelope

Same average period

**Conclusion: For averaged linear responses, only spectrum is important.  
 In a nonlinear case, the phase is a controlling factor.**

## Local Optical Fields in Random Planar Composite at the Instants of their Maxima



**Conclusion: The phase is a controlling factor in random systems as well**

# Femtosecond Imaging of Surface Plasmon Dynamics in a Nanostructured Silver Film

Atsushi Kubo,<sup>†,§</sup> Ken Onda,<sup>†,§</sup> Hrvoje Petek,<sup>\*,†,§</sup> Zhijun Sun,<sup>†,§</sup> Yun S. Jung,<sup>†,§</sup> and Hong Koo Kim<sup>†,§</sup>

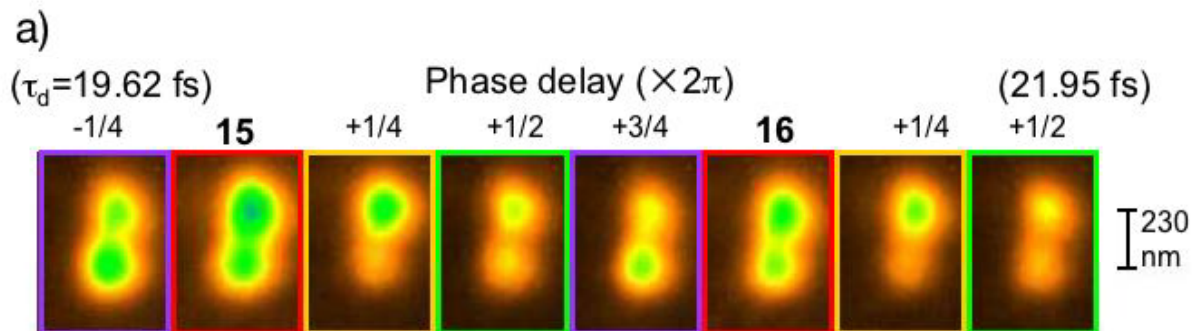
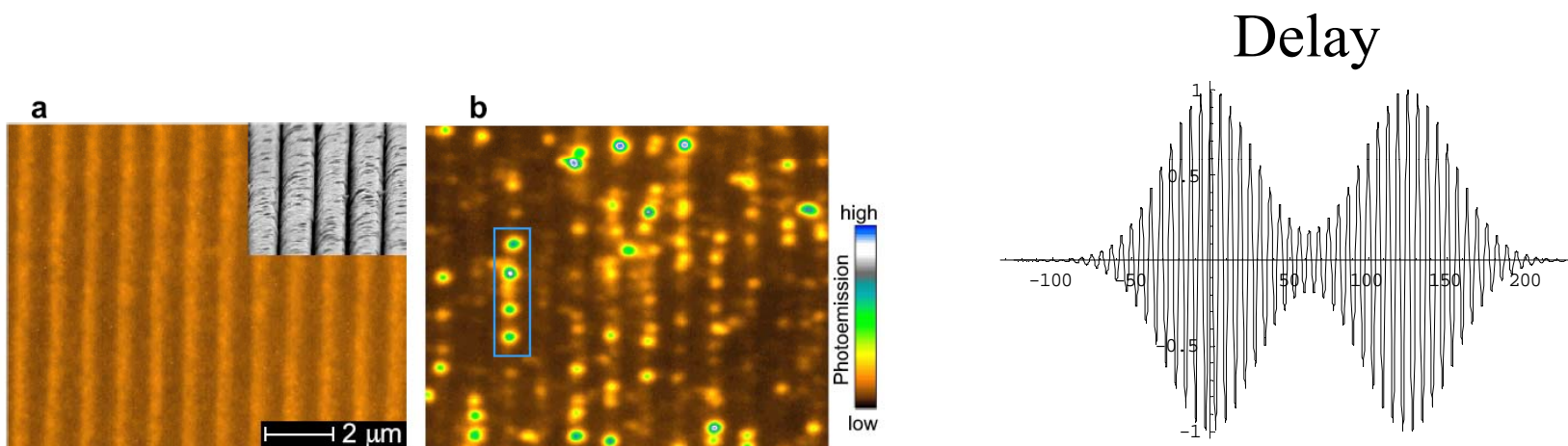
*Department of Physics and Astronomy, Department of Electrical Engineering, and Institute of NanoScience and Engineering, University of Pittsburgh, Pittsburgh, Pennsylvania 15260*

*Received April 10, 2005; Revised Manuscript Received May 6, 2005*

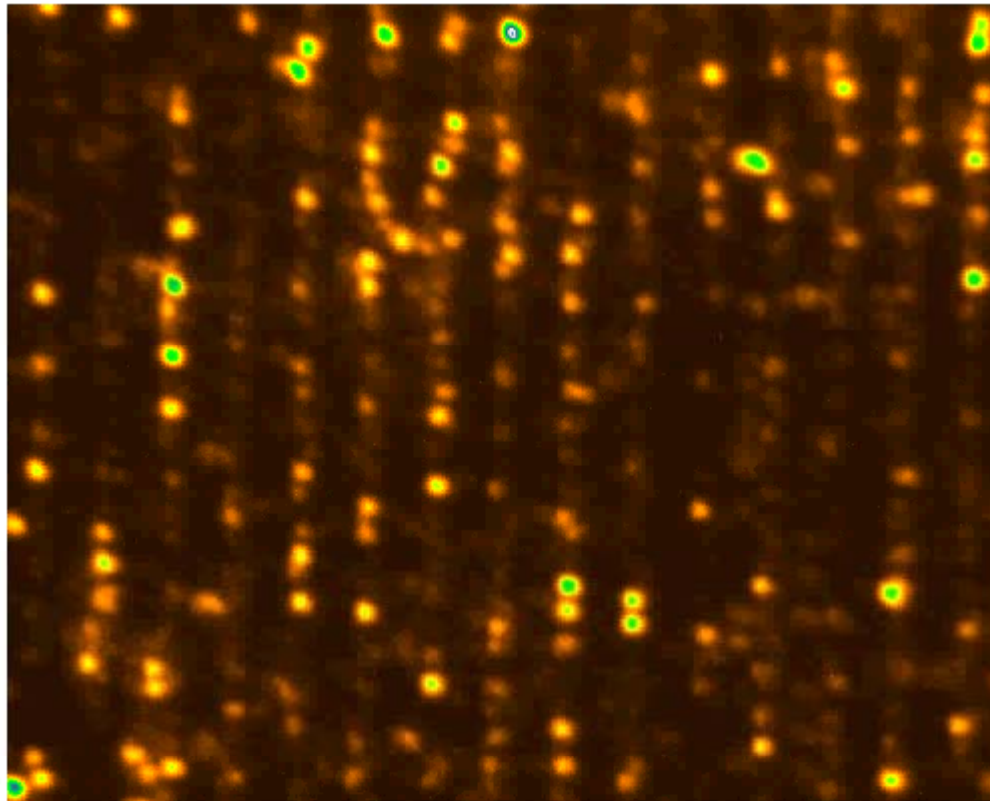
## ABSTRACT

Light interacting with nanostructured metals excites the collective charge density fluctuations known as surface plasmons (SP). Through excitation of the localized SP eigenmodes incident light is trapped on the nanometer spatial and femtosecond temporal scales and its field is enhanced. Here we demonstrate the imaging and quantum control of SP dynamics in a nanostructured silver film. By inducing and imaging the nonlinear two-photon photoemission from the sample with a pair of identical 10-fs laser pulses while scanning the pulse delay, we record a movie of SP fields at a rate of 330-attoseconds/frame.

# Two-Photon Interferometric Coherent Control



## Two-Photon Interferometric Coherent Control (Movie as a function of the delay time between the pulses)



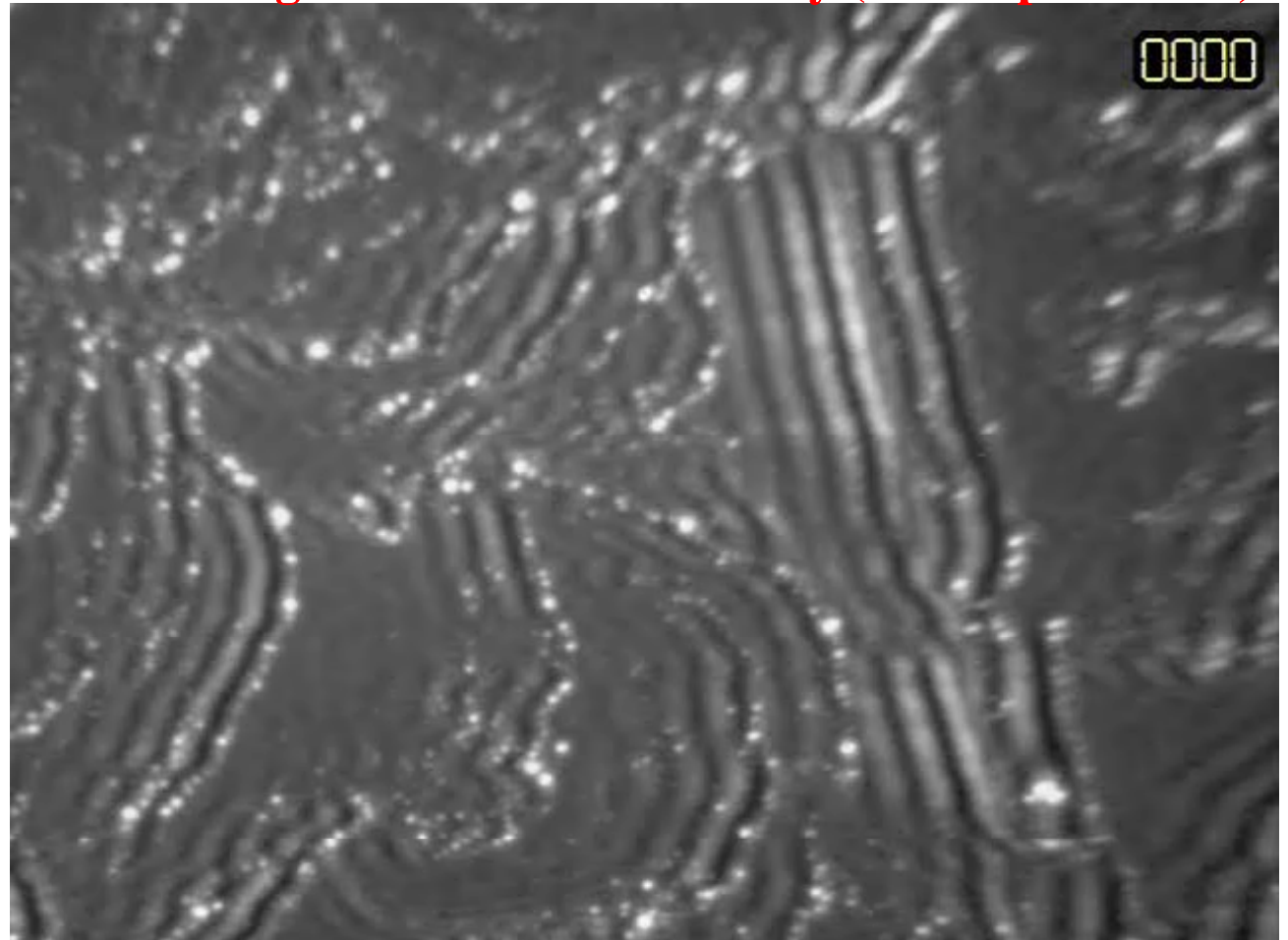
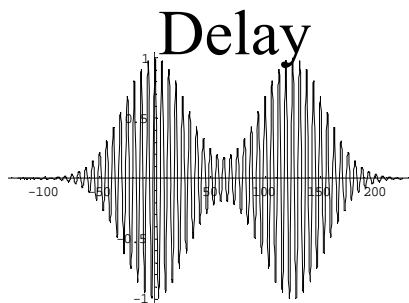
$Dt = 009.75 \times 2\pi$

A. Kubo, K. Onda, H. Petek, Z. Sun, Y. S. Jung, and H. K. Kim, *Femtosecond Imaging of Surface Plasmon Dynamics in a Nanostructured Silver Film*, Nano Lett. 5, 1123 (2005).  
**PEEM Image as a Function of Delay (250 as per frame)**

**200 nm**  
↔

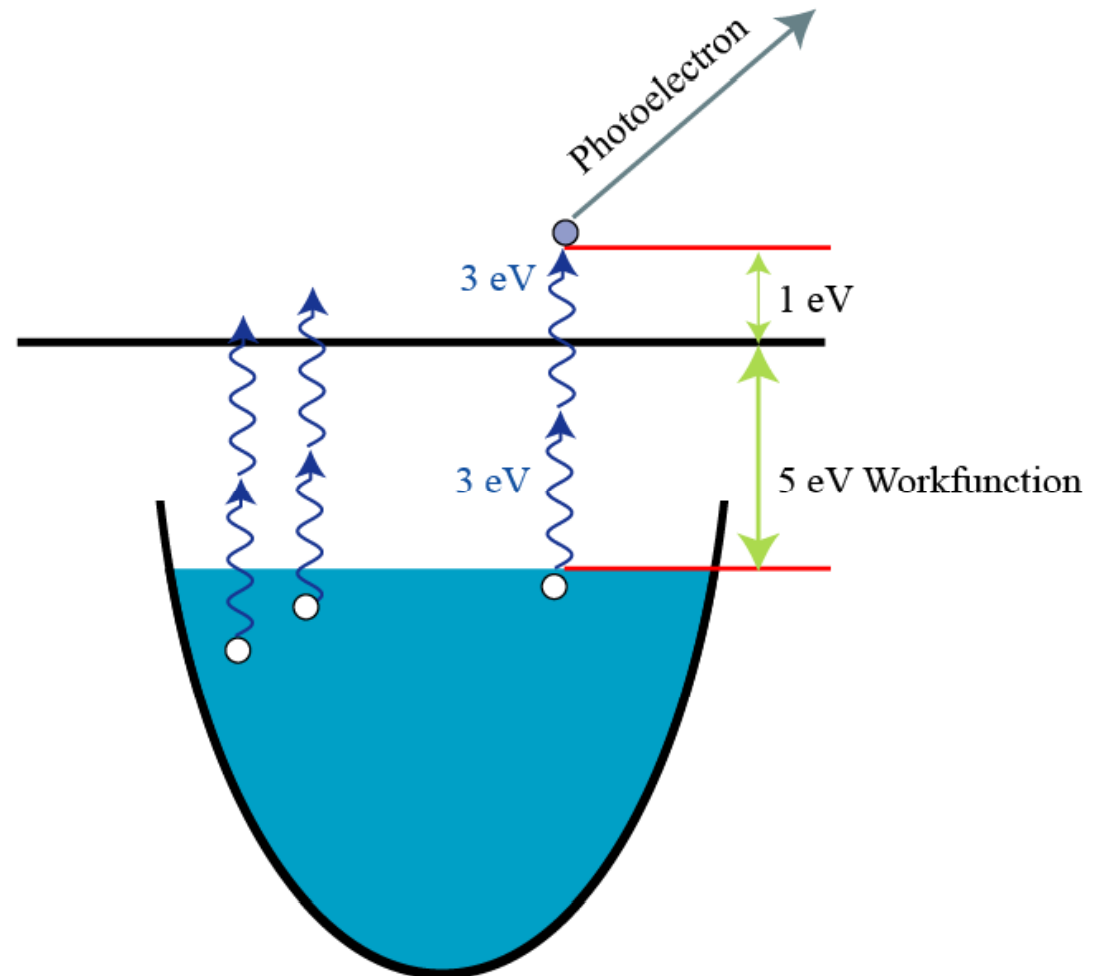
**30 femtoseconds from life  
of a nanoplasmonic  
systems**

**Localized SP hot spots are  
deeply subwavelength as  
seen in PEEM  
(photoemission electron  
microscope)**

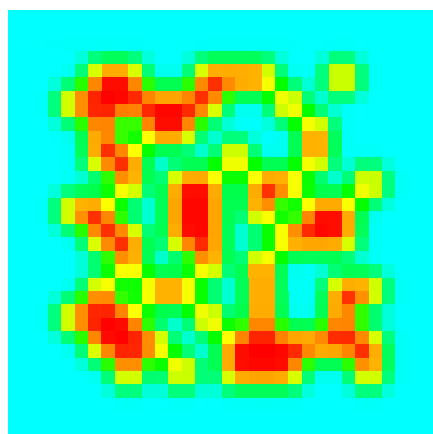


Due to the low photoelectron energy and its large spread, there are large chromatic aberrations in the electron optics of the PEEM

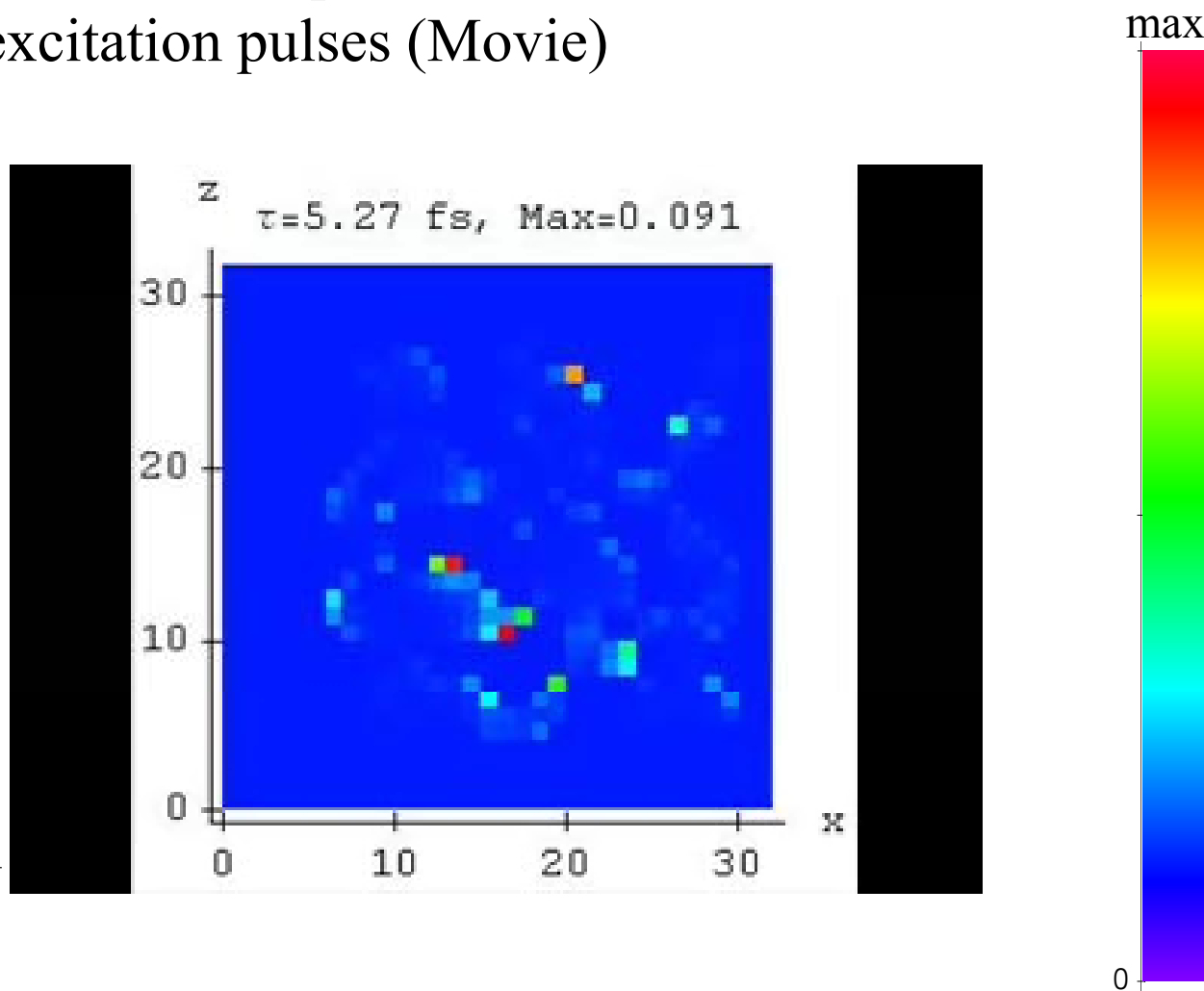
## Two-Photon Electron Emission



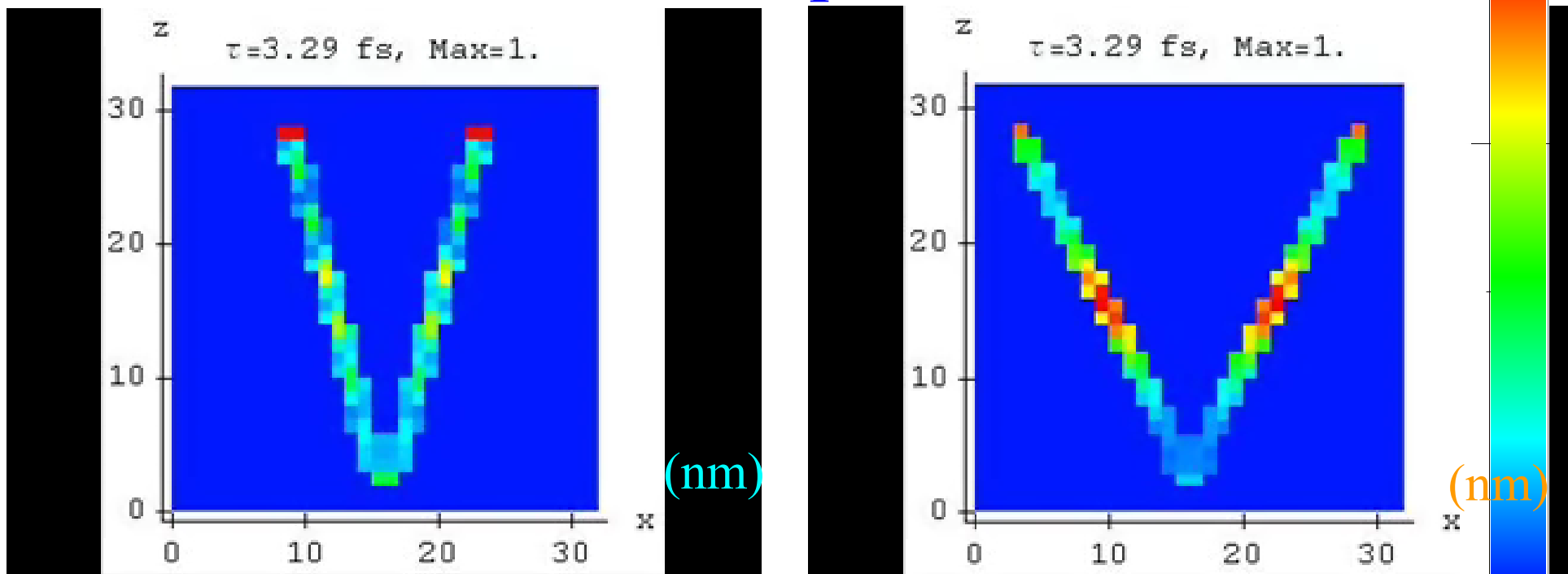
Theory: Spatial distributions of two-photon excitation as a function of delay between the two excitation pulses (Movie)



Geometry of the system



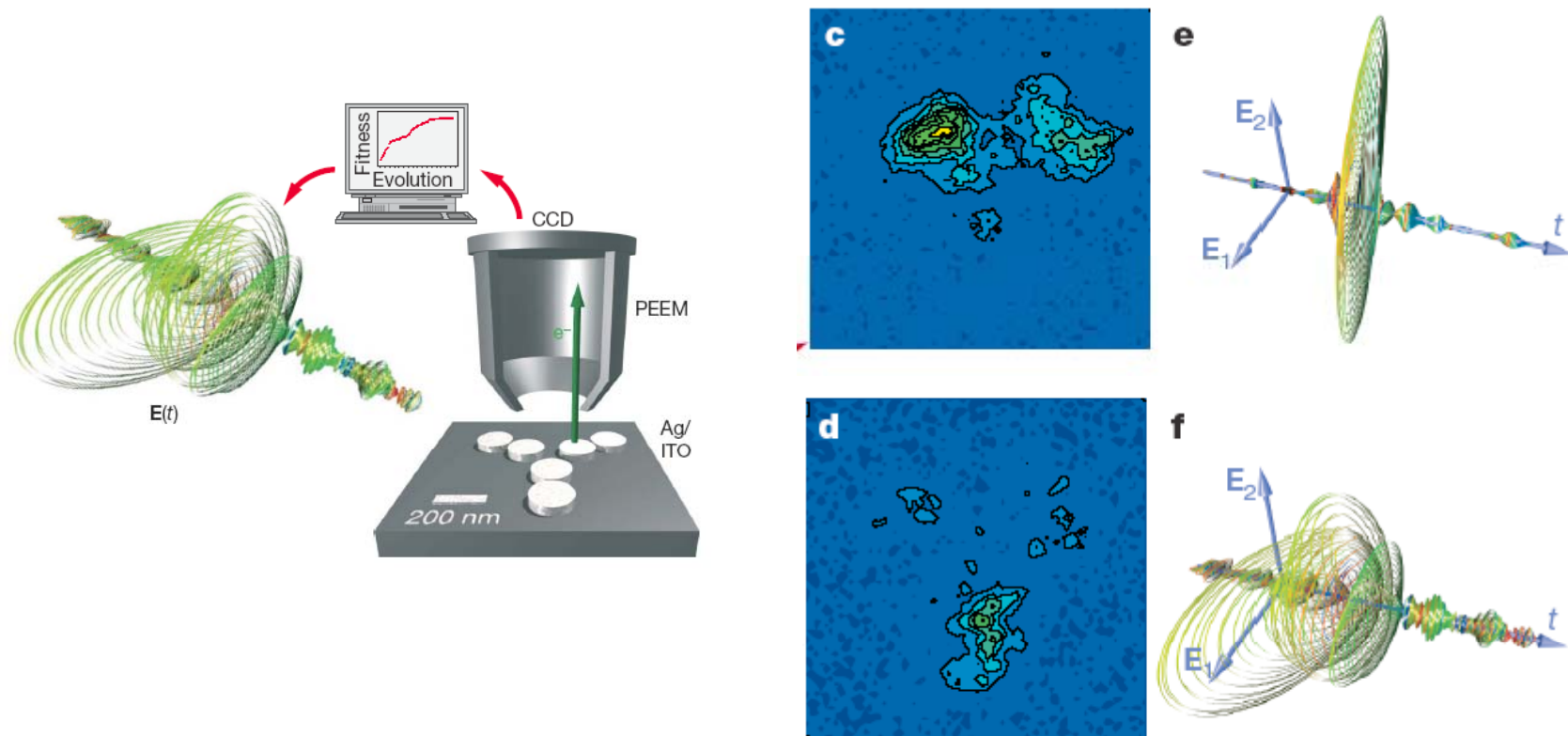
# Coherent Control of Two-Photon Electron Emission in V-Shape Nanoantennas



Time-integrated electron current as a function of interpulse delay  
M.I. Stockman, Nano Lett. **5**, 2325-2329 (2005).

# Adaptive subwavelength control of nano-optical fields

Martin Aeschlimann<sup>1</sup>, Michael Bauer<sup>2</sup>, Daniela Bayer<sup>1</sup>, Tobias Brixner<sup>3</sup>, F. Javier García de Abajo<sup>4</sup>, Walter Pfeiffer<sup>5</sup>, Martin Rohmer<sup>1</sup>, Christian Spindler<sup>3</sup> & Felix Steeb<sup>1</sup>



## CONCLUSIONS

- Phase modulation of the excitation femtosecond pulse provides a functional degree of freedom necessary to control the spatial distribution of the local optical fields in nanosystems on the femtosecond temporal and nanometer spatial scale.
- Both the spectral composition and the phase modulation determine femtosecond-nanometer dynamics of local fields.
- For nonlinear photoprocesses, time-integral spatial distribution is controlled by both the pulse spectrum and its phase modulation. Two-photon processes are locally enhanced at the optimum by a factor of up to  $10^7$ .

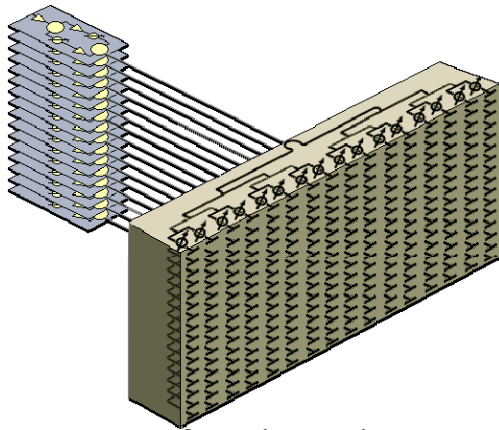


Department of Physics and Astronomy  
Georgia State University  
Atlanta, GA 30303-3083

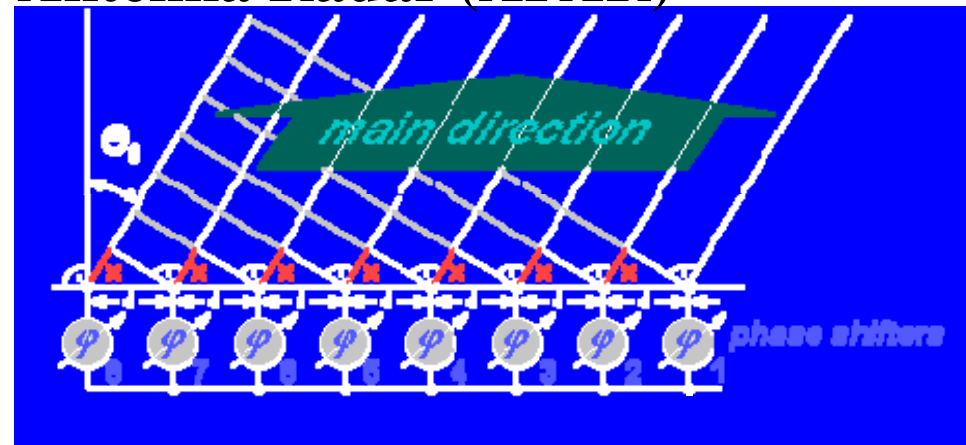
# “Synthetic Aperture Radar” in Nanoplasmonics

M. Durach, A. Rusina, K. Nelson, and M. I. Stockman, *Toward Full Spatio-Temporal Control on the Nanoscale*, arXiv:0705.0725 (2007); *Nano Lett.* **7**, 3145-3149 (2007)

## Radar Basics: Synthetic Aperture Radar (SAR) or Active Phased Array Antenna Radar (APAR)



Planar array of a phased-array antenna



### Space Surveillance Radar

U.S. Space Command's largest surveillance radar. The world's first large phased array radar, the AN/FPS-85 was constructed in the 1960s at Eglin Air Force Base, Florida.

$$x = d \cdot \sin \Theta_s \quad (\text{Sinussatz})$$

$$\frac{360^\circ}{\varphi} = \frac{\lambda}{x} \quad (\text{Dreisatz})$$

$$\Rightarrow \varphi = \frac{360^\circ}{\lambda} \cdot d \cdot \sin \Theta_s$$

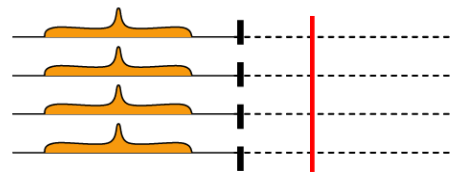
$\varphi$  = phase shift between two successive elements  
 $d$  = distance between the radiating elements  
 $\Theta_s$  = beam steering

## APAR: Active Phased Array Radar

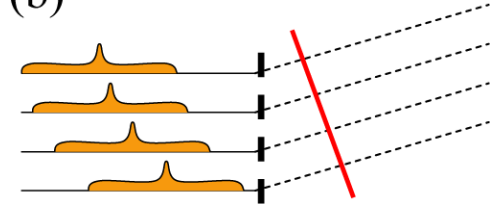
## AESA: Active Electronically Scanned Array



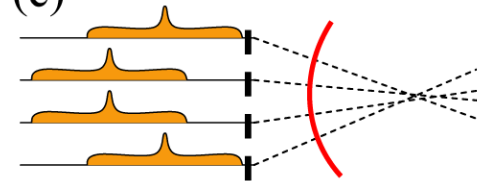
(a) Straight beam



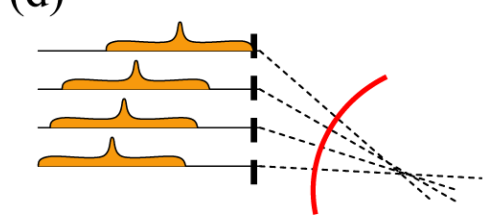
(b) Steering



(c) Focusing



(d) Steering and focusing

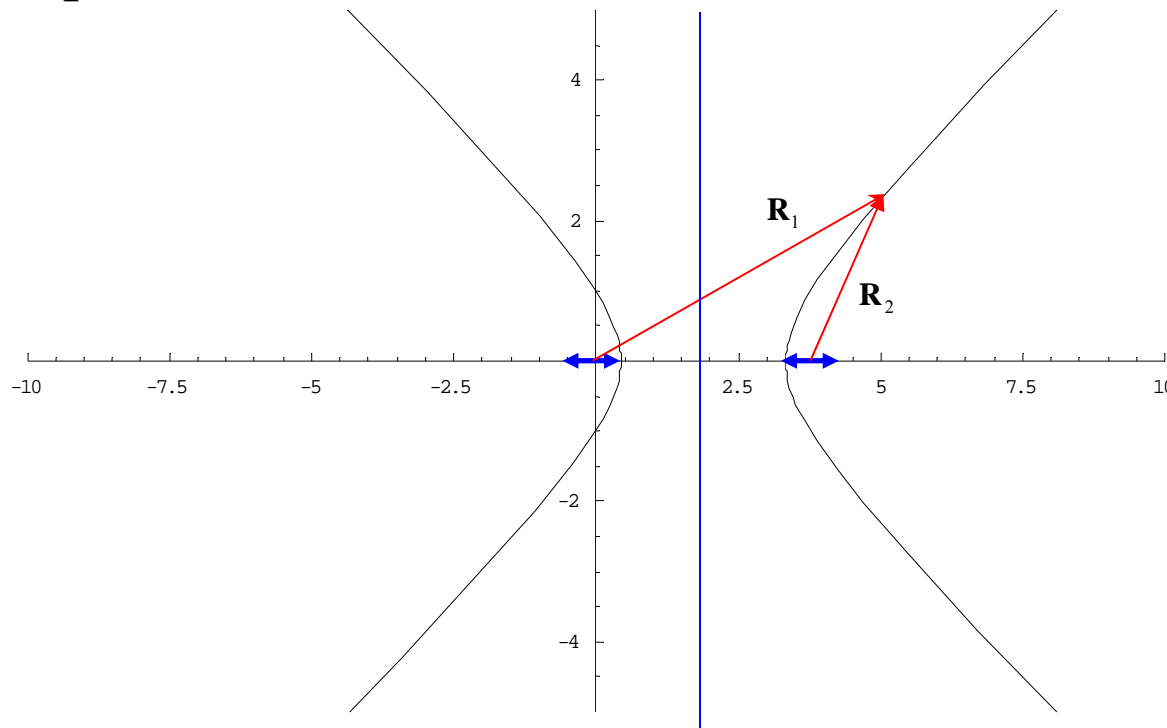


An interference fringe of two coherent EM sources is a line of

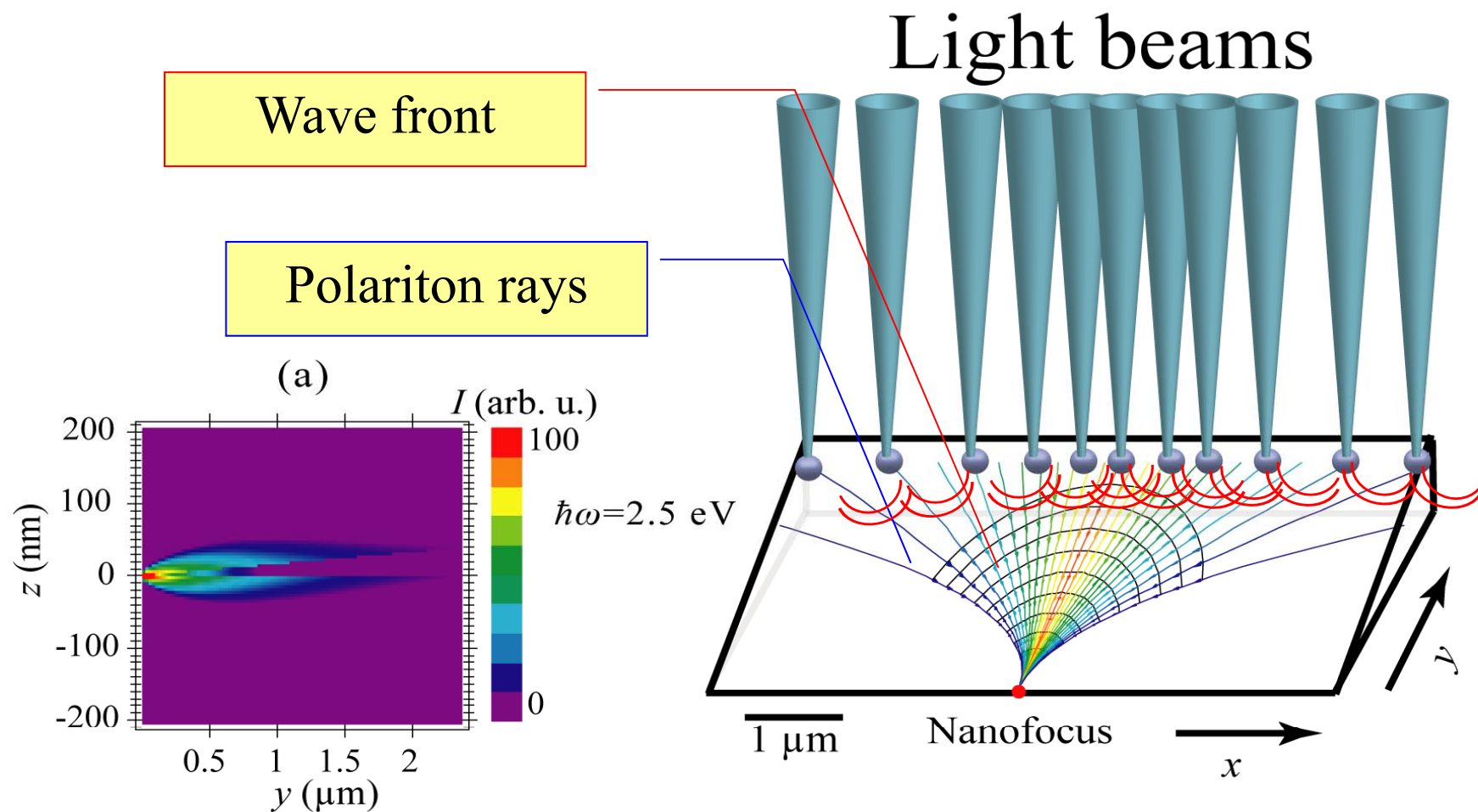
;

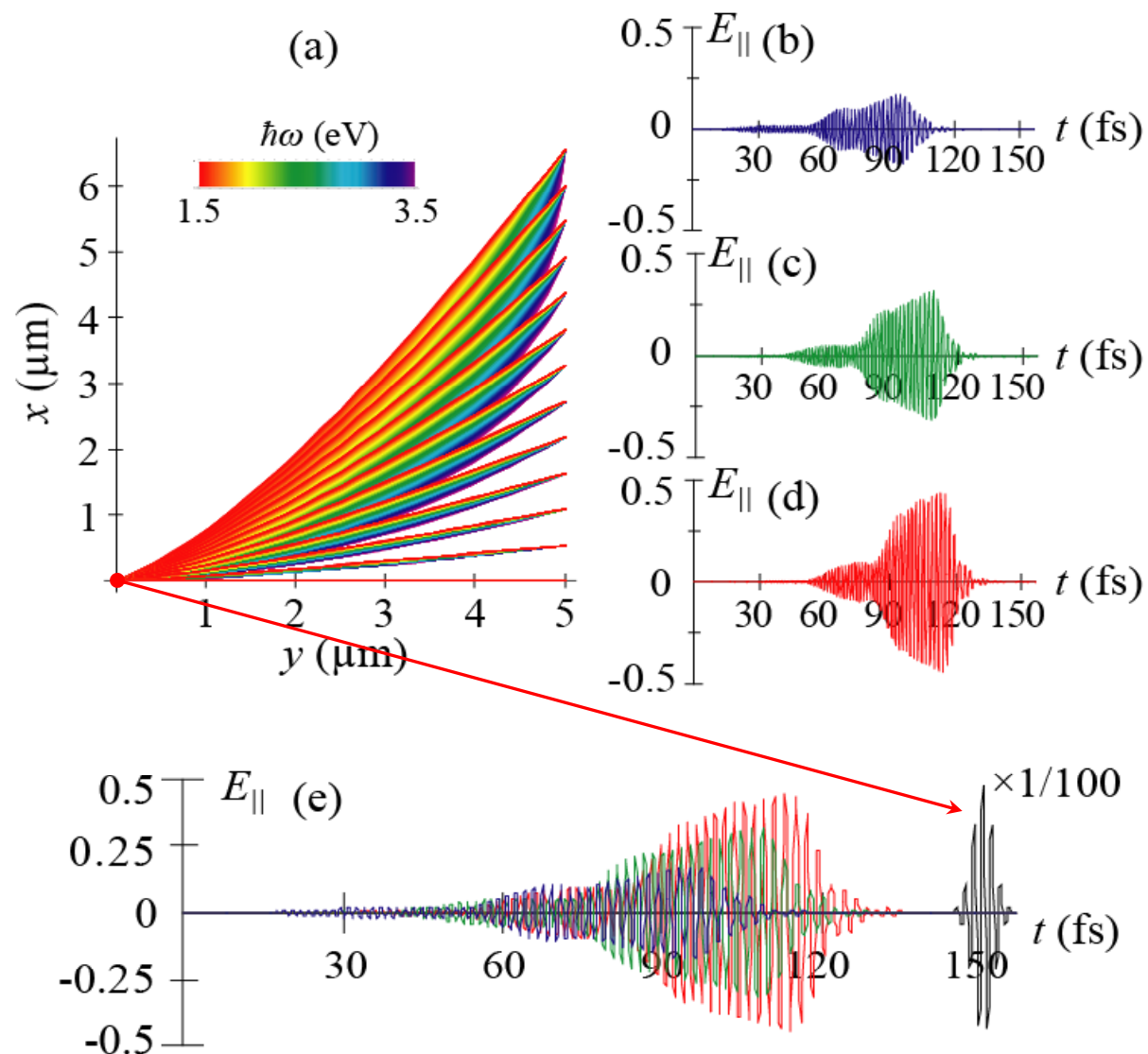
$$R_1 - R_2 = m\lambda, \quad m = 0, \pm 1, \dots$$

It is a hyperbola. This is the first example of coherent control used by the British in operation *Oboe* during WWII to guide bombers over Germany in complete radio silence



M. Durach, A. Rusina, K. Nelson, and M. I. Stockman, *Toward Full Spatio-Temporal Control on the Nanoscale*, arXiv:0705.0725 (2007); Nano Lett. **7**, 3145-3149 (2007)





**Problem: The pulses to control even simplest nanoplasmonic systems found by adaptive algorithms may be very complex.**

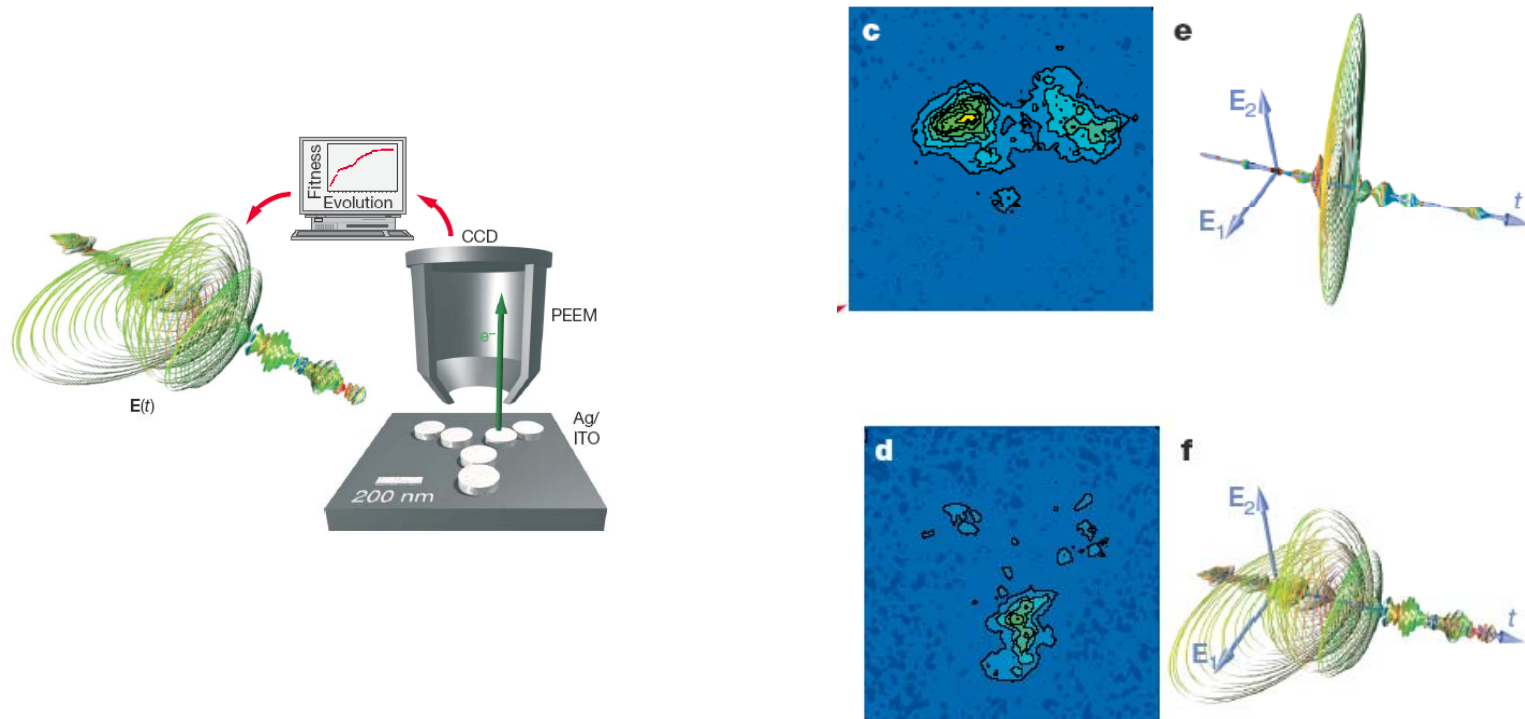
**How to determine a pulse that can localize optical energy at a given site of a nanosystem deterministically and robustly?**

**Solution: Time reversal approach**

X. Li and M. I. Stockman, *Highly efficient spatiotemporal coherent control in nanoplasmonics on a nanometer-femtosecond scale by time reversal*, Phys. Rev. B **77**, 195109 (2008); arXiv:0705.0553

# Adaptive subwavelength control of nano-optical fields

Martin Aeschlimann<sup>1</sup>, Michael Bauer<sup>2</sup>, Daniela Bayer<sup>1</sup>, Tobias Brixner<sup>3</sup>, F. Javier García de Abajo<sup>4</sup>, Walter Pfeiffer<sup>5</sup>, Martin Rohmer<sup>1</sup>, Christian Spindler<sup>3</sup> & Felix Steeb<sup>1</sup>

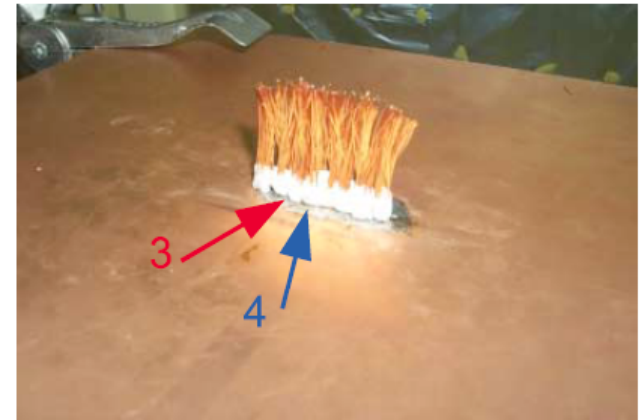
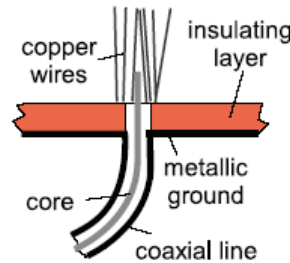
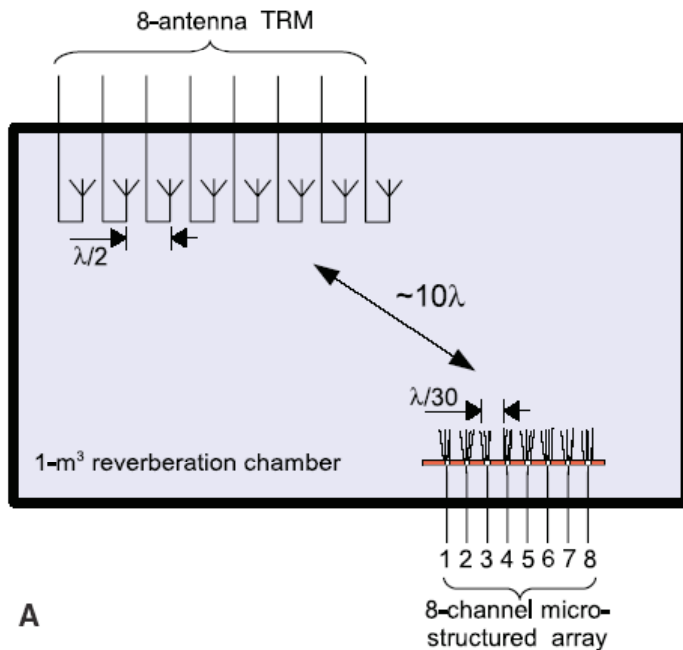


# Focusing Beyond the Diffraction Limit with Far-Field Time Reversal

Geoffroy Lerosey, Julien de Rosny, Arnaud Tourin, Mathias Fink\*

1120

23 FEBRUARY 2007 VOL 315 SCIENCE



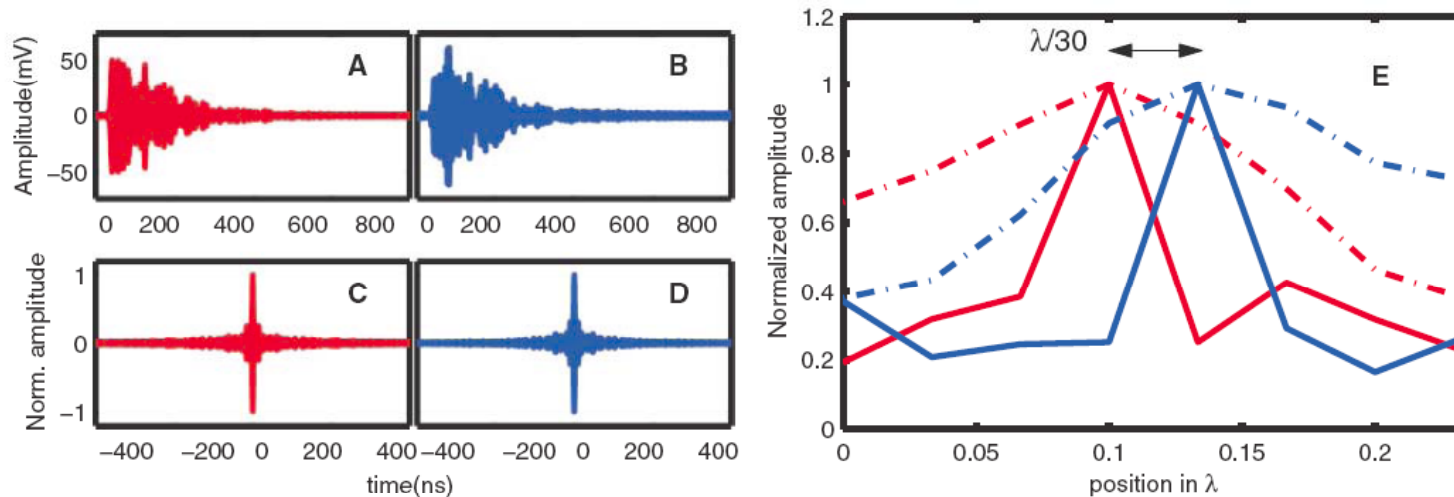


**Fig. 2.** Focusing beyond the diffraction limit. (A and B) show the signal received at one antenna of the TRM when a 10-ns pulse is sent from antennas 3 and 4, respectively, of the microstructured array. The signals in (A) and (B) look considerably different, although antennas 3 and 4 are only  $\lambda/30$  apart. (C and D) show the time compression obtained at antennas 3 and 4, respectively, when the eight signals coming from antennas 3 and 4 are time-

reversed and sent back from the TRM. (E) In full line are shown the focusing spots obtained around antennas 3 and 4. Their typical width is  $\lambda/30$ . Thus, antennas 3 and 4 can be addressed independently. The focal spots obtained when there are no copper wires are shown for comparison (dashed-dotted line). All maxima have been normalized by scaling factors in the ratios: 1 (red and blue dashed-dotted lines), 2.2 (red full line), 2.5 (blue full line).

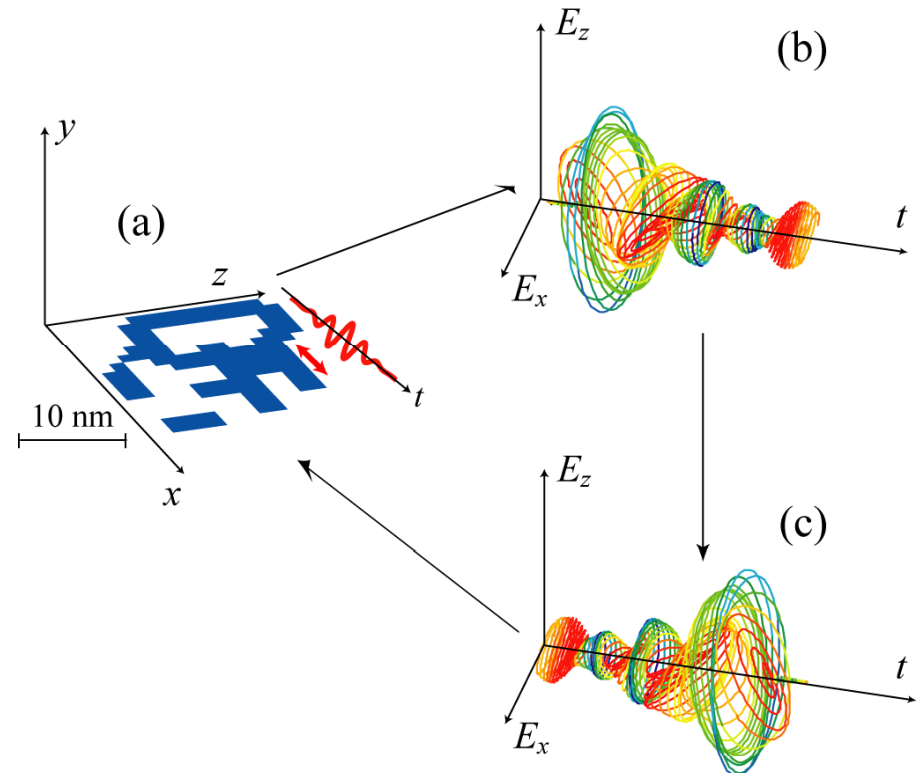
# Nanoplasmonic Energy Localization, Time Reversal, and Coherent Control

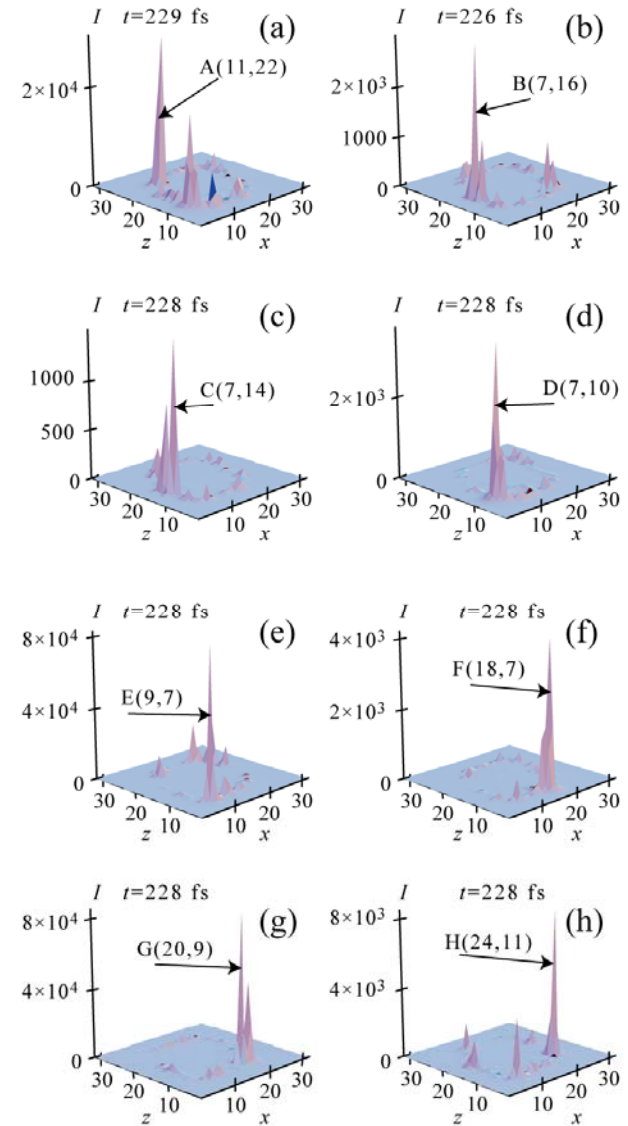
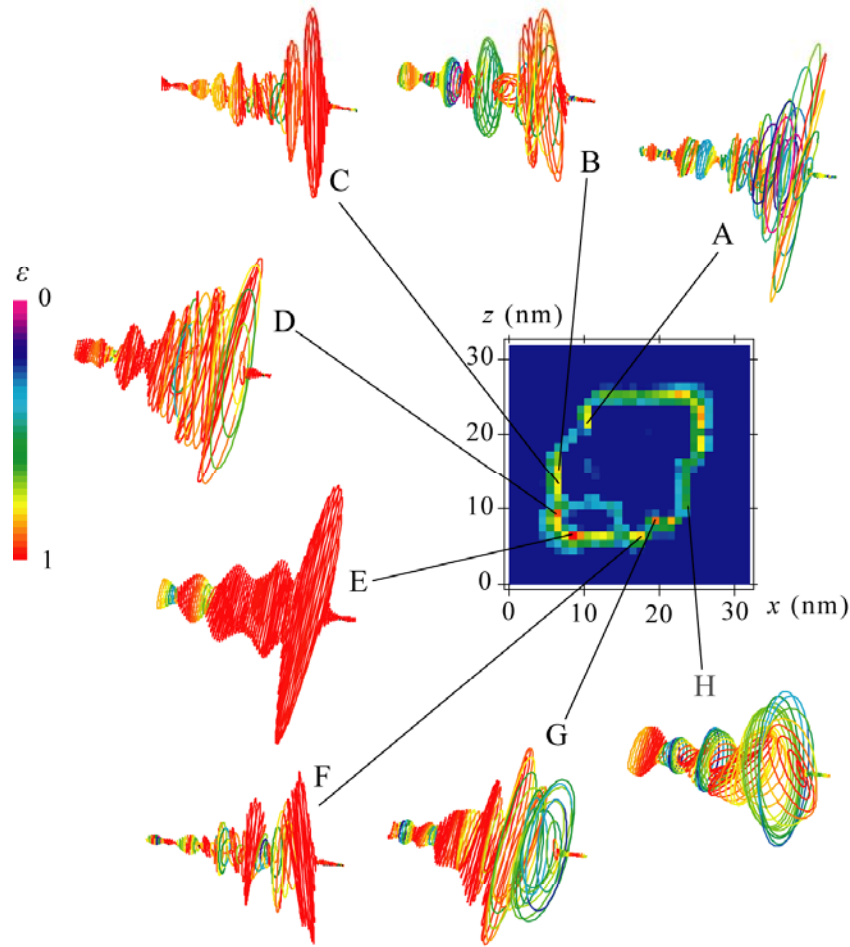
X. Li and M. I. Stockman, *Highly efficient spatiotemporal coherent control in nanoplasmonics on a nanometer-femtosecond scale by time reversal*, Phys. Rev. B **77**, 195109 (2008); arXiv:0705.0553

Idea of time reversal for subwavelength EM-wave localization:

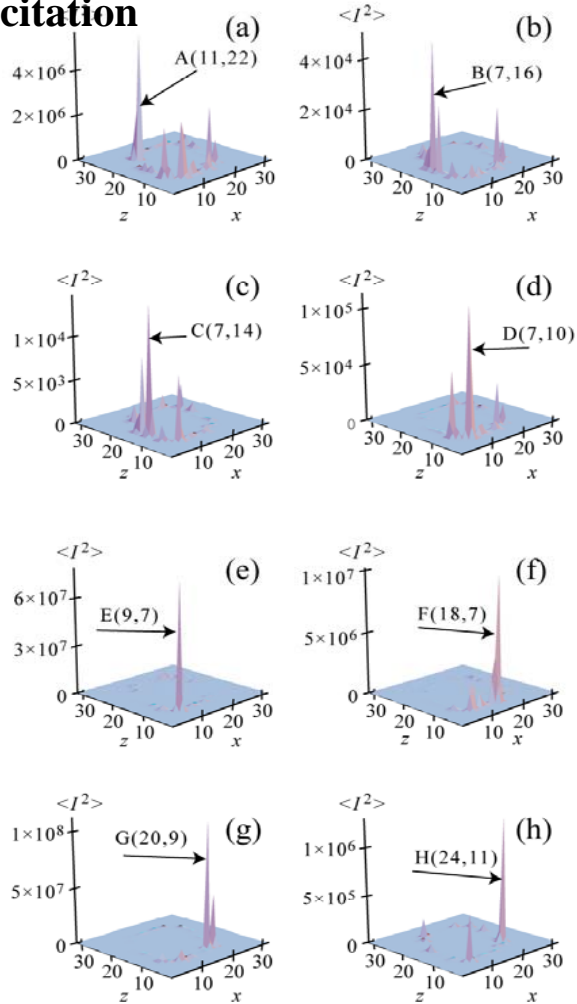
G. Lerosey, J. de Rosny, A. Tourin, and M. Fink, *Focusing Beyond the Diffraction Limit with Far-Field Time Reversal*, Science **315**, 1120-1122 (2007).

A. Derode, A. Tourin, J. de Rosny, M. Tanter, S. Yon, and M. Fink, *Taking Advantage of Multiple Scattering to Communicate with Time-Reversal Antennas*, Phys. Rev. Lett. **90**, 014301 (2003).

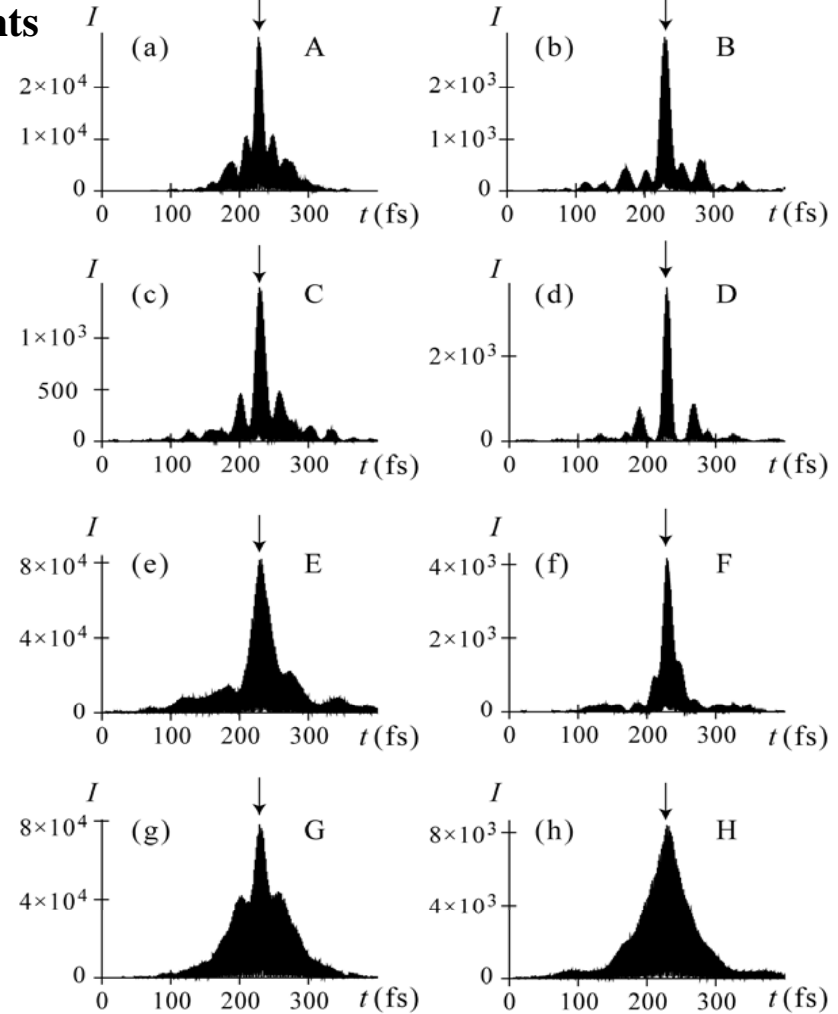




### Time-averaged two-photon excitation



### Time-dependent local field intensity at the target points



### Resonant Metalenses for Breaking the Diffraction Barrier

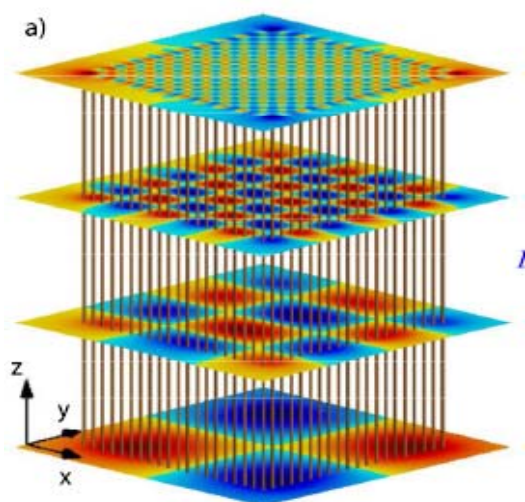
Fabrice Lemoult, Geoffroy Lerosey,\* Julien de Rosny, and Mathias Fink

*Institut Langevin, ESPCI ParisTech & CNRS, Laboratoire Ondes et Acoustique, 10 rue Vauquelin, 75231 Paris Cedex 05, France*  
 (Received 8 January 2010; revised manuscript received 14 April 2010; published 18 May 2010)

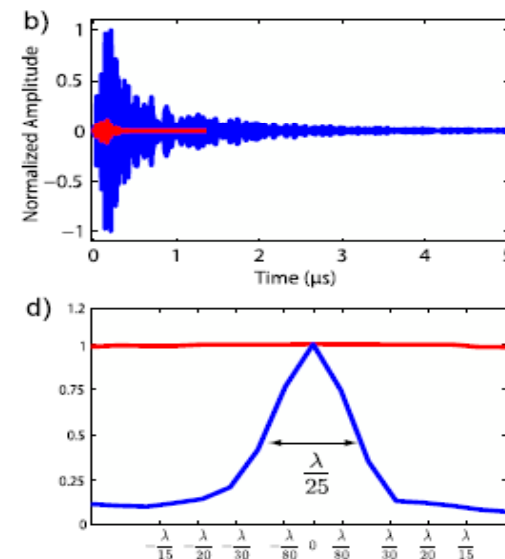
We introduce the resonant metalens, a cluster of coupled subwavelength resonators. Dispersion allows the conversion of subwavelength wave fields into temporal signatures while the Purcell effect permits an efficient radiation of this information in the far field. The study of an array of resonant wires using microwaves provides a physical understanding of the underlying mechanism. We experimentally demonstrate imaging and focusing from the far field with resolutions far below the diffraction limit. This concept is realizable at any frequency where subwavelength resonators can be designed.

DOI: 10.1103/PhysRevLett.104.203901

PACS numbers: 41.20.-q, 78.67.Pt, 81.05.Xj



amplitude of  $E_x$  TEM Bloch modes (1,1), (2,3), (5,6), and (19,19).

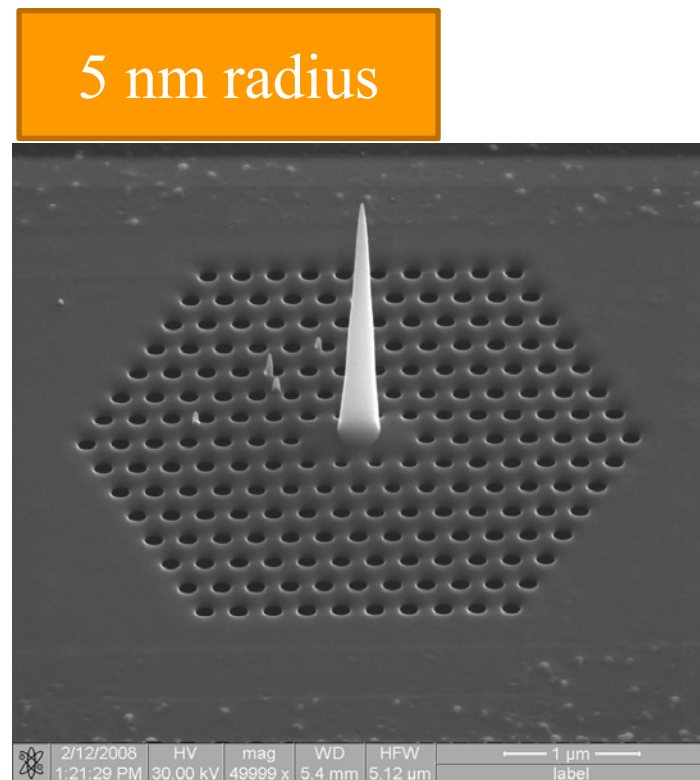
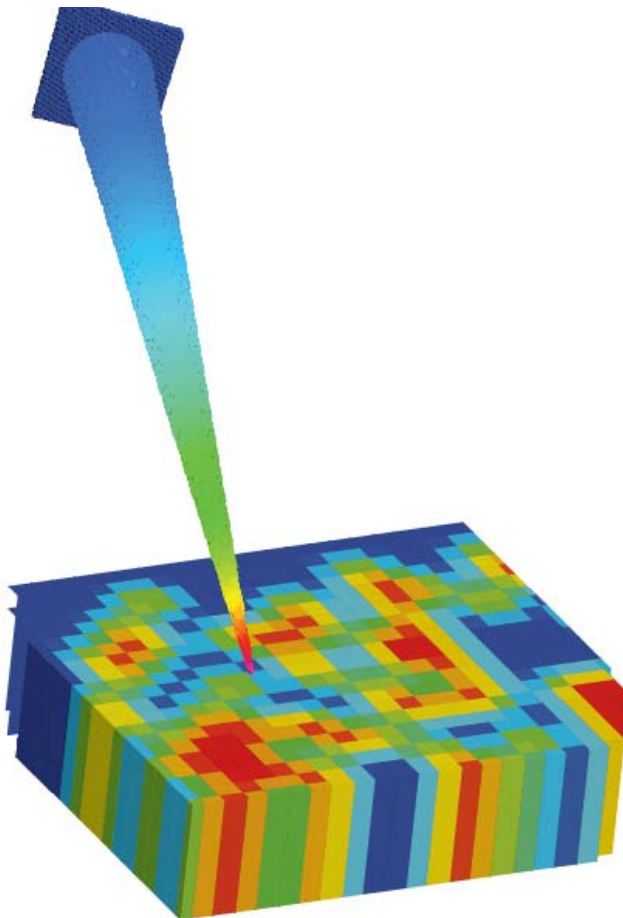


(d) Focal spot obtained after far field time reversal

# Schematic of proposed local excitation with adiabatic cones

M. I. Stockman, *Nanofocusing of Optical Energy in Tapered Plasmonic Waveguides*, Phys. Rev. Lett. **93**, 137404-1-4 (2004)

F. De Angelis, G. Das, P. Candeloro, M. Patrini, M. Galli, A. Bek, M. Lazzarino, I. Maksymov, C. Liberale, L. C. Andreani, and E. Di Fabrizio, *Nanoscale Chemical Mapping Using Three-Dimensional Adiabatic Compression of Surface Plasmon Polaritons*, Nature Nanotechnology **5**, 67-72 (2009).

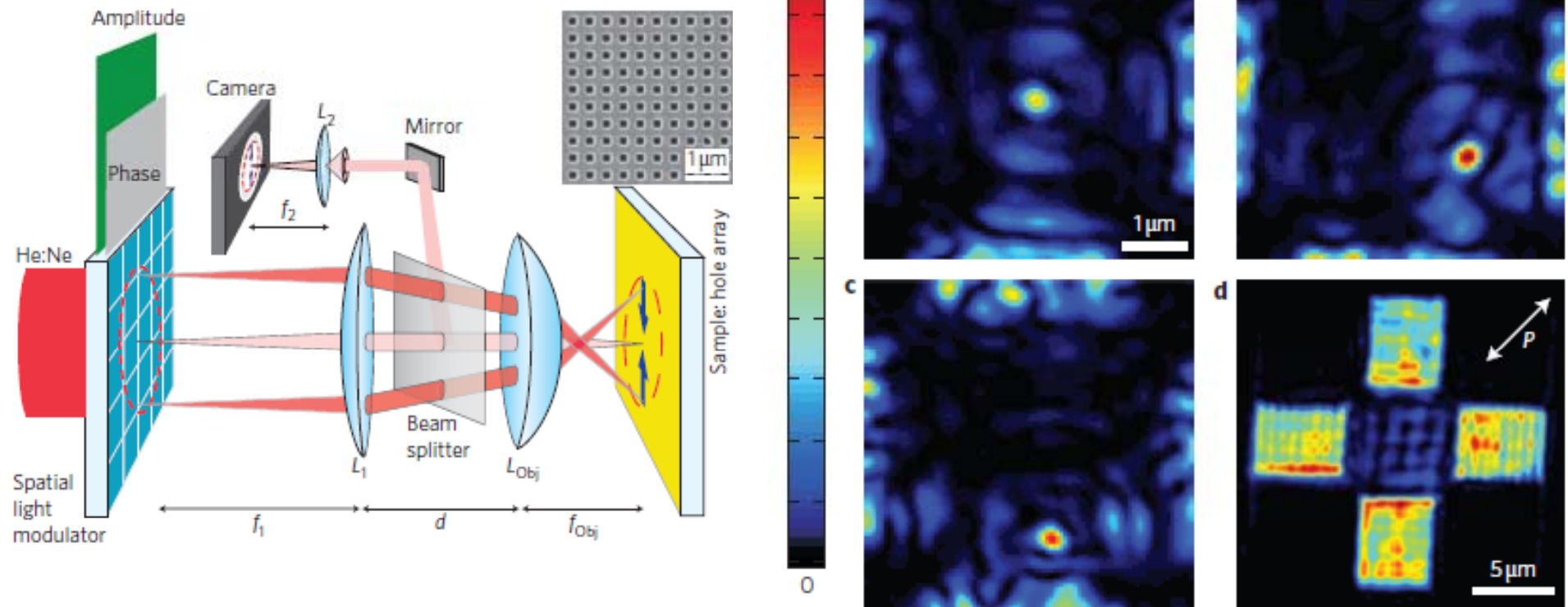


# Active spatial control of plasmonic fields

Bergin Gjonaj<sup>1\*</sup>, Jochen Aulbach<sup>1</sup>, Patrick M. Johnson<sup>1</sup>, Allard P. Mosk<sup>2</sup>, L. Kuipers<sup>1</sup> and Ad Lagendijk<sup>1</sup>

<sup>1</sup>FOM-Institute for Atomic and Molecular Physics AMOLF, Science Park 104, 1098 XG Amsterdam, The Netherlands, <sup>2</sup>Complex Photonic Systems, Faculty of Science and Technology, and MESA+ Institute for Nanotechnology, University of Twente, PO Box 217, 7500 AE Enschede, The Netherlands.

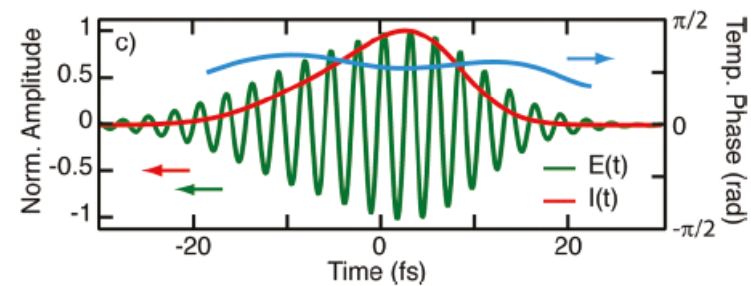
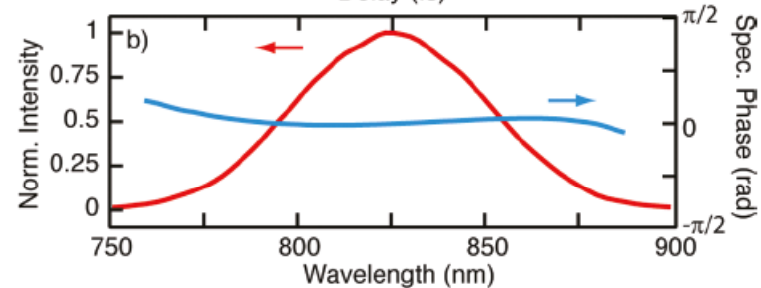
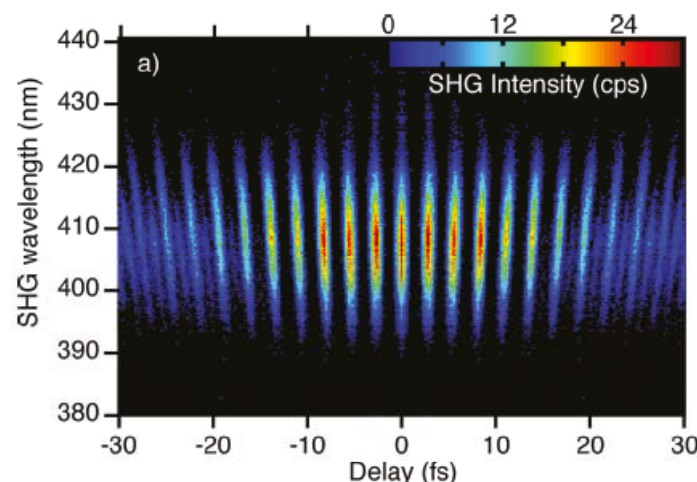
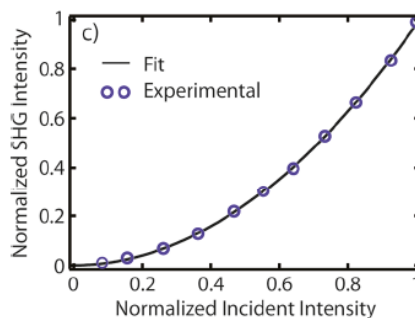
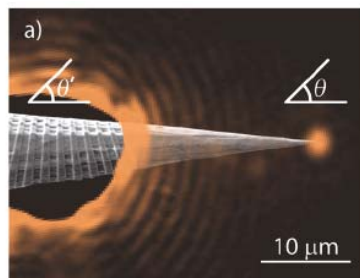
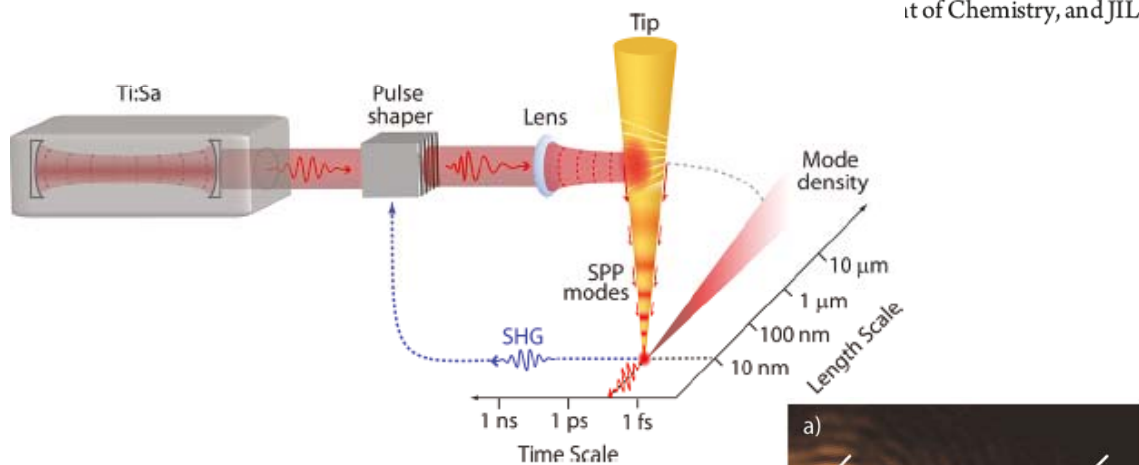
\*e-mail: b.gjonaj@amolf.nl



# Femtosecond Nanofocusing with Full Optical Waveform Control

Samuel Berweger,<sup>†</sup> Joanna M. Atkin,<sup>†</sup> Xiaoji G. Xu, Robert L. Olmon, and Markus B. Raschke\*

<sup>†</sup>Department of Chemistry, and JILA, University of Colorado at Boulder, Boulder, Colorado 80309, United States



## CONCLUSIONS

- In nanoplasmonic systems, optical energy concentrates on the nanoscale in “hot spots” whose characteristic size is limited by the minimum size of the metal nanostructures
- The local optical field enhancement at the hot spots may be very large, up to five orders of magnitude in intensity
- The local optical fields evolve in time on the femtosecond scale, potentially on the attosecond scale
- The optical field nanolocalization is coherently controllable by pulse shaping
- Time reversal gives a convenient and powerful tool to determine the pulse shaping



Department of Physics and Astronomy  
Georgia State University  
Atlanta, GA 30303-3083

**ARTICLES**

# Attosecond nanoplasmonic-field microscope

MARK I. STOCKMAN<sup>1,2\*</sup>, MATTHIAS F. KLING<sup>2</sup>, ULF KLEINEBERG<sup>3</sup> AND FERENC KRAUSZ<sup>2,3\*</sup>

<sup>1</sup>Department of Physics and Astronomy, Georgia State University, Atlanta, Georgia 30303, USA

<sup>2</sup>Max-Planck-Institut für Quantenoptik, Hans-Kopfermann-Straße 1, D-85748 Garching, Germany

<sup>3</sup>Ludwig-Maximilians-Universität München, Department für Physik, Am Coulombwall 1, D-85748 Garching, Germany

\*e-mail: mstockman@gsu.edu; ferenc.krausz@mpq.mpg.de

Published online: 3 September 2007; doi:10.1038/nphoton.2007.169

nature photonics | VOL 1 | SEPTEMBER 2007 | www.nature.com/naturephotonics

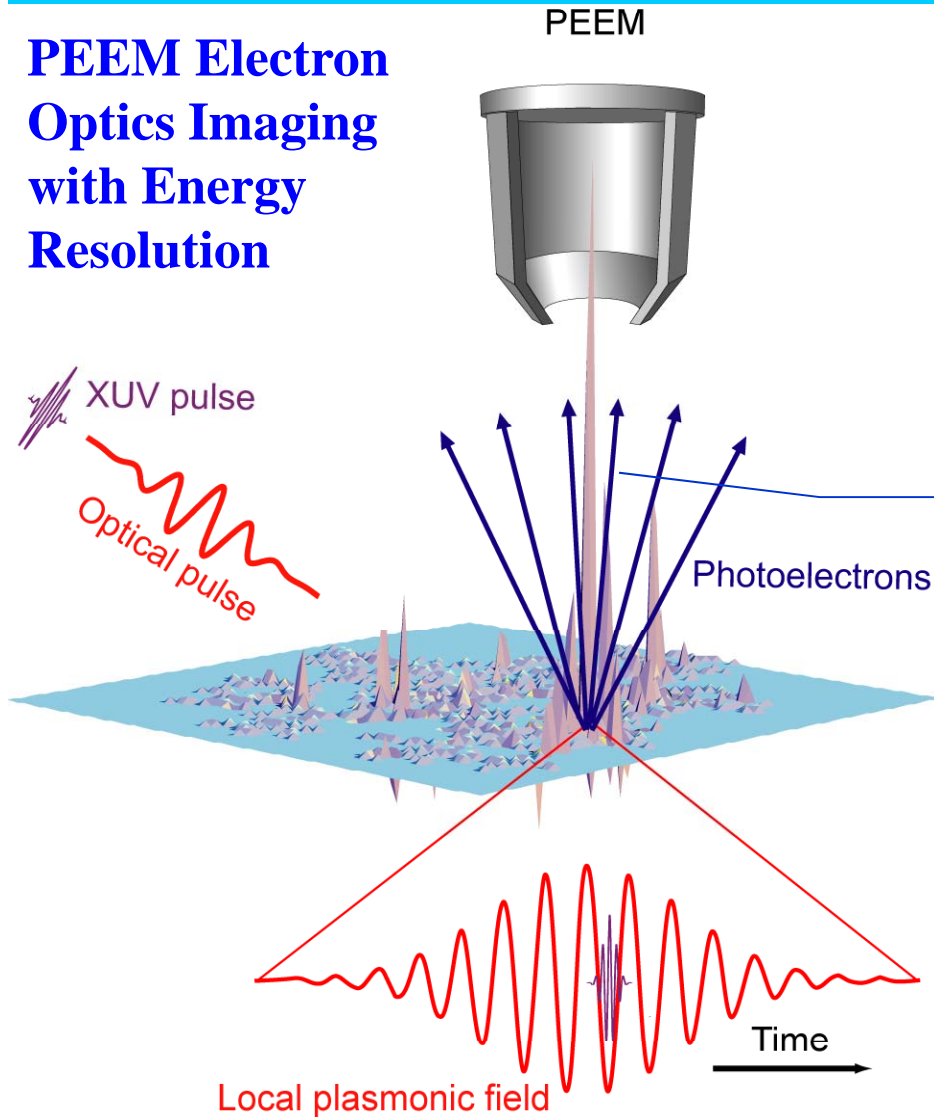
539

Short Course *Nanoplasmonics*  
2015

<http://www.phy-astr.gsu.edu/stockman>  
E-mail: mstockman@gsu.edu

Lecture 3 p.42  
7/10/2015 10:08 AM

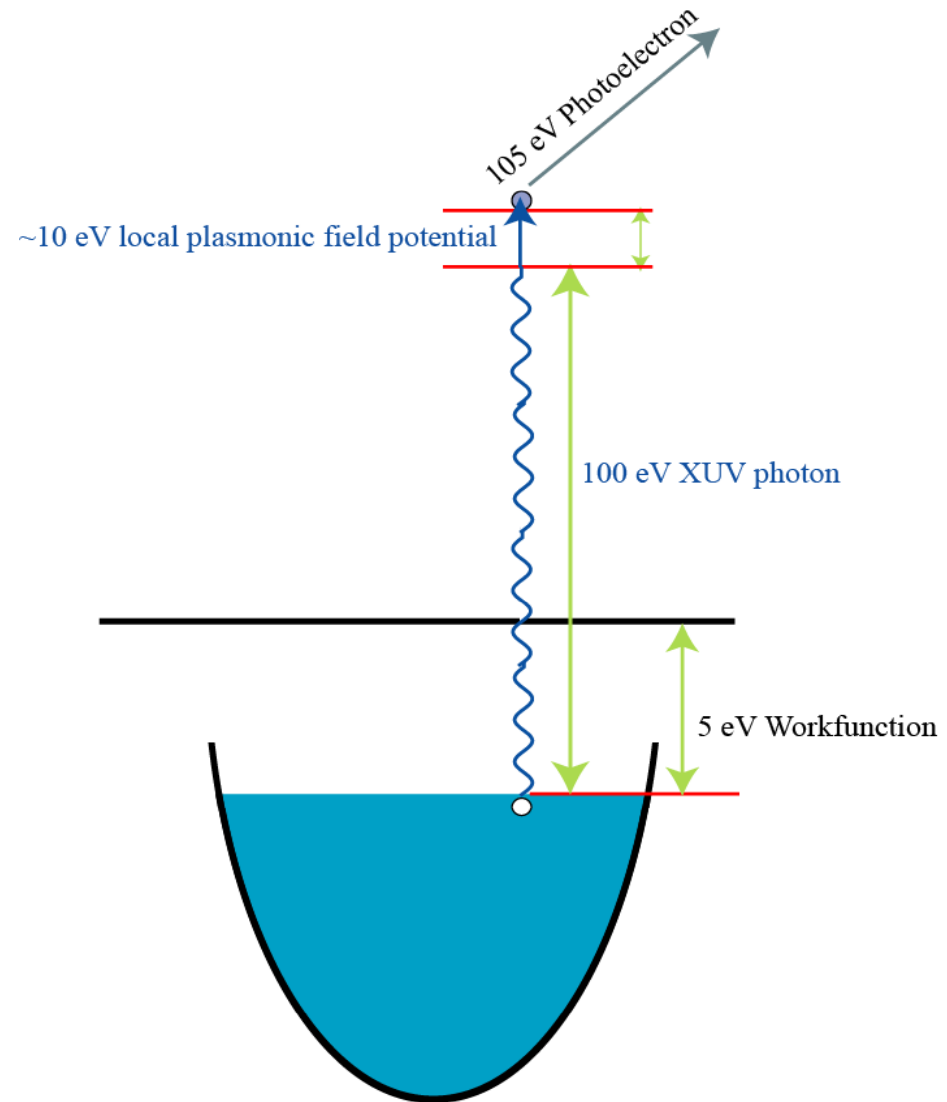
## PEEM Electron Optics Imaging with Energy Resolution



## Schematic of Attosecond Nanoplasmonic Field Microscope

XUV photoelectrons accelerated by enhanced IR plasmonic local fields

Energy of the Fermi-edge photoelectron is  $(\sim 100 \pm 10)$  eV. The local potential of the instantaneous plasmonic fields at the instant of the attosecond pulse arrival adds to the kinetic energy of electrons, acting as a local electrostatic (van de Graaf) accelerator



## Regimes of Electron Emission

Escape (dwelling) time from the local field region:  $\tau_d$

Oscillation period:  $T$

Local field-pulse duration:  $\tau_p$

$$v_d = \sqrt{2(\hbar\omega_X - W_f)/m} = 5.4 \times 10^8 \text{ cm/s}$$

Instantaneous regime:  $\tau_d \ll T$   $\tau_d = 180 \frac{\text{as}}{\text{nm}}$ ,  $\hbar\omega_{\text{XUV}} = 95 \text{ eV}$

$$E_{\text{XUV}} = \hbar\omega_X - W_f + e\phi(\mathbf{r}, t_X)$$

In this case the XUV-electron energy is defined solely by the local, instantaneous electrostatic potential

## Novel Regime of Electron Emission from Nanoplasmonic Systems

The time of flight through the region of local fields for ~100 eV XUV electrons is ~300 as and much less than plasmonic near-IR period. Consequently, electrons are electrostatically accelerated by the instantaneous local field electric potential

Escape (dwelling) time of electron from the local field region:  $\tau_d$

Optical oscillation period:  $T$

Local field-pulse duration:  $\tau_p$  XUV photon energy:  $\hbar\omega_X$

Escape velocity:  $v_d = \sqrt{2(\hbar\omega_X - \dot{W}_f)/m} = 5.4 \times 10^8$  cm/s

**Instantaneous regime:**  $\tau_d \ll T$   $\tau_d = 180 \frac{\text{as}}{\text{nm}}$ ,  $\hbar\omega_X = 95$  eV

The XUV photoelectron energy  $E_e$ :

$$E_e = \hbar\omega_X - W_f + e\phi(\mathbf{r}, t_X)$$

In this case the XUV-electron energy is defined solely by the local, instantaneous electrostatic potential

## Uncertainty Principle and Real-Time Measurement of Local Fields

For any practical purposes, from  $E_e = \hbar\omega_X - W_f + e\phi(\mathbf{r}, t_X)$   
it follows that uncertainty of the local potential  $\Delta\phi = \frac{\hbar}{e}\Delta\omega_X$   
where  $\Delta\omega_X$  is the spectral bandwidth of the XUV pulse.

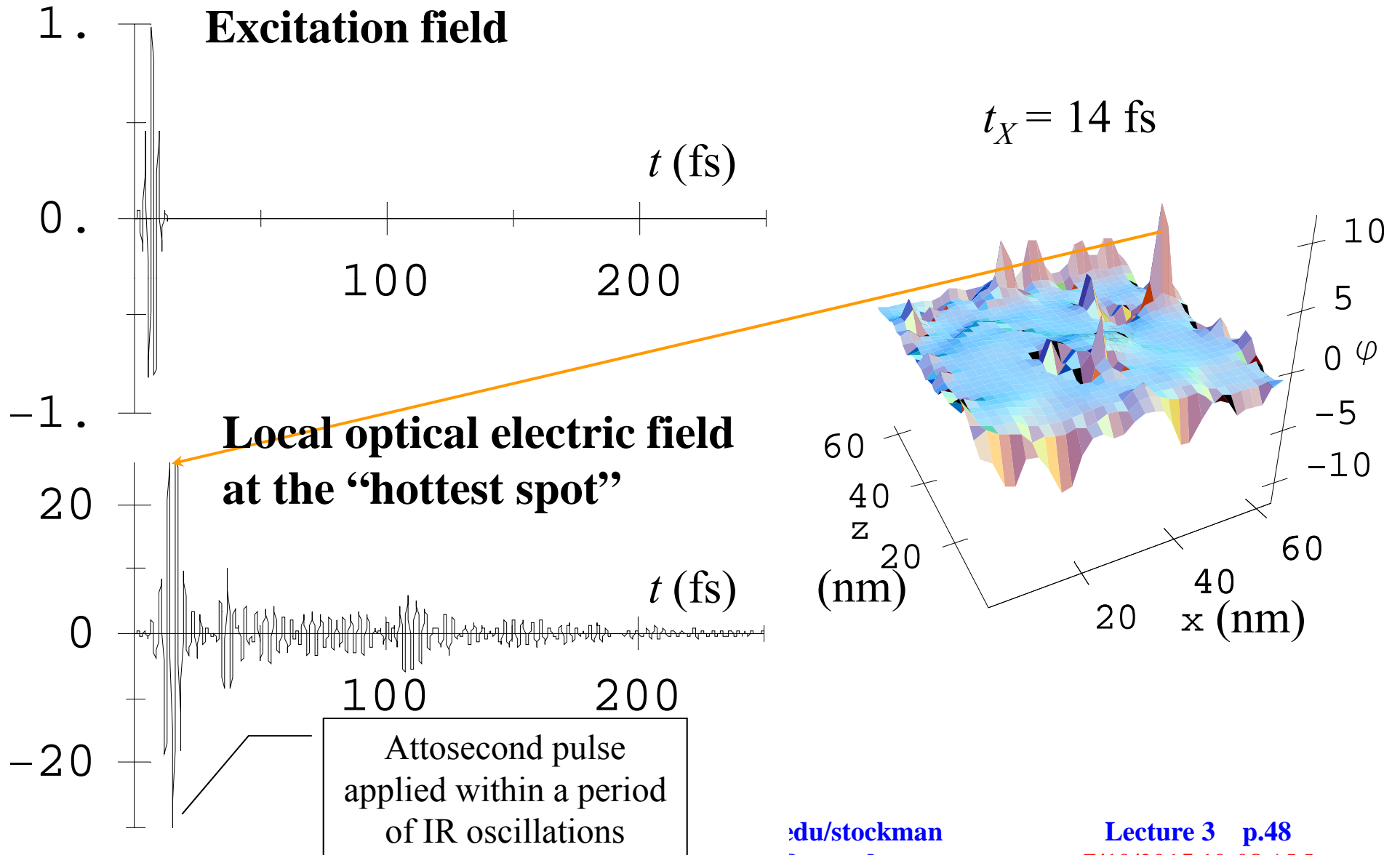
The Heisenberg uncertainty relation is  $\hbar\Delta\omega_X\Delta t_X \geq \frac{\hbar}{2}$

The precision of the instance of measurement is limited by  $\Delta t = \Delta t_X$

Thus, the fundamental limitation on the measurement of  $\phi(\mathbf{r}, t)$  is

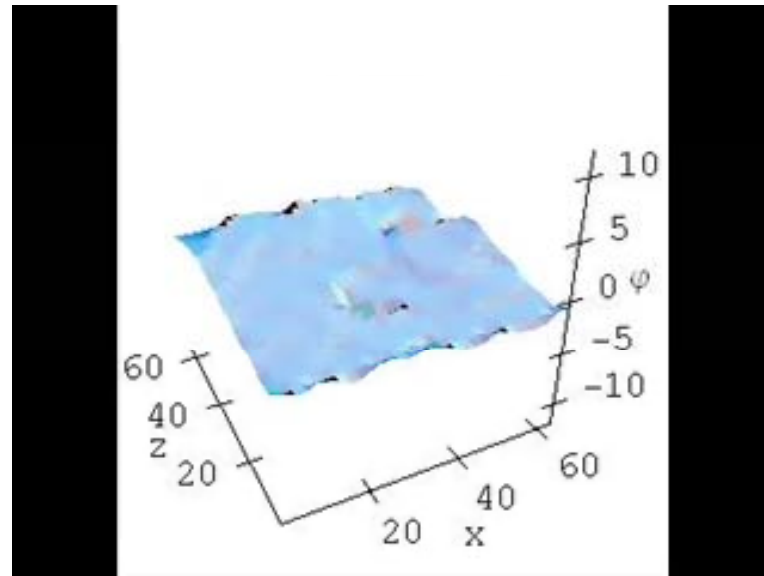
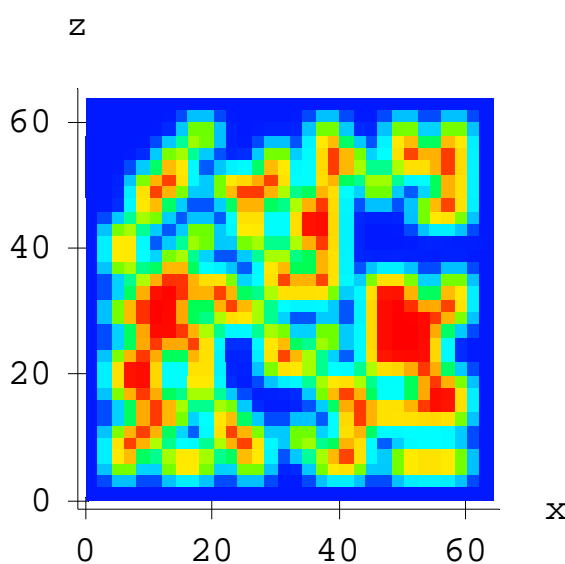
$$\Delta\phi \cdot \Delta t \geq \frac{\hbar}{2e} \quad \text{and} \quad \Delta\phi = \frac{\hbar}{e}\Delta\omega_X$$

**Thus, the instance and the potential cannot be (precisely) measured simultaneously, and the XUV pulse should not be too broadband and too short (though it should have as high energy as possible).**



Energy shift (eV) of electrons emitted by a 95 eV XUV attosecond pulse as a function of the as pulse delay with respect to the infrared-visible excitation pulse (frames are in 200 as) as observed in Photoemission Electron Microscope (PEEM).

**Experiment directly measures instantaneous electric potential of nanoplasmonic oscillations with nm spatial and ~200 as temporal resolution**

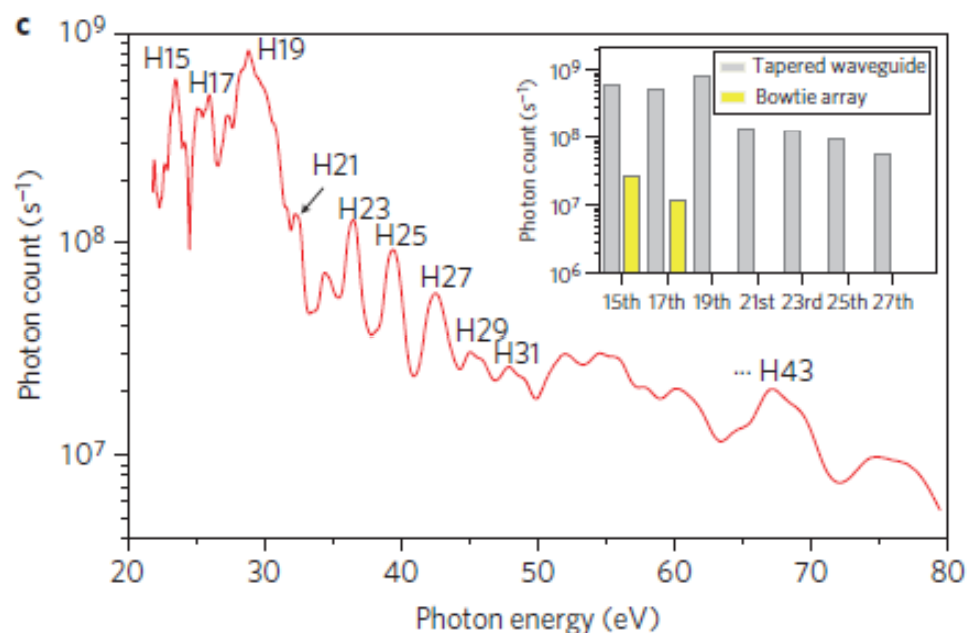
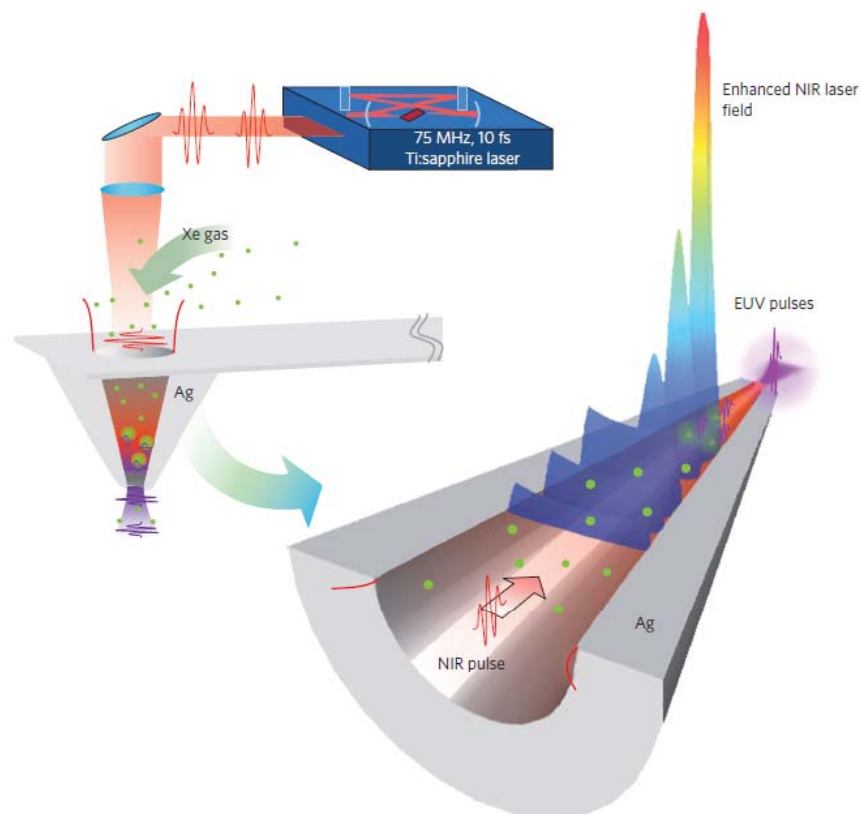


Energy change (eV) of 90 eV XUV photoelectrons from silver nanosystem for 10 GW/cm<sup>2</sup> 800 nm IR power;  $\times 10^{15}$  slowed down

Nanosystem is **60x60 nm** random silver film (50% filling factor)

# Plasmonic generation of ultrashort extreme-ultraviolet light pulses

In-Yong Park<sup>1†</sup>, Seungchul Kim<sup>1†</sup>, Joonhee Choi<sup>1†</sup>, Dong-Hyub Lee<sup>1</sup>, Young-Jin Kim<sup>1</sup>, Matthias F. Kling<sup>2</sup>, Mark I. Stockman<sup>3</sup> and Seung-Woo Kim<sup>1\*</sup>



<sup>1</sup>Ultrafast Optics for Ultraprecision Group, Korea Advanced Institute of Science and Technology (KAIST), Daejeon, 305-701, South Korea, <sup>2</sup>Max Planck Institute of Quantum Optics, Hans-Kopfermann-Str. 1, D-85748 Garching, Germany, <sup>3</sup>Department of Physics and Astronomy, Georgia State University, Atlanta, Georgia 30303, USA; <sup>†</sup>These authors contributed equally to this work as main authors. \*e-mail: swk@kaist.ac.kr



# Dawn of the a new bold era: seminal first paper on laser (originally “optical maser” then laser)

[nature.com](#) | [about npg](#) | [news@nature.com](mailto:news@nature.com) | [naturejobs](#) | [natureevents](#) | [help](#) | [site index](#) |

# nature

[my account](#) | [e-alerts](#) | [subscribe](#) | [register](#)

SEARCH JOURNAL

Go

Thursday 12 September 2013

[Journal Home](#)  
[Current Issue](#)  
[AOP](#)  
[Archive](#)

THIS ARTICLE

[Download PDF](#)  
[References](#)  
[Export citation](#)  
[Export references](#)  
[Send to a friend](#)

More articles like this

[Table of Contents](#)  
[< Previous](#) | [Next >](#)

## letters to nature

*Nature* 187, 493 - 494 (06 August 1960); doi:10.1038/187493a0

## Stimulated Optical Radiation in Ruby

T. H. MAIMAN

Hughes Research Laboratories, A Division of Hughes Aircraft Co., Malibu, California.

Schawlow and Townes<sup>1</sup> have proposed a technique for the generation of very monochromatic radiation in the infra-red optical region of the spectrum using an alkali vapour as the active medium. Javan<sup>2</sup> and Sanders<sup>3</sup> have discussed proposals involving electron-excited gaseous systems. In this laboratory an optical pumping technique has been successfully applied to a fluorescent solid resulting in the attainment of negative temperatures and stimulated optical emission at a wave-length of 6943 Å. ; the active material used was ruby (chromium in corundum).

- Schawlow, A. L. , and Townes, C. H. , *Phys. Rev.*, **112**, 1940 (1958). | [Article](#) | [ISI](#) | [ChemPort](#) |
- Javan, A. , *Phys. Rev. Letters*, **3**, 87 (1959). | [Article](#) | [ISI](#) |
- Sanders, J. H. , *Phys. Rev. Letters*, **3**, 86 (1959). | [Article](#) | [ISI](#) | [ChemPort](#) |
- Maiman, T. H. , *Phys. Rev. Letters*, **4**, 564 (1960). | [Article](#) | [ISI](#) |

# Quantum Nanoplasmonics: Surface Plasmon Amplification by Stimulated Emission of Radiation (SPASER)

1. D. J. Bergman and M. I. Stockman, *Surface Plasmon Amplification by Stimulated Emission of Radiation: Quantum Generation of Coherent Surface Plasmons in Nanosystems*, Phys. Rev. Lett. **90**, 027402-1-4 (2003).
2. M. I. Stockman, *Spasers Explained*, Nat. Phot. **2**, 327-329 (2008) .
3. M. I. Stockman and D. J. Bergman, *Surface Plasmon Amplification by Stimulated Emission of Radiation (SPASER)*, USA Patent No. 7,569,188 (August 4, 2009)
4. M. I. Stockman, *Spaser as Nanoscale Quantum Generator and Ultrafast Amplifier*, Journal of Optics (JOPT) **12**, 024004-1-13 (2010).
5. M. A. Noginov, G. Zhu, A. M. Belgrave, R. Bakker, V. M. Shalaev, E. E. Narimanov, S. Stout, E. Herz, T. Suteewong, and U. Wiesner, *Demonstration of a Spaser-Based Nanolaser*, Nature **460**, 1110-1112 (2009).
6. M. T. Hill, M. Marell, E. S. P. Leong, B. Smalbrugge, Y. Zhu, M. Sun, P. J. van Veldhoven, E. J. Geluk, F. Karouta, Y.-S. Oei, R. Nötzel, C.-Z. Ning, and M. K. Smit, *Lasing in Metal-Insulator-Metal Sub-Wavelength Plasmonic Waveguides*, Opt. Express **17**, 11107-11112 (2009).
7. R. F. Oulton, V. J. Sorger, T. Zentgraf, R.-M. Ma, C. Gladden, L. Dai, G. Bartal, and X. Zhang, *Plasmon Lasers at Deep Subwavelength Scale*, Nature **461**, 629-632 (2009).
8. R.-M. Ma, R. F. Oulton, V. J. Sorger, G. Bartal, and X. Zhang, *Room-Temperature Sub-Diffraction-Limited Plasmon Laser by Total Internal Reflection*, Nat. Mater. **10**, 110-113 (2010). DOI 10.1038/nmat2919
9. R. A. Flynn, C. S. Kim, I. Vurgaftman, M. Kim, J. R. Meyer, A. J. Mäkinen, K. Bussmann, L. Cheng, F. S. Choa, and J. P. Long, *A Room-Temperature Semiconductor Spaser Operating near 1.5 Micron*, Opt. Express **19**, 8954-8961 (2011), and many others

# Spasers explained

nature photonics | VOL 2 | JUNE 2008 |

MARK I. STOCKMAN

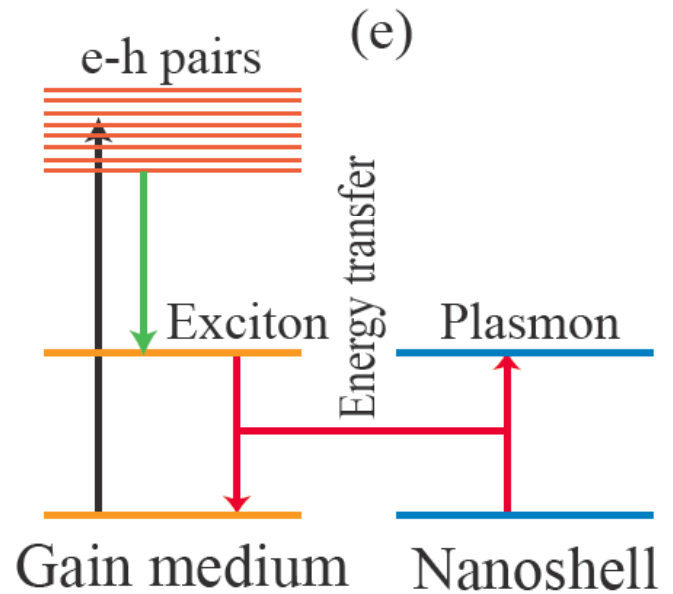
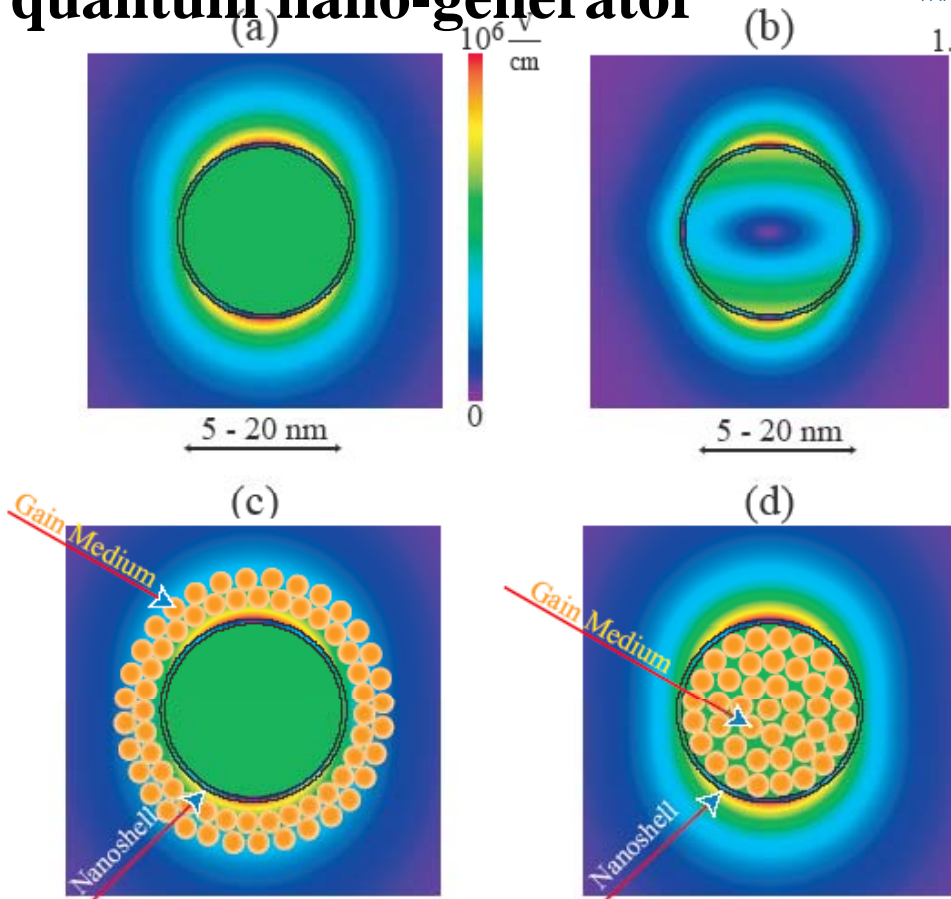
is in the Department of Physics and  
e-mail: mstockman@gsu.edu

The spaser is a proposed  
ring lab  
including

For small nanoparticles,  
radiative loss is  
negligible.

Spaser is fully scalable

## Spaser is the ultimately smallest quantum nano-generator



D. J. Bergman and M. I. Stockman, *Surface Plasmon Amplification by Stimulated Emission of Radiation: Quantum Generation of Coherent Surface Plasmons in Nanosystems*, Phys. Rev. Lett. **90**, 027402-1-4 (2003).

## THEORETICAL APPROACH

Because the characteristic size of a spaser is much smaller than the wavelength, the quasistatic approximation in field equations is valid. Surface plasmon field equations and boundary conditions in a material-independent form, where  $s_n$  are eigenvalues and  $\varphi_n$  are eigenfunctions:

$$\frac{\partial}{\partial \mathbf{r}} \theta(\mathbf{r}) \frac{\partial}{\partial \mathbf{r}} \varphi_n(\mathbf{r}) = s_n \frac{\partial^2}{\partial \mathbf{r}^2} \varphi_n(\mathbf{r}),$$

where  $\theta(\mathbf{r} \in \text{metal}) = 1$  and  $\theta(\mathbf{r} \in \text{elsewhere}) = 0$ ;

$\varphi_n(x, y, 0) = \varphi_n(x, y, L_z) = 0$ , and

$$\frac{\partial}{\partial x} \varphi_n(x, y, z) \Big|_{x=0, L_x} = \frac{\partial}{\partial y} \varphi_n(x, y, z) \Big|_{y=0, L_y} = 0.$$

Spectral parameter:  $s(\omega) = [1 - \epsilon_m(\omega) / \epsilon_d]^{-1}$

Frequency  $\omega_n$  and decay rate  $\gamma_n$  of surface plasmons:

$$\text{Re}[s(\omega_n)] = s_n, \quad \gamma_n = \frac{\text{Im}[s(\omega_n)]}{s'_n}, \quad \text{where } s'_n \equiv \frac{d \text{Re}[s(\omega_n)]}{d\omega_n}$$

Quasielectrostatic Hamiltonian of an inhomogeneous dispersive nanosystem:

$$H = \frac{1}{4\pi} \int_{-\infty}^{\infty} \frac{d[\omega \epsilon(\mathbf{r}, \omega)]}{d\omega} \mathbf{E}(\mathbf{r}, \omega) \mathbf{E}^+(\mathbf{r}, \omega) \frac{d\omega}{2\pi} d^3r$$

where is  $\mathbf{E}(\mathbf{r}, \omega) = -\nabla \phi(\mathbf{r}, \omega)$  the electric field operator.

Quantized potential operator as an expansion over surface plasmons:

$$\hat{\phi}(\mathbf{r}, t) = \sum_n \sqrt{\frac{4\pi\hbar s_n}{\epsilon_d s_n'}} \phi_n(\mathbf{r}) \left[ a_n e^{-i\omega_n t} + a_n^+ e^{i\omega_n t} \right]$$

where  $a_n^+$  and  $a_n$  are the surface plasmon creation and annihilation operators. With this, the Hamiltonian becomes  $H = \sum_n \hbar\omega_n \left( a_n^+ a_n + \frac{1}{2} \right)$

The interaction Hamiltonian of the surface plasmons and two-level systems (quantum dots) of the active medium:

$$H' = \sum_a \mathbf{d}^{(a)} \nabla \hat{\phi}(\mathbf{r}_a, t)$$

Using the perturbation theory, kinetic equation for the population number of surface plasmons in an  $n$ -th mode is:

$$\frac{dN_n}{dt} = (B_n - \gamma_n) N_n + A_n$$

The Einstein stimulated emission coefficient is

$$B_n = \frac{4\pi}{3\hbar} \frac{s_n |\mathbf{d}_{10}|^2 p_n q_n}{\epsilon_h s'_n \gamma_n} > \gamma_n \Rightarrow \boxed{\frac{|\mathbf{d}_{10}|^2 N_{QD} Q}{\hbar R^3 \Gamma} \geq 1}$$

Here  $p_n$  is the spatial overlap factor,  $q_n$  is the spectral overlap factor between the eigenmode intensity and the population inversion,  $\Gamma$  is the spectral width of the gain medium emission,  $Q = \omega_n / \gamma$  is the plasmon quality factor.

$$p_n = \int [\nabla \varphi_n(\mathbf{r})]^2 [\rho_1(\mathbf{r}) - \rho_0(\mathbf{r})] d^3 r, \quad q_n = \int F(\omega) [1 + (\omega - \omega_n)^2 \gamma_n^2] d\omega$$

Spaser gain

$$\alpha_n = \frac{B - \gamma_n}{\gamma_n}$$

shows how many times faster the surface plasmons are born by the stimulated emission than they decay.

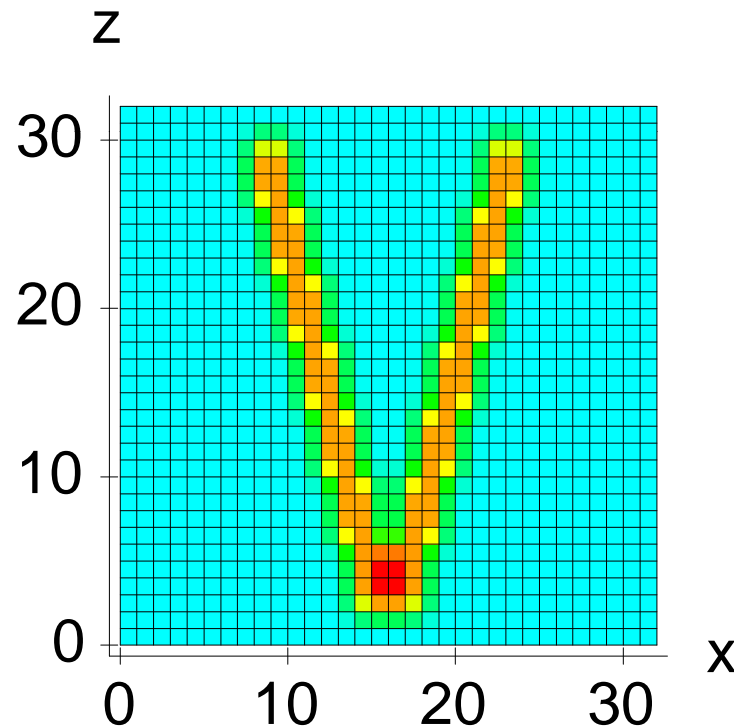
The local RMS field produced by spaser:  $E(\mathbf{r}) = \langle [\nabla \phi(\mathbf{r})]^2 \rangle^{1/2}$   
is calculated as:

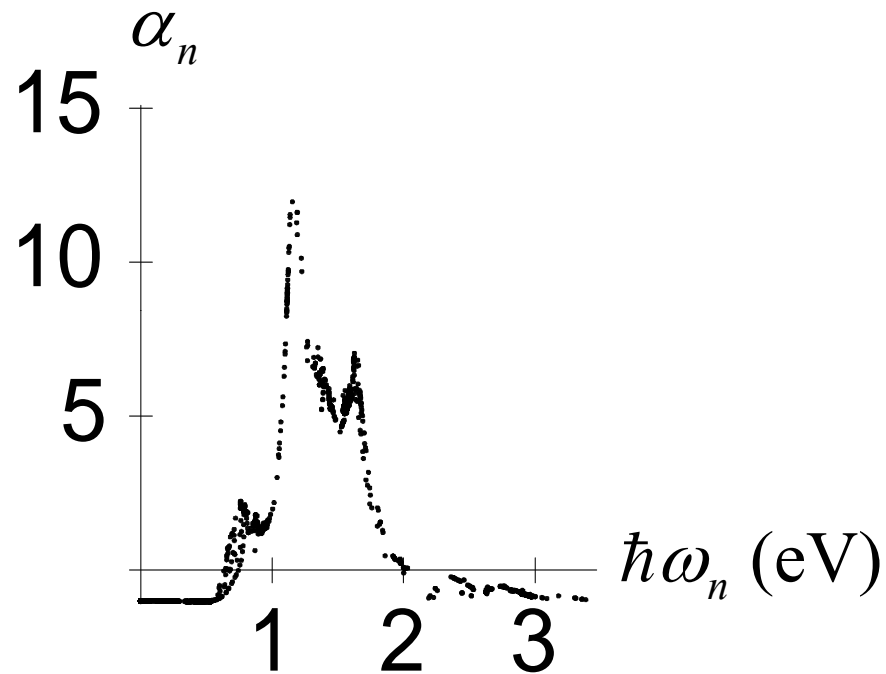
$$E(\mathbf{r}) = E_n(\mathbf{r}) \left( N_n + \frac{1}{2} \right)^{1/2}, \text{ where}$$

$$E_n(\mathbf{r}) = \left\{ \frac{4\pi\hbar s_n}{\epsilon_h s'_n} \langle [\nabla \varphi_n(\mathbf{r})]^2 \rangle \right\}^{1/2}$$

## RESULTS

The resonant nanoparticle is an “engineered” V-shape. The material is silver; the spatial scale is 2-5 nm/grid unit.



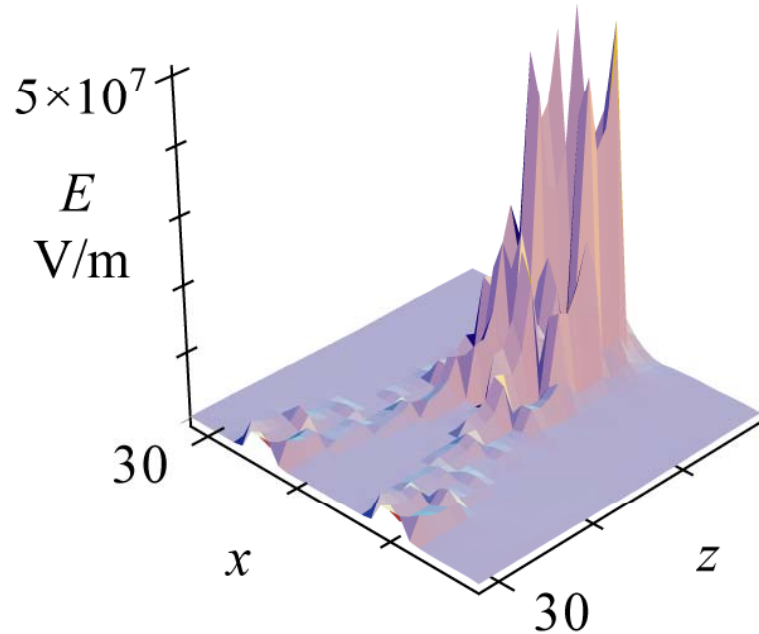


Calculated gain for thin (three monolayers of quantum dots) active medium

## Eigenmodes with highest yields for the spectral maximum at 1.2 eV

$$\hbar\omega = 1.15 \text{ eV}$$

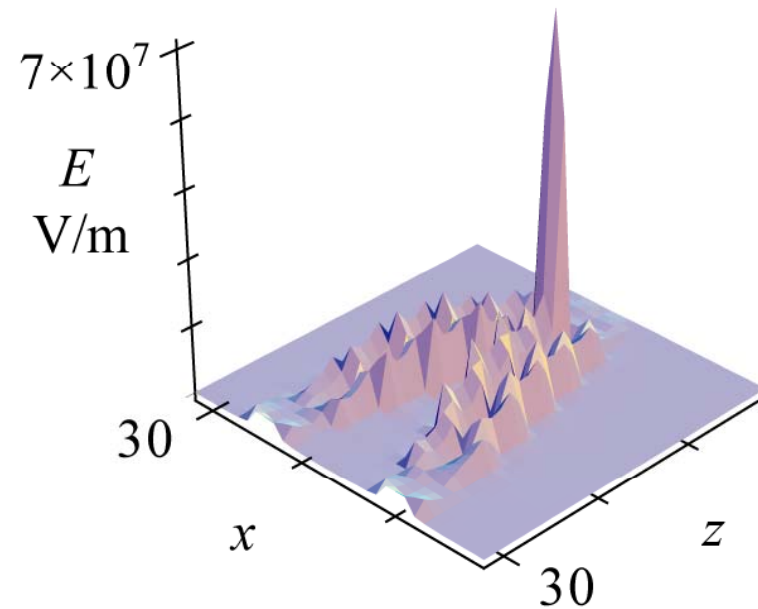
$$\alpha = 12, f = 0.005$$



**Bright mode**

$$\hbar\omega = 1.18 \text{ eV}$$

$$\alpha = 11, f = 10^{-12}$$



**Dark mode**



Quantization of the SP system, valid in the quasistatic regime for times shorter than the SP lifetime  $\tau_n \equiv 1/\gamma_n$ , is carried out by using the following approximate expression for the energy  $H$  of an electric field  $\mathbf{E}(\mathbf{r}, t)$ , which is obtained for a dispersive system by following Ref. [13],

$$H = \frac{1}{4\pi T} \int_{-\infty}^{\infty} \frac{d[\omega \varepsilon(\mathbf{r}, \omega)]}{d\omega} \mathbf{E}(\mathbf{r}, \omega) \mathbf{E}(\mathbf{r}, -\omega) \frac{d\omega}{2\pi} d^3r. \quad (2)$$

The electric field operator<sup>40</sup> of the quantized SPs is<sup>4</sup>

$$\mathbf{E}(\mathbf{r}) = - \sum_n A_n \nabla \varphi_n(\mathbf{r}) (\hat{a}_n + \hat{a}_n^\dagger), \quad A_n = \left( \frac{4\pi \hbar s_n}{\varepsilon_d s'_n} \right)^{1/2}$$

$s(\omega) = \varepsilon_d / [\varepsilon_d - \varepsilon_m(\omega)]$  is Bergman's spectral parameter,  $\varepsilon_d$  is the permittivity of the ambient dielectric, and  $\varepsilon_m(\omega)$  is the metal permittivity.

The spaser Hamiltonian has the form

$$H = H_g + \hbar \sum_n \omega_n \hat{a}_n^\dagger \hat{a}_n - \sum_p \mathbf{E}(\mathbf{r}_p) \mathbf{d}^{(p)},$$

where  $H_g$  is the Hamiltonian of the gain medium,

D. J. Bergman and M. I. Stockman, *Surface Plasmon Amplification by Stimulated Emission of Radiation: Quantum Generation of Coherent Surface Plasmons in Nanosystems*, Phys. Rev. Lett. **90**, 027402-1-4 (2003)

Introducing a rate constant  $\Gamma_{12}$  to describe the polarization relaxation and a difference  $n_{21}^{(p)} = \rho_{22}^{(p)} - \rho_{11}^{(p)}$  as the population inversion on this spasing transition, we derive an equation of motion for the non-diagonal element of the density matrix as

$$\dot{\rho}_{12}^{(p)} = - [i(\omega - \omega_{12}) + \Gamma_{12}] \bar{\rho}_{12}^{(p)} + i n_{21}^{(p)} \Omega_{12}^{(a)*}, \quad (4)$$

where  $\Omega_{12}^{(p)} = -A_n \mathbf{d}_{12}^{(p)} \nabla \varphi_n(\mathbf{r}_p) a_{0n} / \hbar$  is the Rabi frequency for the spasing transition in a  $p$ th chromophore, and  $\mathbf{d}_{12}^{(p)}$  is the corresponding transitional dipole element.

$$\dot{\bar{n}}_{21}^{(p)} = -4\text{Im} [\bar{\rho}_{12}^{(p)} \Omega_{21}^{(p)}] - \gamma_2 (1 + n_{21}^{(p)}) + g (1 - n_{21}^{(p)})$$

$$\dot{a}_{0n} = [i(\omega - \omega_n) - \gamma_n] a_{0n} + i \sum_p \rho_{12}^{(p)*} \Omega^{(p)12}$$

As in Schawlow-Towns theory of laser-line width, this spontaneous emission of SPs leads to the diffusion of the phase of the spasing state. This defines width  $\gamma_s$  of the spasing line as

$$\gamma_s = \frac{\sum_p (1 + n_{21}^{(p)}) \gamma_2^{(p)}}{2(2N_p + 1)}. \quad (8)$$

## Theory of Spaser in Stationary Regime

Physically, the spaser action is a result of spontaneous symmetry breaking when the phase of the coherent SP field is established from the spontaneous noise. Mathematically, the spaser is described by homogeneous differential Eqs. (4)-(6) derived and solved in Sec. IIB. These equations become homogeneous algebraic equations for the stationary (CW) case. These equations always have a trivial, zero solution. However, when their determinant vanishes, they also possess a nontrivial solution describing spasing, whose condition is

$$(\omega_s - \omega_n + i\gamma_n)^{-1} \times (\omega_s - \omega_{21} + i\Gamma_{12})^{-1} \sum_p \left| \tilde{\Omega}_{12}^{(p)} \right|^2 n_{21}^{(p)} = -1, \quad (9)$$

where  $\omega_s$  is the spasing frequency,  $\tilde{\Omega}_{12}^{(p)} = -A_n \mathbf{d}_{12}^{(p)} \nabla \varphi_n(\mathbf{r}_p) / \hbar$  is the single-plasmon Rabi frequency,  $\mathbf{d}_{12}^{(p)}$  is the transition dipole moment of a  $p$ th chromophore,  $\varphi_n(\mathbf{r}_p)$  is the electric potential of the spasing mode at the position this chromophore,  $\gamma_n$

$$n_{21}^{(p)} = (g - \gamma_2) \times \left\{ g + \gamma_2 + 4 \left| \tilde{\Omega}_{12}^{(p)} \right|^2 / \left[ (\omega_s - \omega_{21})^2 + \Gamma_{12}^2 \right] \right\}^{-1}, \quad (10)$$

From the imaginary part of Eq. (10) we immediately find the spasing frequency

$$\omega_s = (\gamma_n \omega_{21} + \Gamma_{12} \omega_n) / (\gamma_n + \Gamma_{12}), \quad (11)$$

which generally does not coincide with either the gain transition frequency  $\omega_{21}$  or the SP frequency  $\omega_n$ , but is between them (this is a frequency walk-off phenomenon similar to that of laser physics). Substituting Eq. (11) back to Eqs. (10)-(11), we obtain a system of equations

$$\frac{(\gamma_n + \Gamma_{12})^2}{\gamma_n \Gamma_{12} \left[ (\omega_{21} - \omega_n)^2 + (\Gamma_{12} + \gamma_n)^2 \right]} \times \sum_p \left| \tilde{\Omega}_{12}^{(p)} \right|^2 n_{21}^{(p)} = 1, \quad (12)$$

$$n_{21}^{(p)} = (g - \gamma_2) \times \left[ g + \gamma_2 + \frac{4N_n \left| \tilde{\Omega}_{12}^{(p)} \right|^2 (\Gamma_{12} + \gamma_n)}{(\omega_{12} - \omega_n)^2 + (\Gamma_{12} + \gamma_n)^2} \right]^{-1}. \quad (13)$$

This system defines the stationary (CW) number of SPs per spasing mode  $N_n$ .

## SPASER Threshold Condition [Consistent with PRL 90, 027402-1-4 (2003)]:

Since  $n_{21}^{(p)} \leq 1$ , from Eqs. (12), (13) we immediately obtain a necessary condition of the existence of spasing,

$$\frac{(\gamma_n + \Gamma_{12})^2}{\gamma_n \Gamma_{12} \left[ (\omega_{21} - \omega_n)^2 + (\Gamma_{12} + \gamma_n)^2 \right]} \sum_p \left| \tilde{\Omega}_{12}^{(p)} \right|^2 \geq 1. \quad (14)$$

[arXiv:0908.3559](https://arxiv.org/abs/0908.3559)  
 Journal of Optics,  
 024004-1-13 (2010).

This expression is fully consistent with [4]. The following order of magnitude estimate of this spasing condition has a transparent physical meaning and is of heuristic value:

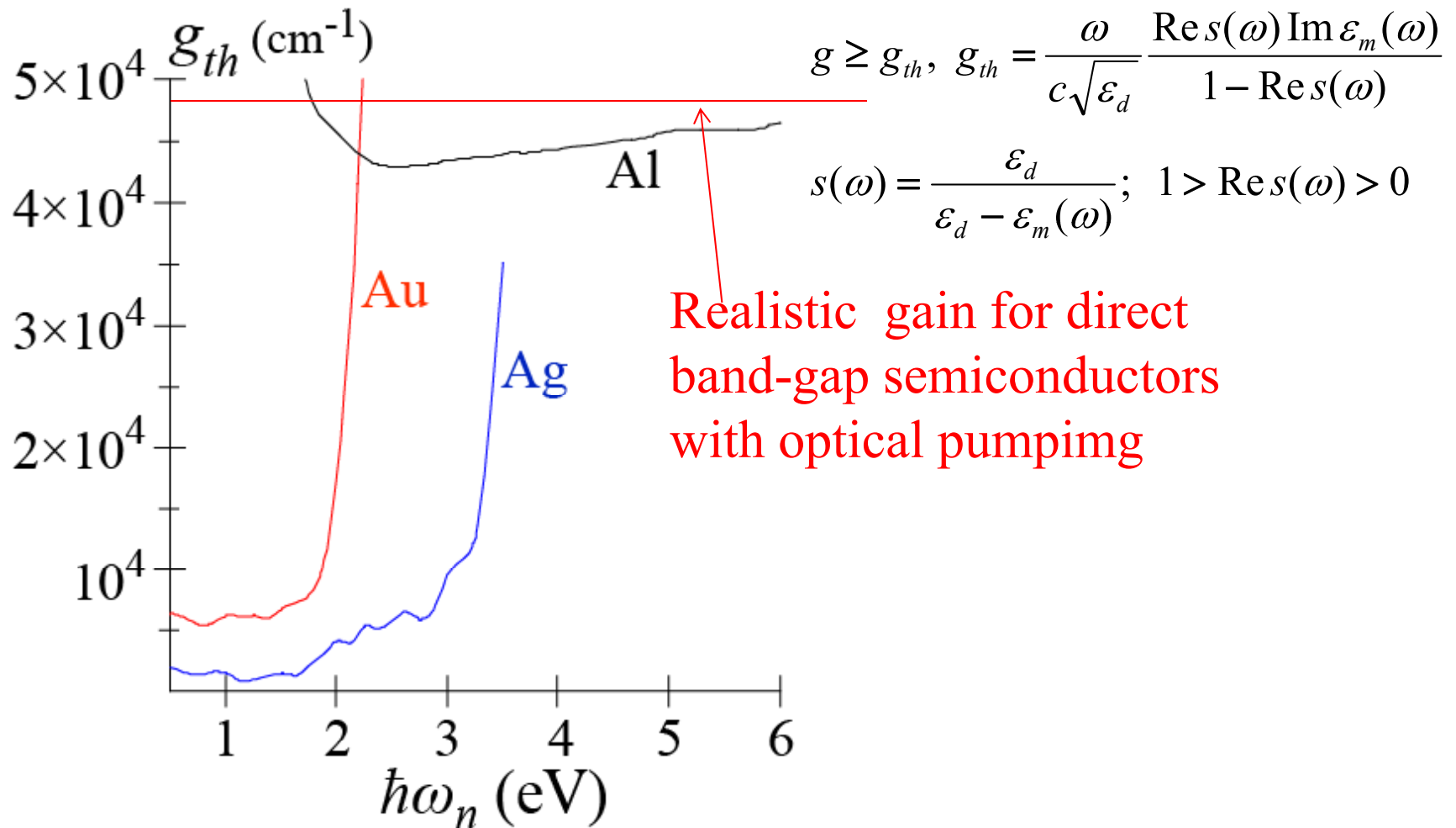
$$\boxed{\frac{d_{12}^2 Q N_c}{\hbar \Gamma_{12} V_n} \gtrsim 1,} \quad (15)$$

where  $Q = \omega/\gamma_n$  is the quality factor of SPs,  $V_n$  is the volume of the spasing SP mode, and  $N_c$  is the number of gain medium chromophores within this volume. Deriving this estimate, we have neglected the detuning, i.e., set  $\omega_{21} - \omega_n = 0$ .

The spasing is essentially a quantum effect.

It is non-relativistic: does not depend on  $c$

**Gain of bulk medium required for spasing and for loss compensation by gain:** M. I. Stockman, *Spaser Action, Loss Compensation, and Stability in Plasmonic Systems with Gain*, Phys. Rev. Lett. **106**, 156802-1-4 (2011); Phil. Trans. R. Soc. A **369**, 3510 (2011).



# Stationary (CW) spaser regime

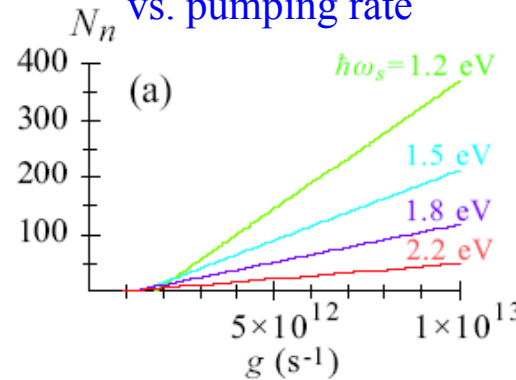
Physics and Astronomy  
University  
Atlanta, GA 30303-3083

This quasilinear dependence  $N_n(g)$  is a result of the very strong feedback in spaser due to the small modal volume

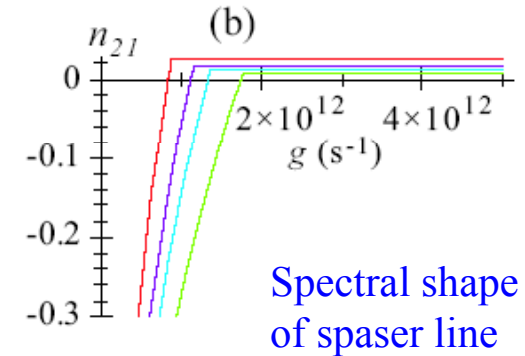
M. I. Stockman, *The Spaser as a Nanoscale Quantum Generator and Ultrafast Amplifier*, *Journal of Optics* **12**, 024004-1-13 (2010)

Spectral line width  $\propto 1/N_{SP}$

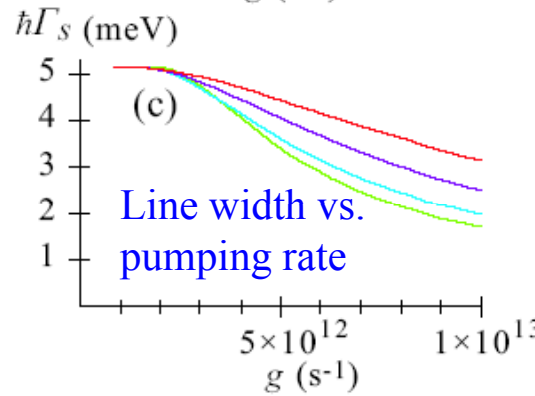
Plasmon number vs. pumping rate



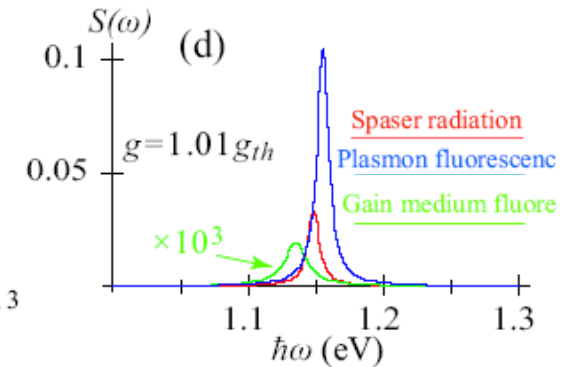
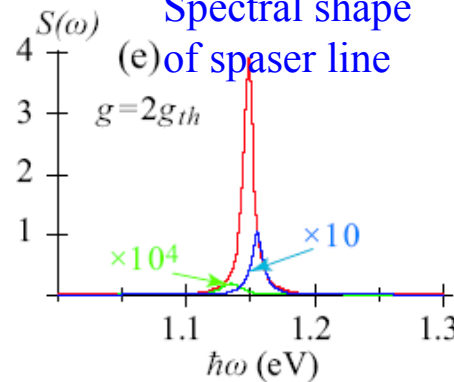
Inversion vs. pumping rate



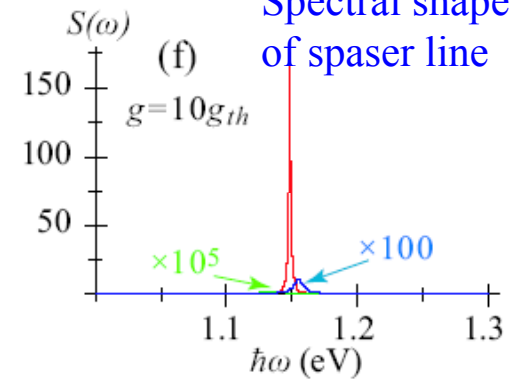
Spectral shape of spaser line



Spectral shape of spaser line



Spectral shape of spaser line



# This invention changed civilization as we know it

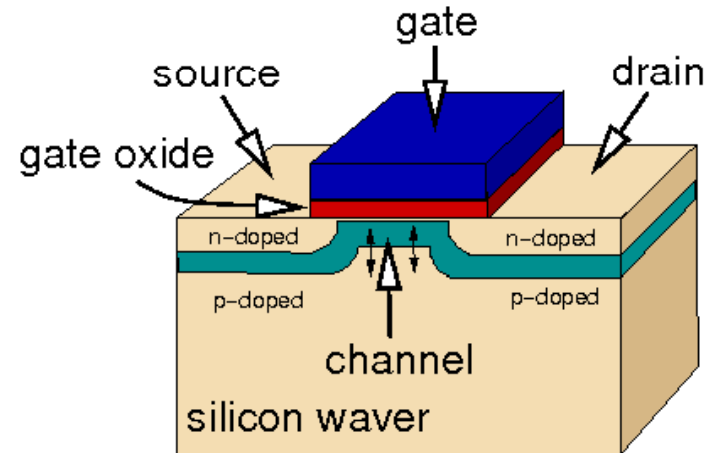
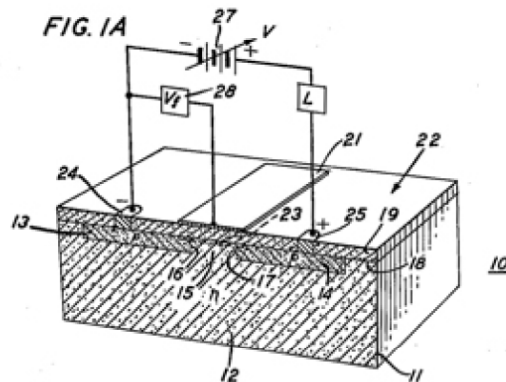
This invention is used in more copies than all others combined

This is the most valuable element of nanotechnology: nanoamplifier, which in c-MOS technology pairs forms a digital nanoamplifier and bistable element for information processing

Aug. 27, 1963      DAWON KAHNG      3,102,230

ELECTRIC FIELD CONTROLLED SEMICONDUCTOR DEVICE

Filed May 31, 1960



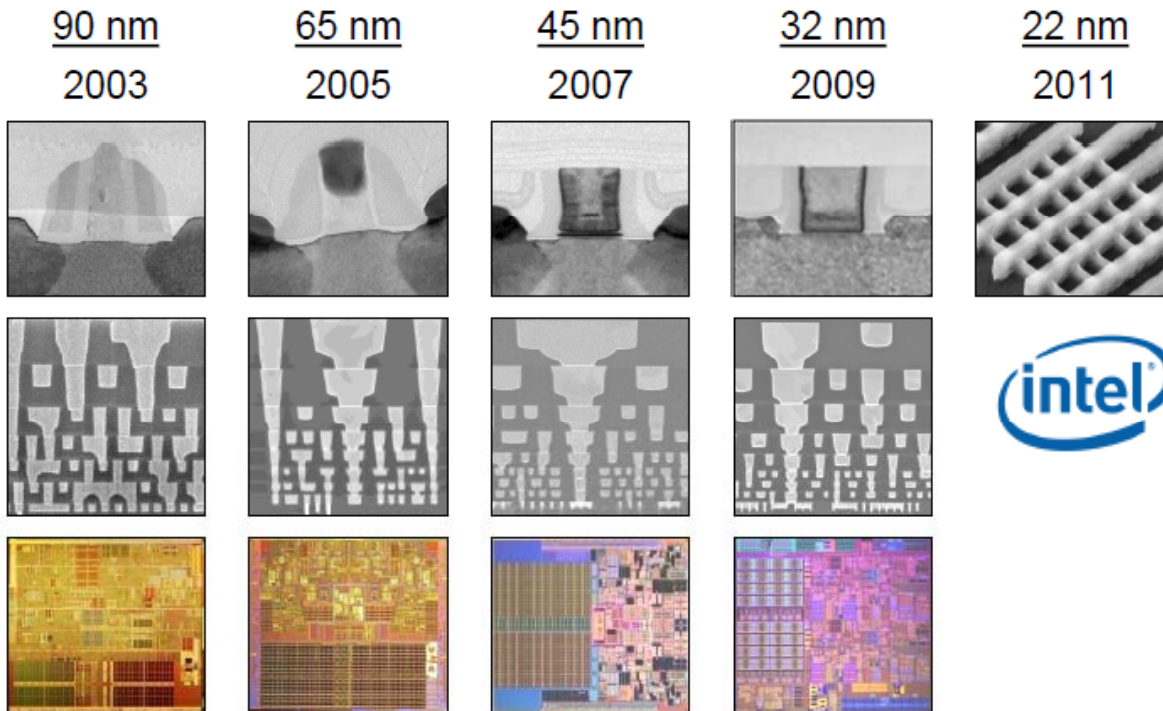
Metal-Oxide Field-Effect Transistor (MOSFET)

Bandwidth ~ 10-100 GHz  
 Low resistance to ionizing radiation

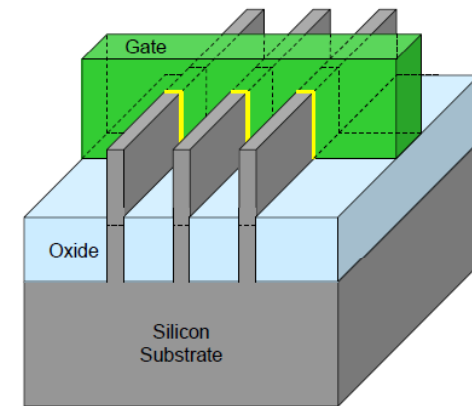
P. Packan et al., in 2009 IEEE International Electron Devices Meeting (IEDM), *High Performance 32nm Logic Technology Featuring Second Generation High-K + Metal Gate Transistors* (Baltimore, MD, 2009), Vol. IEDM09-662, p. 28.4.1-28.4.4

**Abstract:**

A 32nm logic technology for high performance microprocessors is described. 2nd generation high-k + metal gate transistors provide record drive currents at the tightest gate pitch reported for any 32 nm or 28nm logic technology. NMOS drive currents are 1.62mA/um  $I_{dsat}$  and 0.231mA/um  $I_{dlin}$  at 1.0V and 100nA/um  $I_{off}$ . PMOS drive currents are 1.37mA/um  $I_{dsat}$  and 0.240mA/um  $I_{dlin}$  at 1.0V and 100nA/um  $I_{off}$ . The impact of SRAM cell and array size on  $V_{ccmin}$  is reported.



22 nm Tri-Gate Transistor



Tri-Gate transistors can have multiple fins connected together to increase total drive strength for higher performance

## The spaser as a Nanoamplifier

Major problem: any quantum amplifier (laser and spaser) in a CW regime possesses exactly **zero amplification** (it is actually a condition for the CW operation).

We have proposed to set the spaser as a nanoamplifier in two ways:

1. In transient mode (before reaching the CW regime), the spaser still possesses non-zero amplification
2. With a saturable absorber, the spaser can be bistable. There are two stable states: with the zero coherent SP population (“logical zero”) and with a high SP population that saturates the absorber (“logical one” state). Such a spaser will function as a threshold (digital) amplifier

## Scaling of Spaser

Field in spaser:  $E \sim \frac{\hbar\omega}{R^{3/2}} \sqrt{N_p} \sim \left(\frac{R}{10 \text{ nm}}\right)^{-3/2} \sqrt{N_p} \frac{\text{MV}}{\text{cm}}$

Heat per flop:  $H = \hbar\omega N_p$

Threshold:  $g \geq g_{th}$ ,  $g_{th} = \frac{\omega}{c\sqrt{\epsilon_d}} \frac{\text{Re}s(\omega) \text{Im}\epsilon_m(\omega)}{1 - \text{Re}s(\omega)}$ ,  $s(\omega) = \frac{\epsilon_d}{\epsilon_d - \epsilon_m(\omega)}$

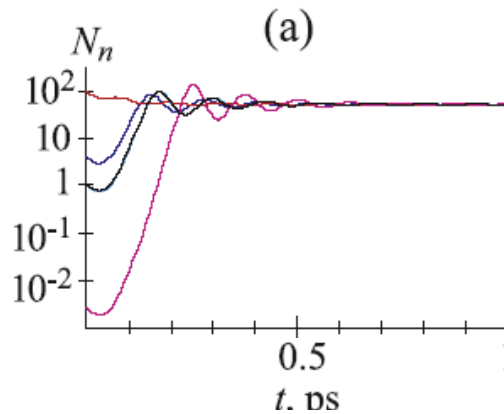
Switching time:  $\tau \sim \left(\frac{10 \text{ nm}}{R}\right)^3 \frac{100}{N_p} \text{ fs}$

Conclusion: Spaser is orders of magnitude more efficient (less heat per flop) and much faster than transistor. It can operate close to the quantum limit.

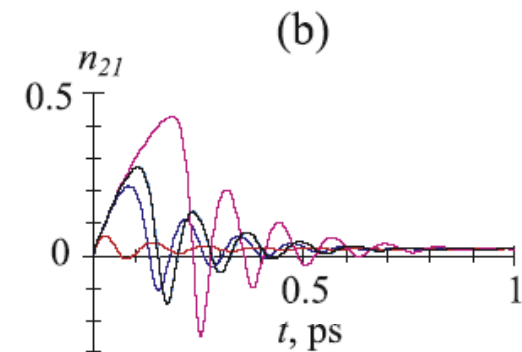
# Amplification in Spaser without a Saturable Absorber

Stationary pumping

SP coherent population

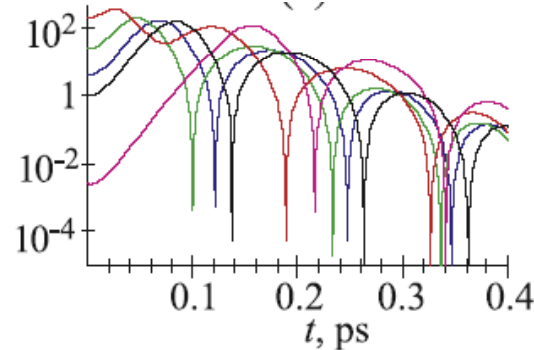


Population inversion

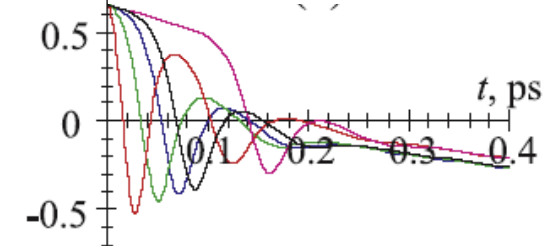


Pulse pumping

SP coherent population



n Population inversion

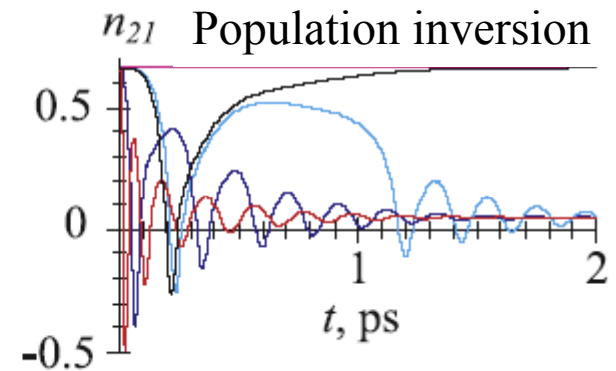
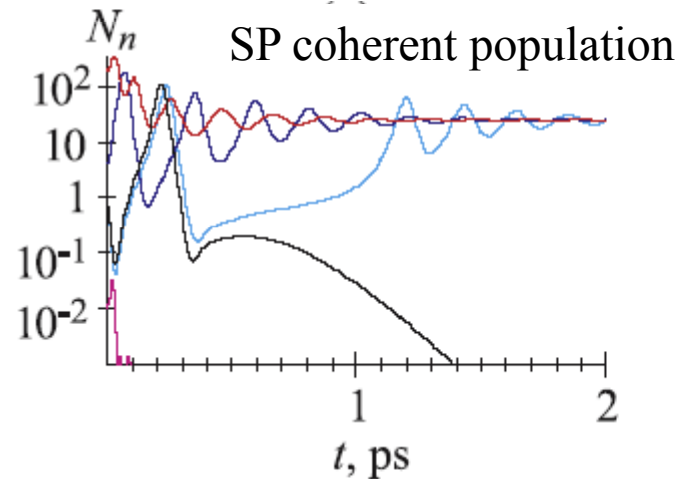


Bandwidth  $\sim 10\text{-}100$  THz

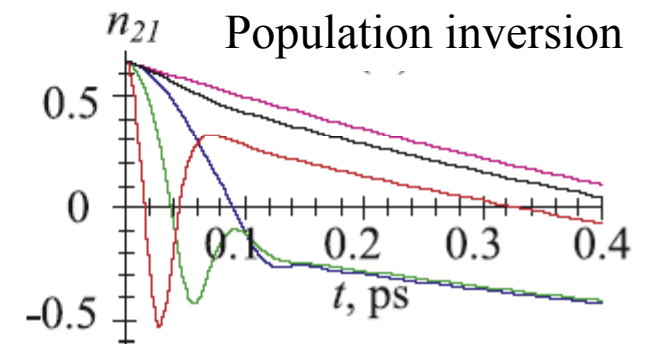
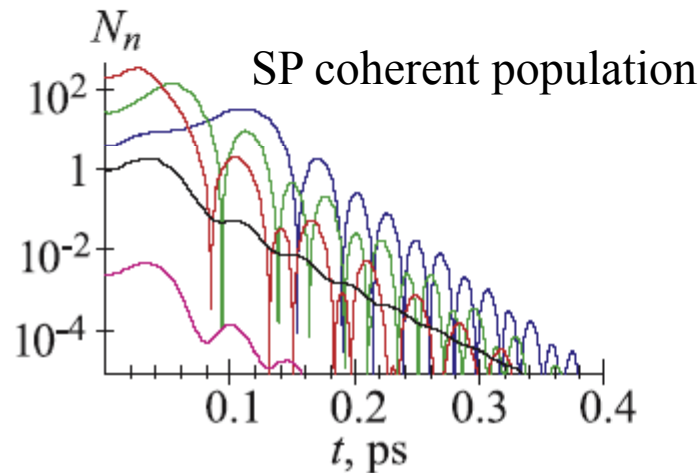
Very high resistance to ionizing radiation

## Amplification in Spaser with a Saturable Absorber (1/3 of the gain chromophores)

Stationary pumping



Pulse pumping



## Demonstration of a spaser-based nanolaser

M. A. Noginov<sup>1</sup>, G. Zhu<sup>1</sup>, A. M. Belgrave<sup>1</sup>, R. Bakker<sup>2</sup>, V. M. Shalaev<sup>2</sup>, E. E. Narimanov<sup>2</sup>, S. Stout<sup>1,3</sup>, E. Herz<sup>3</sup>, T. Suteewong<sup>3</sup> & U. Wiesner<sup>3</sup>

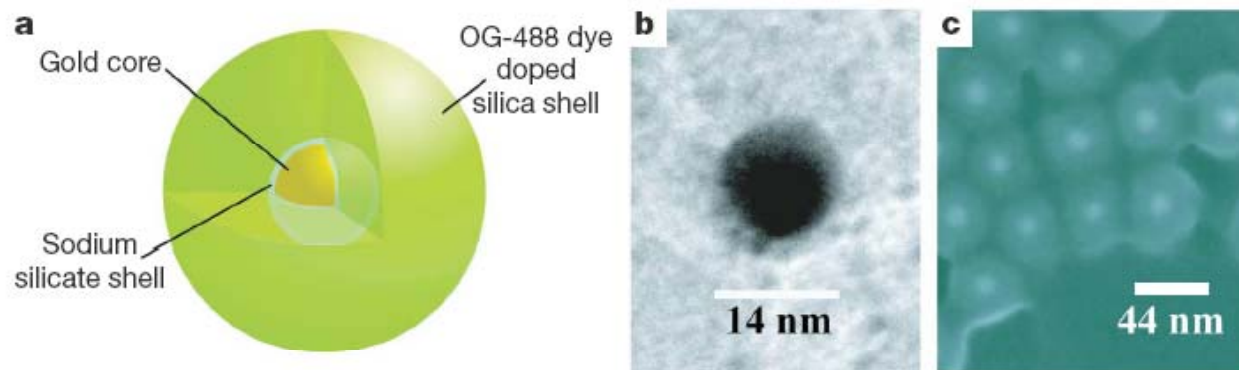


**Figure 1 | Spaser design.** **a**, Diagram of the hybrid nanoparticle architecture (not to scale), indicating dye molecules throughout the silica shell. **b**, Transmission electron microscope image of Au core. **c**, Scanning electron microscope image of Au/silica/dye core-shell nanoparticles. **d**, Spaser mode (in false colour), with  $\lambda = 515$  nm. The white circles represent the 14-nm Au cores. The colour strength colour scheme is shown in the inset.

<sup>1</sup>Center for Materials Research, Norfolk State University, Norfolk, Virginia 23504, USA. <sup>2</sup>School of Electrical & Computer Engineering, Purdue University, West Lafayette, Indiana 47907, USA. <sup>3</sup>Materials Science and Engineering Department, Cornell University, Ithaca, New York 14853, USA.

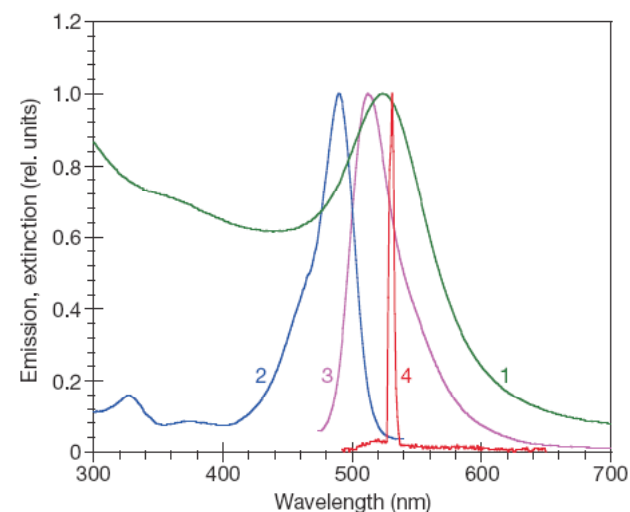


**Figure 2 | Spectroscopic results.** Normalized extinction (1), excitation (2), spontaneous emission (3), and stimulated emission (4) spectra of Au/silica/dye nanoparticles. The peak extinction cross-section of the nanoparticles is  $1.1 \times 10^{-12} \text{ cm}^2$ . The emission and excitation spectra were measured in a spectrofluorometer at low fluence.

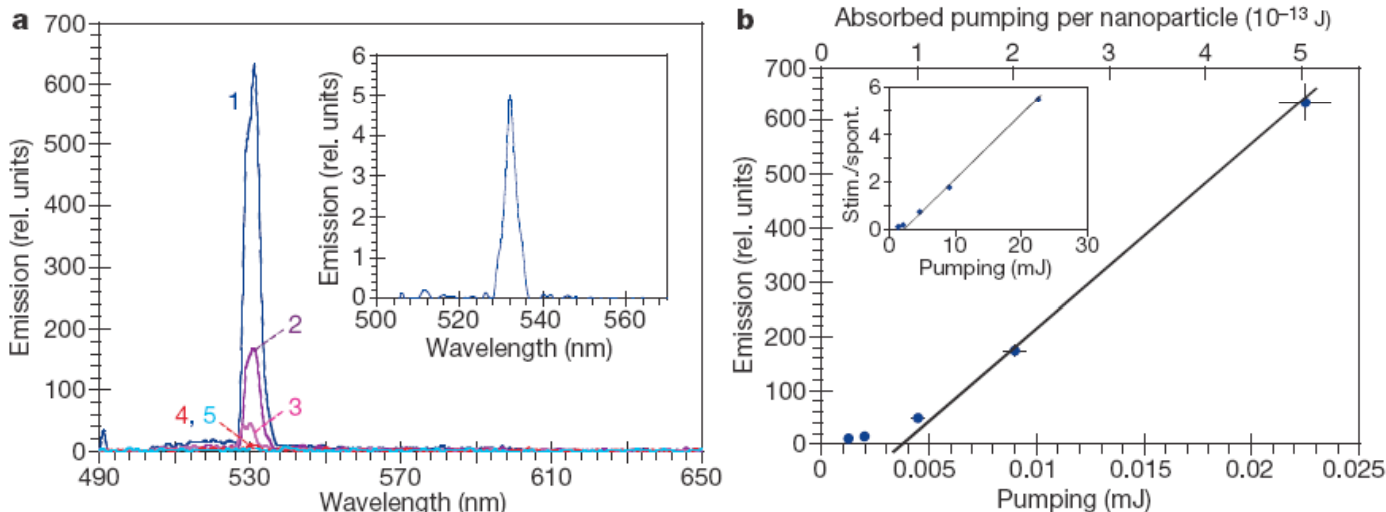


**Figure 4 | Stimulated emission.** **a**, Main panel, stimulated emission spectra of the nanoparticle sample pumped with 22.5 mJ (1), 9 mJ (2), 4.5 mJ (3), 2 mJ (4) and 1.25 mJ (5) 5-ns optical parametric oscillator pulses at  $\lambda = 488 \text{ nm}$ . **b**, Main panel, corresponding input–output curve (lower axis, total launched pumping energy; upper axis, absorbed pumping energy per

by the noise of the photodetector and the instability of the pumping laser) do not exceed the size of the symbol. Inset of **a**, stimulated emission spectrum at more than 100-fold dilution of the sample. Inset of **b**, the ratio of the stimulated emission intensity (integrated between 526 nm and 537 nm) to the spontaneous emission background (integrated at  $< 526 \text{ nm}$  and

# Lasing in metal-insulator-metal sub-wavelength plasmonic waveguides

Martin T. Hill<sup>1\*</sup>, Milan Marell<sup>1</sup>, Eunice S. P. Leong<sup>2</sup>, Barry Smalbrugge<sup>1</sup>, Youcai Zhu<sup>1</sup>, Minghua Sun<sup>2</sup>, Peter J. van Veldhoven<sup>1</sup>, Erik Jan Geluk<sup>1</sup>, Fouad Karouta<sup>1</sup>, Yok-Siang Oei<sup>1</sup>, Richard Nötzel<sup>1</sup>, Cun-Zheng Ning<sup>2</sup>, and Meint K. Smit<sup>1</sup>

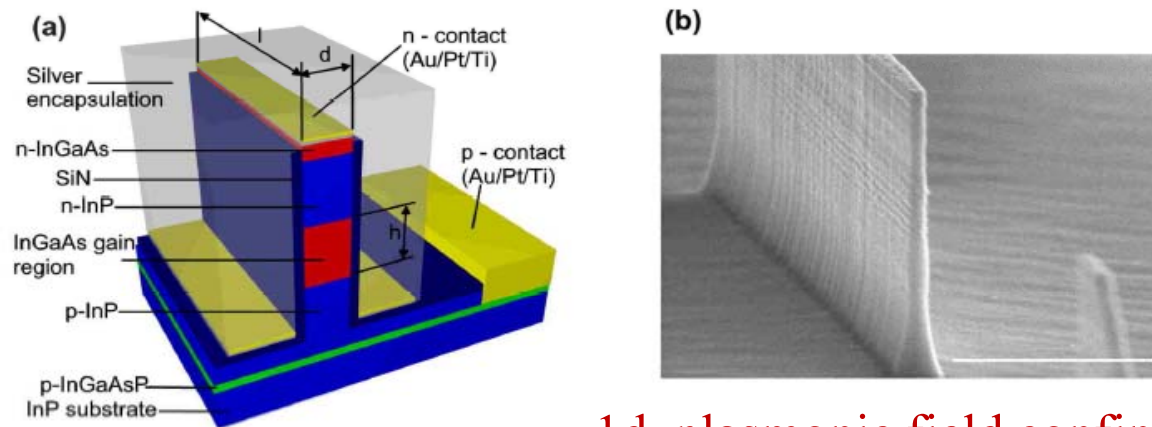
<sup>1</sup>COBRA Research Institute, Technische Universiteit Eindhoven, Postbus 513, 5600 MB Eindhoven, The Netherlands

<sup>2</sup>Department of Electrical Engineering, Arizona State University, Tempe AZ 85287, USA

\*m.t.hill@ieee.org

Received 14 Apr 2009; revised 8 Jun 2009; accepted 9 Jun 2009; published 18 Jun 2009

22 June 2009 / Vol. 17, No. 13 / OPTICS EXPRESS 11107



1d plasmonic field confinement

Fig. 1. Structure of cavity formed by a rectangular semiconductor pillar encapsulated in Silver. (a) Schematic showing the device layer structure. (b) Scanning electron microscope image showing the semiconductor core of one of the devices. The scale bar is 1 micron.

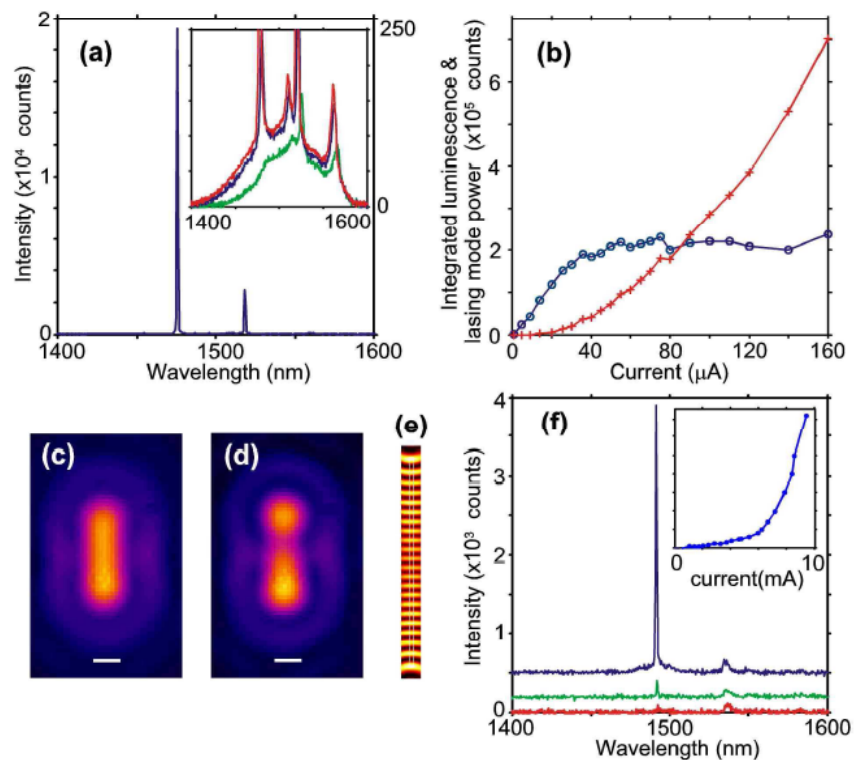
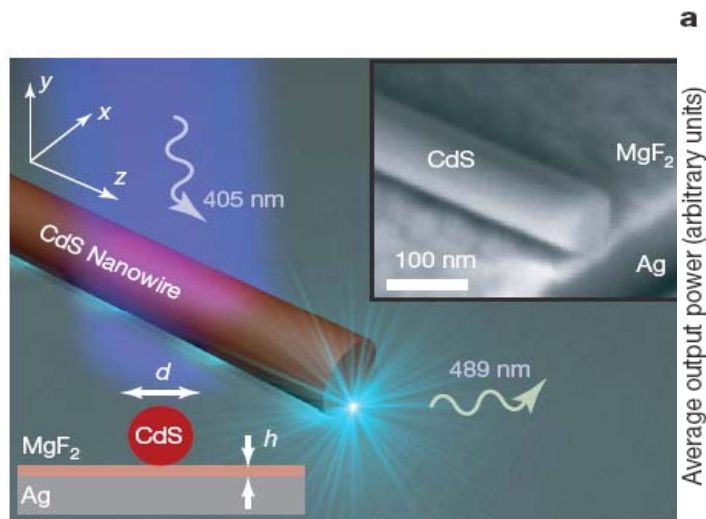


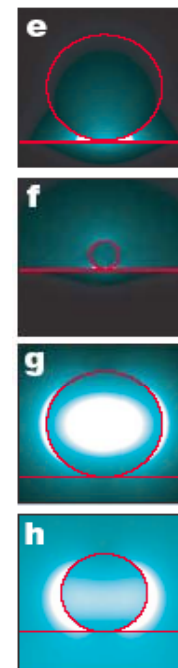
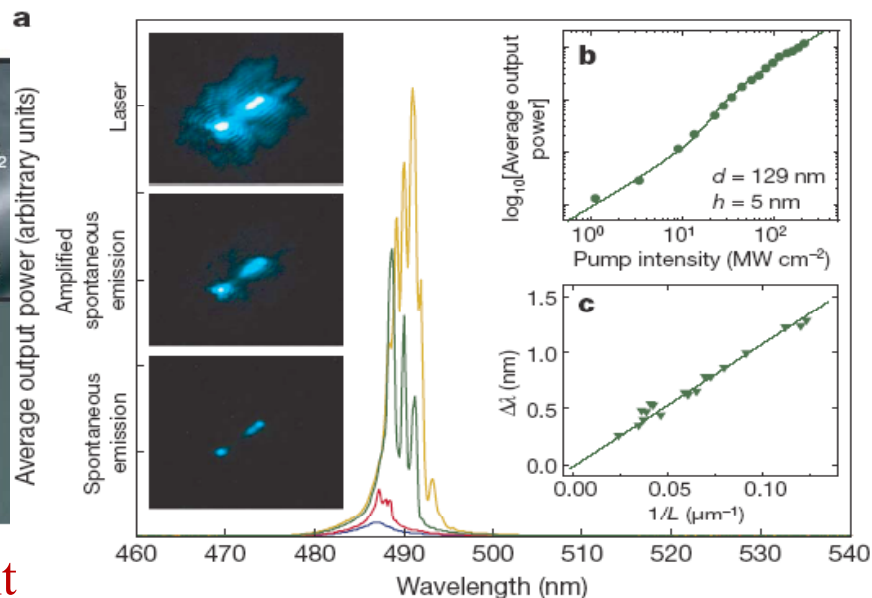
Fig. 2. Spectra and near field patterns showing lasing in devices. (a) Above threshold emission spectrum for 3 micron long device with semiconductor core width  $d \sim 130\text{nm}$  ( $\pm 20\text{nm}$ ), with pump current  $180\ \mu\text{A}$  at  $78\text{K}$ . Inset: emission spectra for  $20$  (green),  $40$  (blue) and  $60$  (red)  $\mu\text{A}$ , all at  $78\text{K}$ . (b) Lasing mode light output (red crosses), integrated luminescence (blue circles), versus pump current for  $78\text{K}$ . (c) Actual near field pattern (in  $x$ - $y$  plane) for  $6$  micron ( $d = 130\text{nm}$ ) device captured with  $100\times$ ,  $0.7$  NA long working distance microscope objective and infrared camera, the scale bar is  $2$  micron, for below threshold  $30\ \mu\text{A}$ , and (d) above threshold  $320\ \mu\text{A}$ . (e) Simulated vertical ( $z$ ) component of the Poynting vector taken at  $0.7$  microns below the pillar base, shows most emitted light at ends of device. (f) Spectra for a  $6$  micron long device with  $d \sim 310\text{nm}$  at  $298\text{K}$ , pulsed operation ( $28$  ns wide pulses,  $1\text{MHz}$  repetition). Spectra for peak currents of  $5.2\text{mA}$  (red),  $5.9\text{mA}$  (green) and  $7.4\text{mA}$  (blue), (currents were estimated from the applied voltage pulse amplitude). The spectra for  $5.9$  and  $7.4$  mA are offset from  $0$  for clarity. Inset shows the total light collected by the spectrometer from the device for currents ranging from  $0$  to  $10\text{mA}$ .

## Plasmon lasers at deep subwavelength scale

Rupert F. Oulton<sup>1\*</sup>, Volker J. Sorger<sup>1\*</sup>, Thomas Zentgraf<sup>1\*</sup>, Ren-Min Ma<sup>3</sup>, Christopher Gladden<sup>1</sup>, Lun Dai<sup>3</sup>, Guy Bartal<sup>1</sup> & Xiang Zhang<sup>1,2</sup>



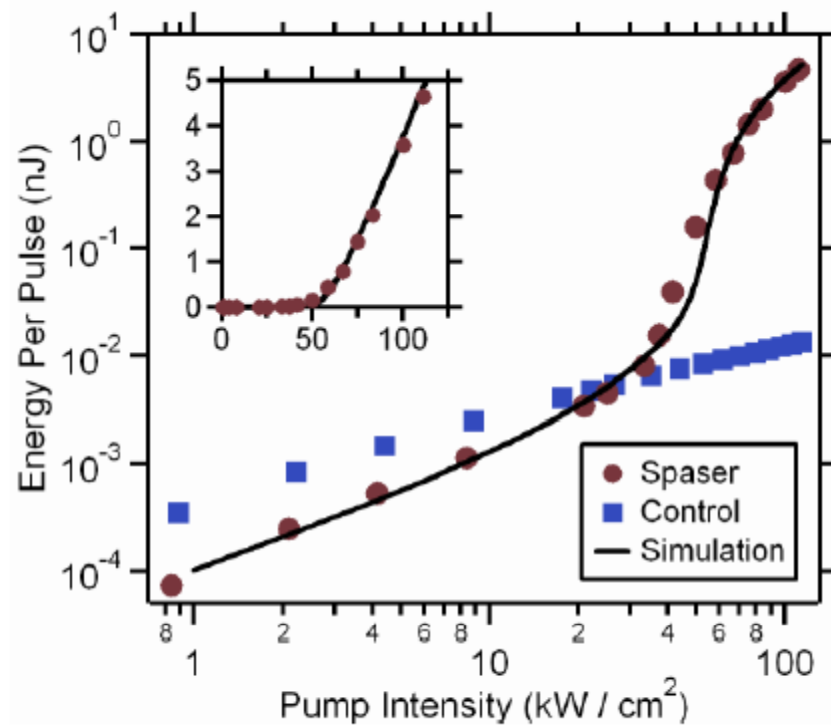
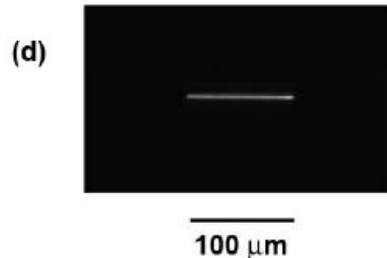
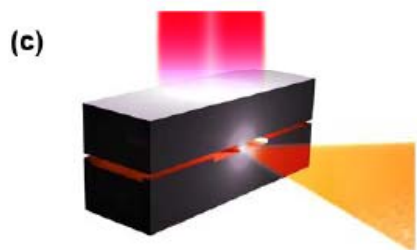
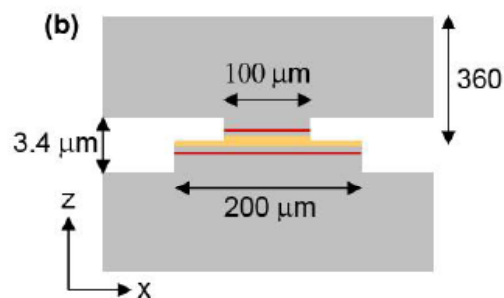
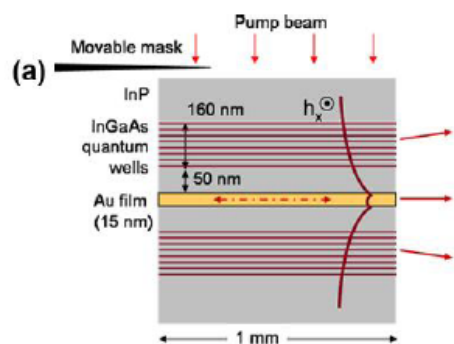
2d plasmonic field confinement



# A room-temperature semiconductor spaser operating near 1.5 $\mu\text{m}$

R. A. Flynn,<sup>1</sup> C. S. Kim,<sup>1</sup> I. Vurgaftman,<sup>1</sup> M. Kim,<sup>1</sup> J. R. Meyer,<sup>1</sup> A. J. Mäkinen,<sup>1</sup>  
 K. Bussmann,<sup>2</sup> L. Cheng,<sup>3</sup> F.-S. Choa,<sup>3</sup> and J. P. Long<sup>4,\*</sup>

25 April 2011 / Vol. 19, No. 9 / OPTICS EXPRESS 8954



# Plasmonic Nanolaser Using Epitaxially Grown Silver Film

Yu-Jung Lu,<sup>1\*</sup> Jisun Kim,<sup>2\*</sup> Hung-Ying Chen,<sup>1</sup> Chihhui Wu,<sup>2</sup> Nima Dabidian,<sup>2</sup> Charlotte E. Sanders,<sup>2</sup> Chun-Yuan Wang,<sup>1</sup> Ming-Yen Lu,<sup>3</sup> Bo-Hong Li,<sup>4</sup> Xianggang Qiu,<sup>4</sup> Wen-Hao Chang,<sup>5</sup> Lih-Juann Chen,<sup>3</sup> Gennady Shvets,<sup>2</sup> Chih-Kang Shih,<sup>2†</sup> Shangjr Gwo<sup>1†</sup>

Having developed epitaxially grown, atomically smooth Ag films as a scalable plasmonic platform, we report a SPASER under CW operation with an ultralow lasing threshold at liquid nitrogen temperature and a mode volume well below the 3D diffraction limit. The device has

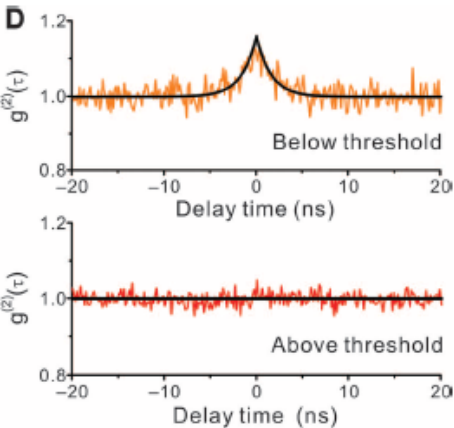
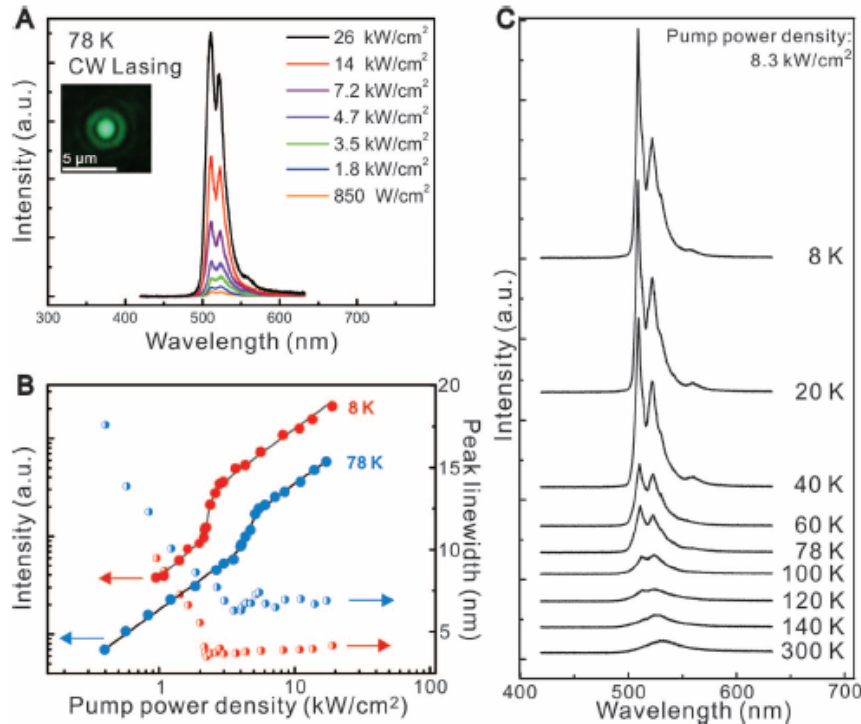
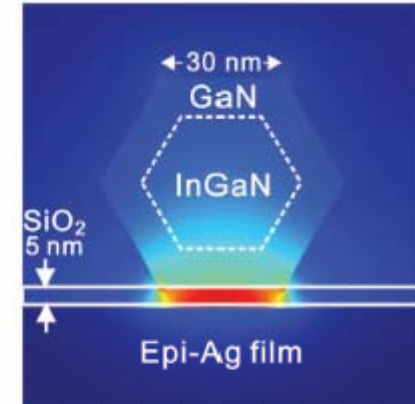
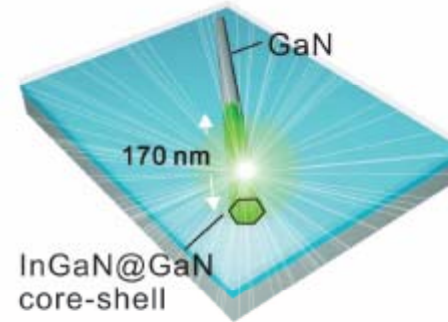
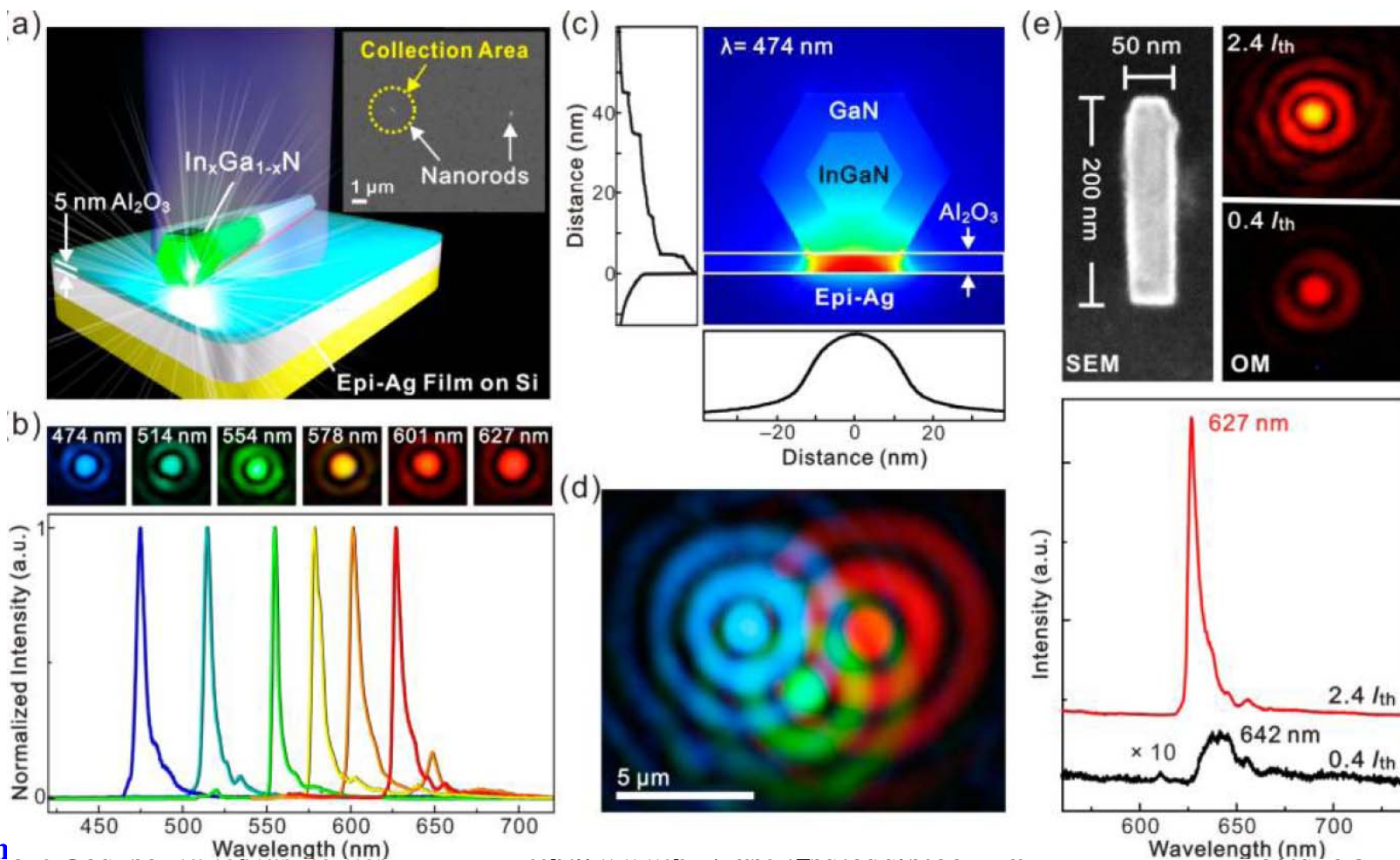


**Fig. 3.** (A) Lasing spectra for pumping by a CW 405-nm semiconductor diode laser. (Inset) The far-field laser spot, with contrast fringes indicative of spatial coherence resulting from lasing. a.u., arbitrary units. (B) Temperature-dependent lasing thresholds of the plasmonic cavity. The  $I$ - $P$  plots at the main lasing peak (510 nm) are shown with the corresponding linewidth-narrowing behavior when the plasmonic laser is measured at 8 K (red) and 78 K (blue), with lasing thresholds of 2.1 and 3.7 kW/cm<sup>2</sup>, respectively. (C) Temperature-dependent lasing behavior from 8 to 300 K. (D) Second-order photon correlation function measurements at 8 K.

Y.-J. Lu *et al.*, Nano Lett. **14**, 4381 (2014)

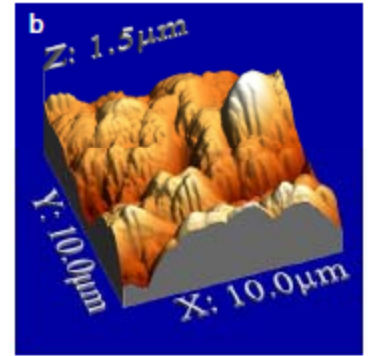
# All-Color Plasmonic Nanolasers with Ultralow Thresholds: Autotuning Mechanism for Single-Mode Lasing

Yu-Jung Lu,<sup>†</sup> Chun-Yuan Wang,<sup>†</sup> Jisun Kim,<sup>‡</sup> Hung-Ying Chen,<sup>†</sup> Ming-Yen Lu,<sup>||</sup> Yen-Chun Chen,<sup>⊥</sup> Wen-Hao Chang,<sup>⊥</sup> Lih-Juann Chen,<sup>||</sup> Mark I. Stockman,<sup>§,¶,||</sup> Chih-Kang Shih,<sup>\*,‡</sup> and Shangjr Gwo<sup>\*,†</sup>

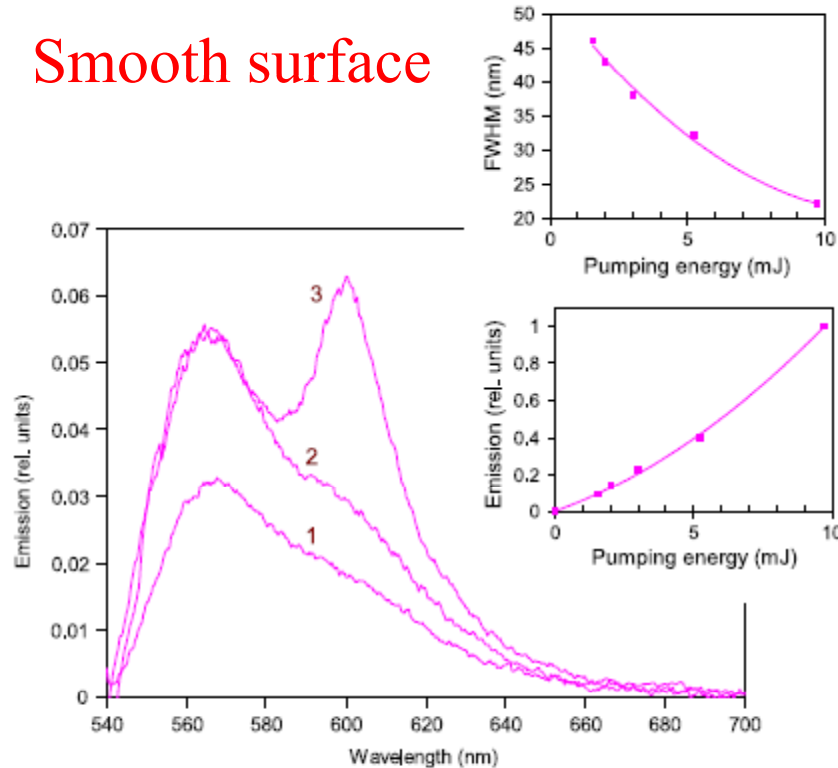


# Stimulated emission of surface plasmon polaritons on smooth and corrugated silver surfaces

J K Kitur, G Zhu, Yu A Barnakov and M A Noginov



Smooth surface



Random Spaser

Rough surface

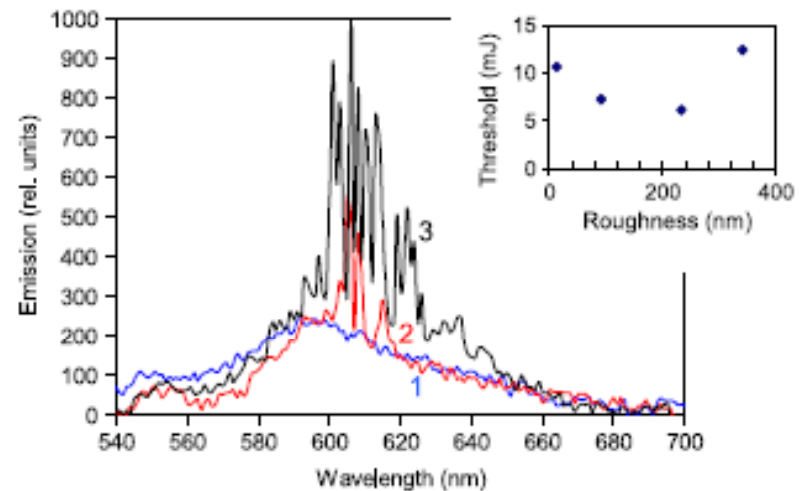


Figure 5. Emission spectra in the RB:PMMA film deposited on a roughened silver with surface roughness equal to 234 nm, pumped with 7 mJ (1), 13 mJ (2) and 20 mJ (3) laser pulses. Inset: stimulated emission threshold as a function of the surface roughness.

# Surface plasmon lasing observed in metal hole arrays

Frerik van Beijnum,<sup>1</sup> Peter J. van Veldhoven,<sup>2</sup> Erik Jan Geluk,<sup>2</sup>  
 Michiel J.A. de Dood,<sup>1</sup> Gert W. 't Hooft,<sup>1,3</sup> and Martin P. van Exter<sup>1</sup>

<sup>1</sup>Leiden University, Huygens Laboratory, P.O. Box 9504, 2300 RA Leiden, The Netherlands

<sup>2</sup>COBRA Research Institute, Technische Universiteit Eindhoven,  
 Postbus 513, 5600 MB Eindhoven, The Netherlands

<sup>3</sup>Philips Research Laboratories, Prof. Holstlaan 4, 5656 AA Eindhoven, Netherlands

Phys. Rev.  
 Lett. **110**,  
 206802-1-5  
 (2013)

See also: W. Zhou, M. Dridi, J. Y. Suh, C. H. Kim, D. T. Co, M. R. Wasielewski, G. C. Schatz, and T. W. Odom, *Lasing Action in Strongly Coupled Plasmonic Nanocavity Arrays*, Nature Nanotechnology **8**, 506-511 (2013)

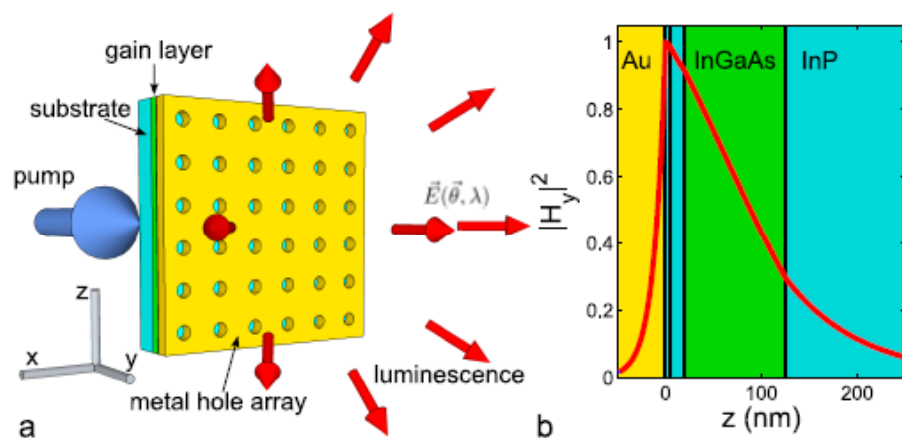
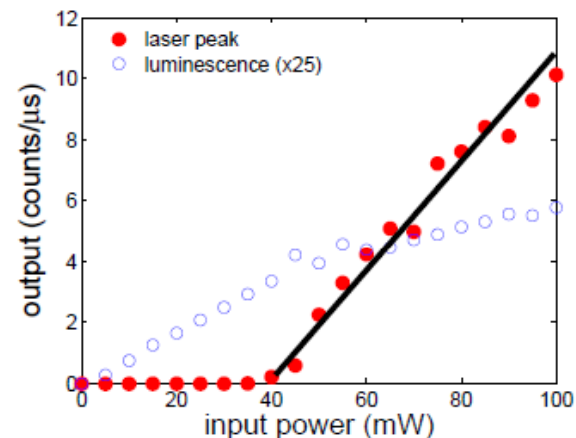
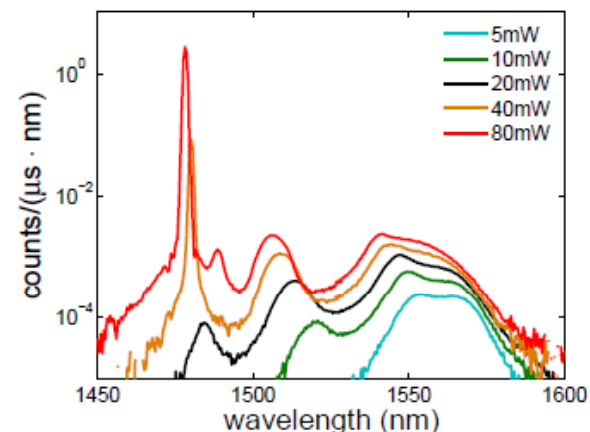
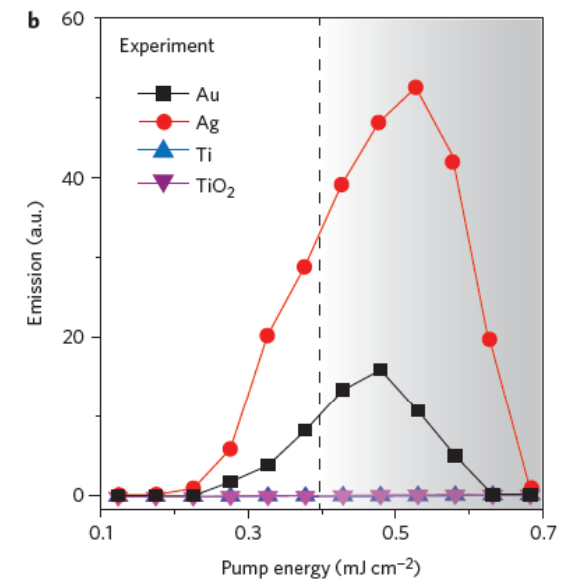
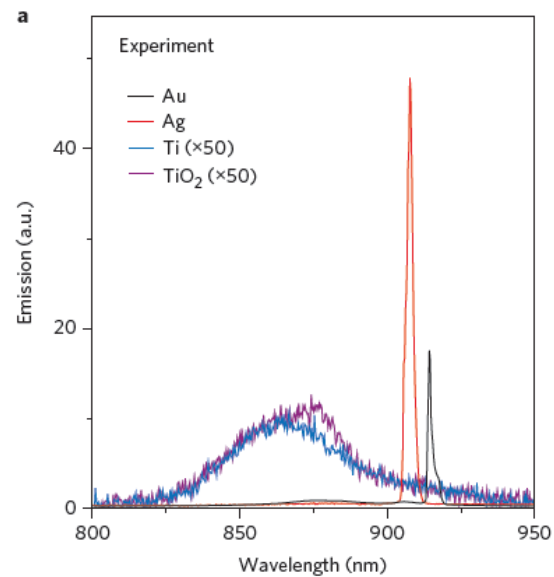
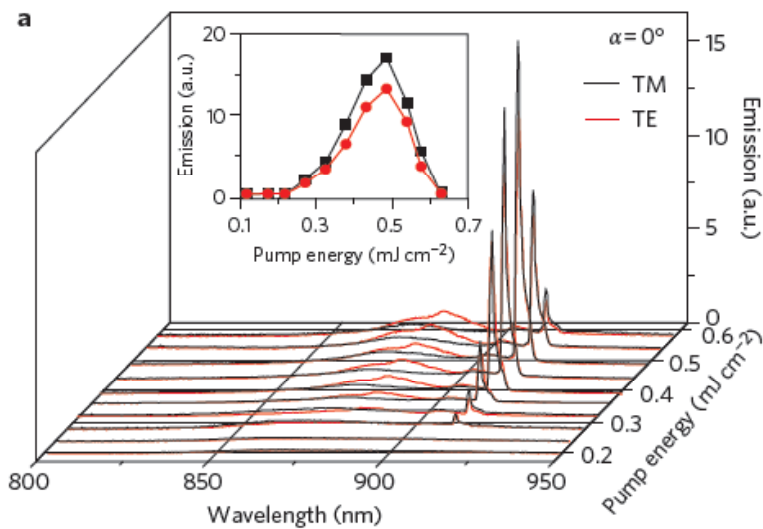
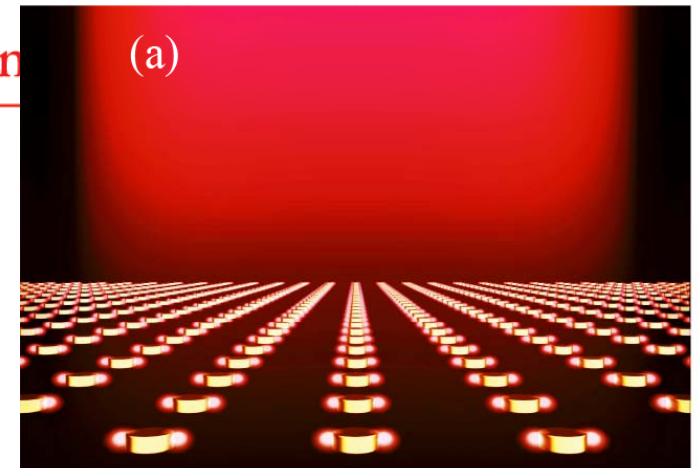


FIG. 2. (a) Luminescence spectra as a function of pump power, plotted on a semilog scale. For increasing pump power the bandwidth of the luminescence increases until the device starts lasing. Above threshold, the emission of the non-lasing resonances starts to saturate at a maximum intensity. 80 mW corresponds to  $\sim 11 \text{ kW/cm}^2$  (b) The output in the lasing peak and in the luminescence in the range of 1485 – 1600 nm. The power in the lasing peak shows a clear threshold (red). The black line is a guide to the eye. The luminescence outside the lasing peak starts to level off, as expected for lasing in semiconductor devices (blue).



# Lasing action in strongly coupled plasmonic nanocavity arrays

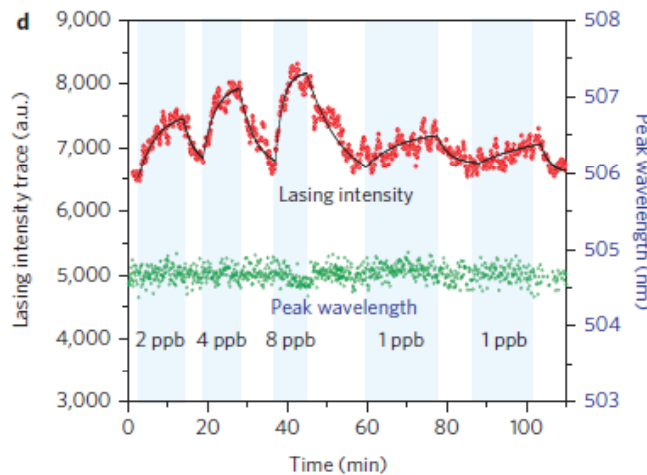
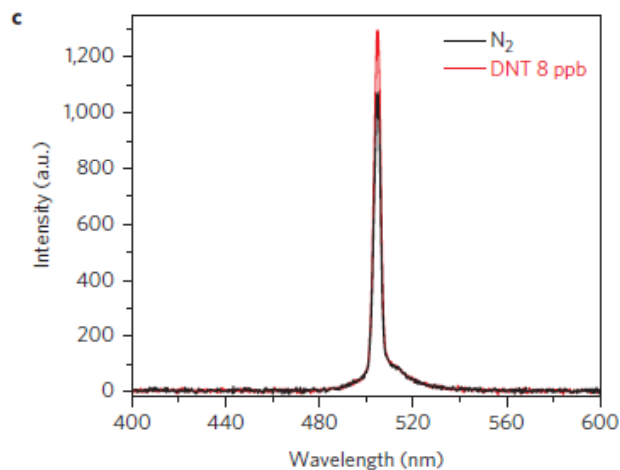
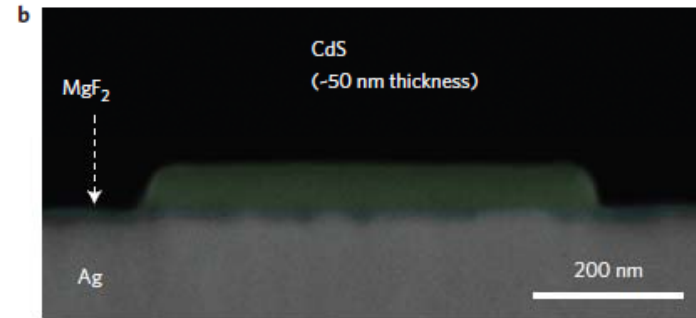
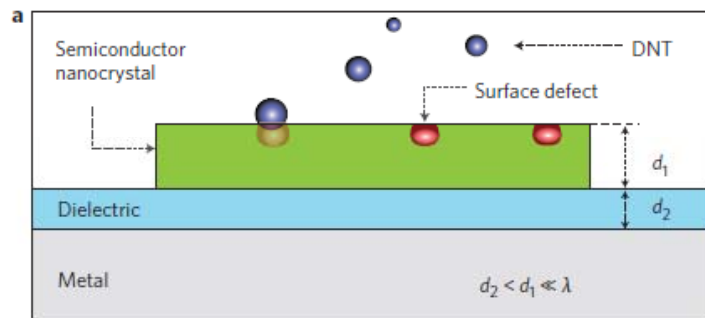
Wei Zhou<sup>1†</sup>, Montacer Dridi<sup>2</sup>, Jae Yong Suh<sup>2</sup>, Chul Hoon Kim<sup>2,3†</sup>, Dick T. Co<sup>2,3</sup>,  
Michael R. Wasielewski<sup>2,3</sup>, George C. Schatz<sup>2</sup> and Teri W. Odom<sup>1,2,3\*</sup>



# Explosives detection in a lasing plasmon nanocavity

Ren-Min Ma<sup>†</sup>, Sadao Ota<sup>†</sup>, Yimin Li<sup>1</sup>, Sui Yang<sup>1</sup> and Xiang Zhang<sup>1,2\*</sup>

<sup>1</sup>NSF Nanoscale Science and Engineering Centre, 3112 Etcheverry Hall, University of California, Berkeley, California 94720, USA, <sup>2</sup>Materials Sciences Division, Lawrence Berkeley National Laboratory, 1 Cyclotron Road, Berkeley, California 94720, USA,



Explosive (DNT) detection

ARTICLE

Received 28 Dec 2013 | Accepted 11 Aug 2014 | Published 23 Sep 2014

DOI: 10.1038/ncomms5953

# A room temperature low-threshold ultraviolet plasmonic nanolaser

Qing Zhang<sup>1</sup>, Guangyuan Li<sup>1</sup>, Xinfeng Liu<sup>1</sup>, Fang Qian<sup>2</sup>, Yat Li<sup>3</sup>, Tze Chien Sum<sup>1,4</sup>, Charles M. Lieber<sup>5</sup> & Qihua Xiong<sup>1,6</sup>

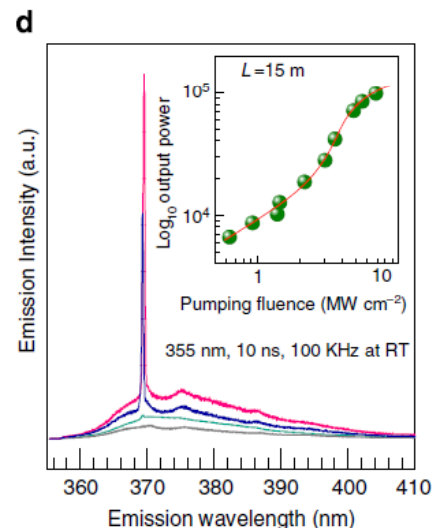
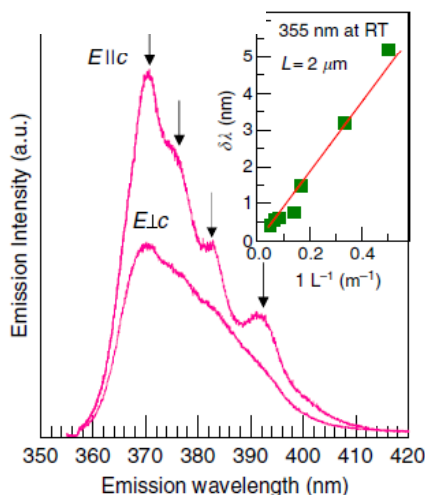
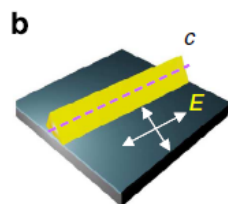
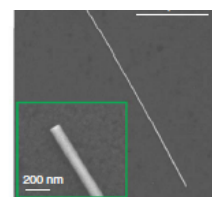
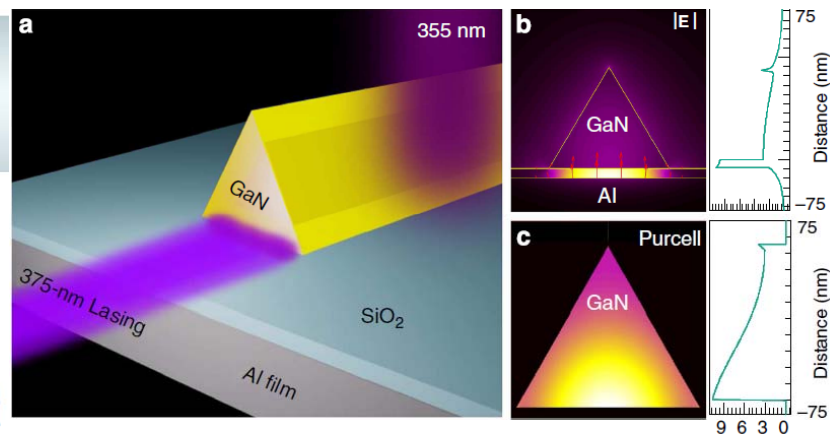


**Figure 2 | Room temperature ultraviolet plasmonic lasing characterization.** (a) Scanning electron microscopy (SEM) image of a GaN nanowire sitting on SiO<sub>2</sub>/Al film. Inset: magnified scanning electron microscopy image of one end of the GaN nanowire. The nanowire length and diameter is 15 μm and 100 nm, respectively. (b) Schematic of optical measurement and polarization detection setup. c is defined as the orientation of nanowire. The incidence excitation laser is circular polarized and the focused laser beam can cover the whole nanowire. The emission scattered out from two ends is collected and the polarization property along and perpendicular to nanowire axis c is analysed. (c) Spontaneous emission of as-fabricated plasmonic device below lasing threshold at room temperature under a power fluence of 0.5 MW cm<sup>-2</sup>. Arrows highlight the Fabry-Pérot peaks. The nanowire length is 2 μm. Inset: cavity mode spacing  $\delta\lambda$  variation with nanowire length  $L$  (green dots).  $\delta\lambda$  versus  $1/L$  can be well fitted with a linear function (red curve), suggesting a high group index  $n_g$  ( $n_g = \lambda^2/2L$ ) of 7.61 due to the high gain requirement of the plasmonic laser device. (d) Power-dependent emission spectra of the plasmonic devices. One sharp peak with a maximum full width at half maximum (FWHM)  $\sim 0.8$  nm appears above the spontaneous emission background. The nanowire length is 15 μm. Inset: integrated emission versus pumping intensity. The S-shaped plot suggests the evolution from a spontaneous emission, amplified spontaneous emission to lasing process.

# Ultrafast plasmonic nanowire lasers near the surface plasmon frequency

Themistoklis P. H. Sidiropoulos<sup>1\*</sup>, Robert Röder<sup>2</sup>, Sebastian Geburt<sup>2</sup>, Ortwin Hess<sup>1</sup>, Stefan A. Maier<sup>1</sup>, Carsten Ronning<sup>2</sup> and Rupert F. Oulton<sup>1\*</sup>

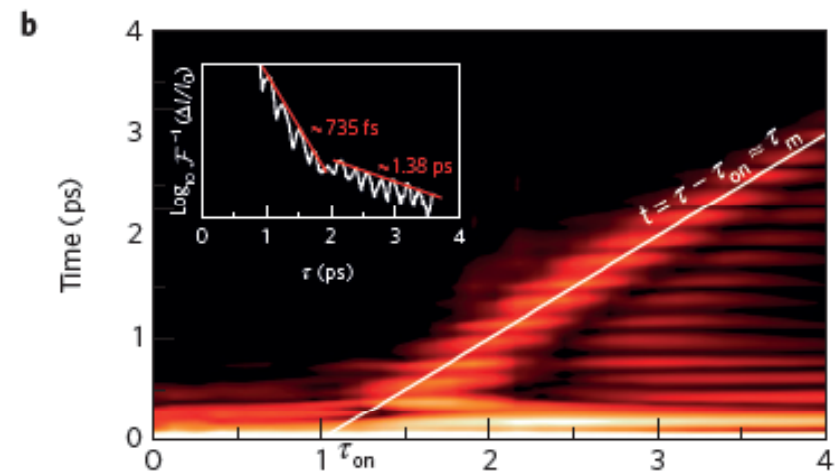
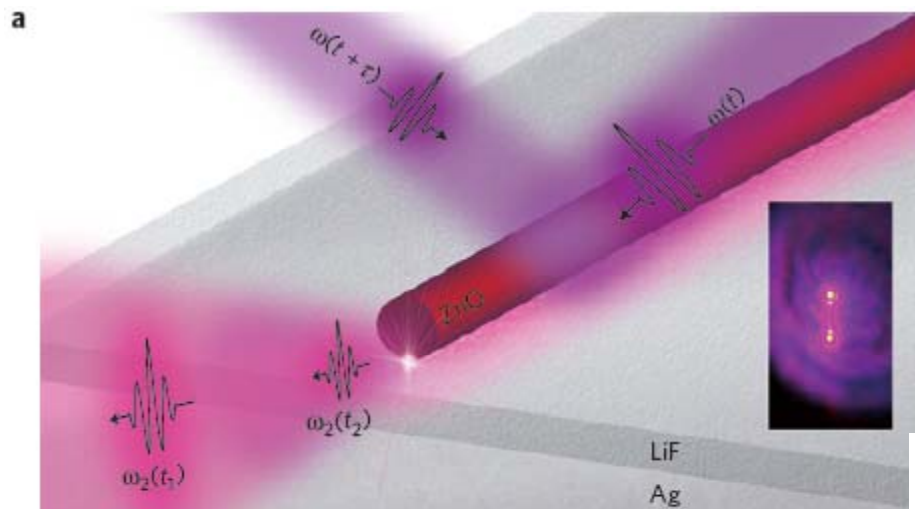
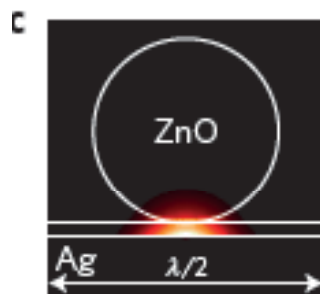


**Figure 5 | Measured spectra versus double-pump pulse delay for the plasmonic nanowire laser and its Fourier transform. a**, Normalized difference spectrum,  $\Delta I(\lambda, \tau)/I_0(\lambda) - I(\lambda, \tau)/I_0(\lambda) - 1$ , of the plasmonic nanowire laser for  $\tau \geq 0$ , where  $I(\lambda, \tau)$  is the spectrum under double-pump excitation and  $I_0(\lambda)$  is the single strong pump pulse spectrum. The two upper panels show the  $\Delta I/I_0$  spectra for the pulse delays,  $\tau = 2.0$  ps and  $\tau = 3.1$  ps, indicating the increasing spectral modulation frequency with pulse delay. **b**, Fourier transform of each spectrum shown in **a** versus pulse delay. The white trend line follows  $t = \tau - \tau_{\text{on}} \approx \tau_m$ , indicating a turn-on time of  $\tau_{\text{on}} = 1.1$  ps. The inset shows the amplitude decay of the Fourier transform along the white trend line, with linear fits (red lines) to the modulation peaks. The presented data in this figure correspond to measurements at the highest pump power (situation i) shown in Fig. 4a.





# Graphene spaser

Vadym Apalkov<sup>1</sup> and Mark I. Stockman<sup>1,2,3</sup>

<sup>1</sup>Department of Physics and Astronomy, Georgia State University, Atlanta, Georgia 30303, USA

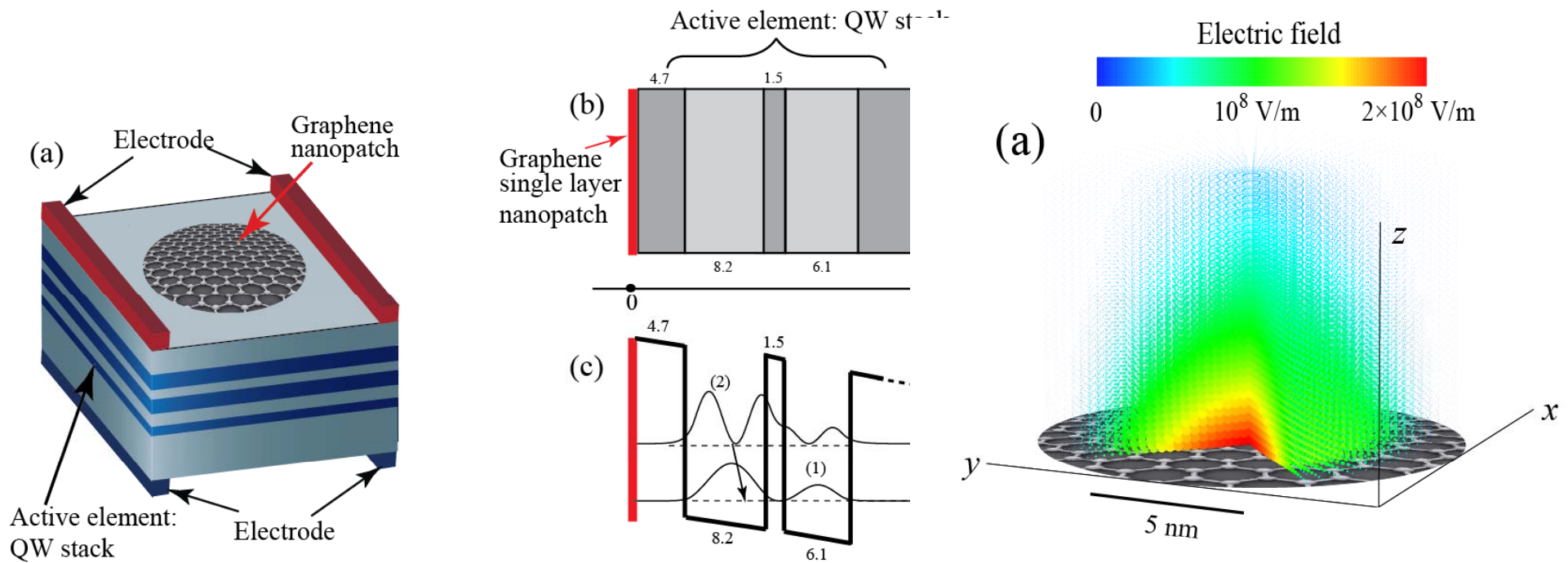
<sup>2</sup>Fakultät für Physik, Ludwig-Maximilians-Universität, Geschwister-Scholl-Platz 1, D-80539 München, Germany

<sup>3</sup>Max-Planck-Institut für Quantenoptik, Hans-Kopfermann-Strasse 1, D-85748 Garching, Germany

(Dated: May 10, 2013)

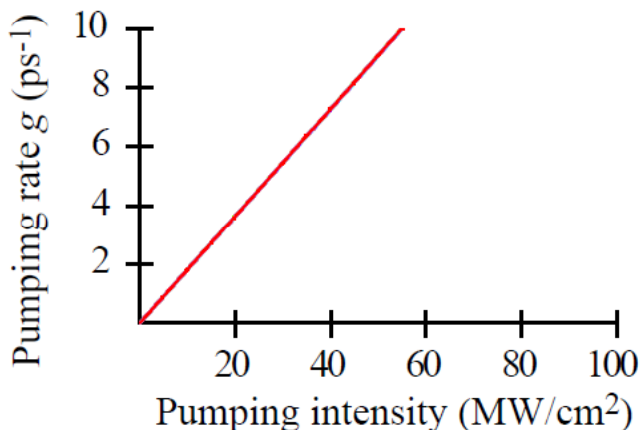
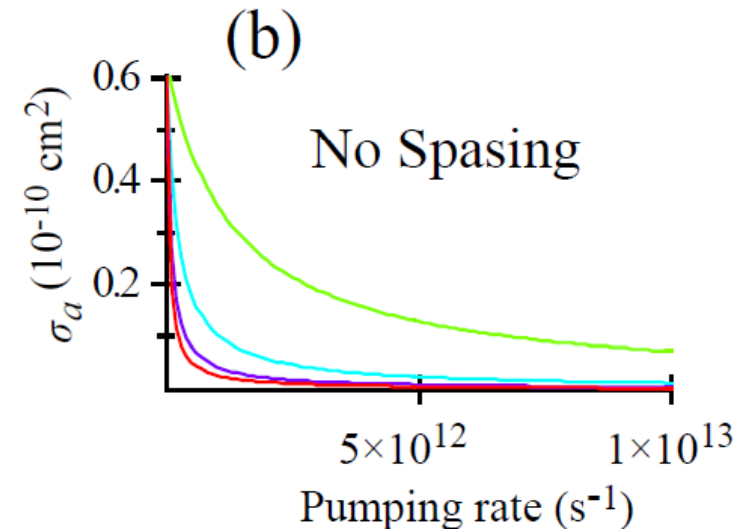
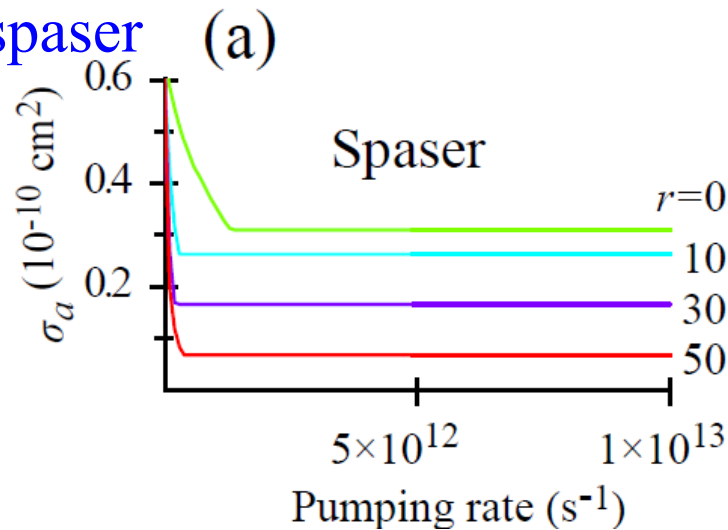
We propose a graphene spaser, which is a coherent quantum generator of surface plasmons in nanostructured graphene. The plasmonic core of this spaser is a graphene monolayer nanopatch and its active (gain) element is a multi-quantum well system with a design similar to the design of an active element of quantum cascade laser. For realistic parameters of the multi-quantum well system, the spasing in graphene monolayer can be achieved at a finite doping of graphene and at a plasmon frequency,  $\approx 0.15$  eV, close to the typical frequency of intersubband transitions in multi-quantum well systems. The proposed graphene spaser will be an efficient source of intense and coherent nanolocalized fields in the mid-infrared spectral region with wide perspective applications in mid-infrared nanoscopy, nano-spectroscopy, and nano-lithography.

V. Apalkov and M. I. Stockman, *Proposed Graphene Nanospaser*, NPG: Light Sci. Appl. **3**, e191 (2014).



**Applications in Biomedicine:** Why spaser is efficient as fluorescent, photothermal and photoacoustic agent? It does not saturate!

Absorption cross section as a function of the pumping rate for different loads  $r$  of spaser



H. Koochaki and M. Stockman (In preparation)

# Spaser as Versatile Biomedical Tool



Ekaterina I. Galanzha,<sup>1</sup> Robert Weingold,<sup>1</sup> Dmitry A. Nedosekin<sup>1</sup>, Mustafa Sarimollaoglu,<sup>1</sup>  
Alexander S. Kuchyanov<sup>2</sup>, Roman G. Parkhomenko<sup>3</sup>, Alexander I. Plekhanov<sup>2</sup>, Mark I.  
Stockman<sup>4</sup>, Vladimir P. Zharov<sup>1</sup>

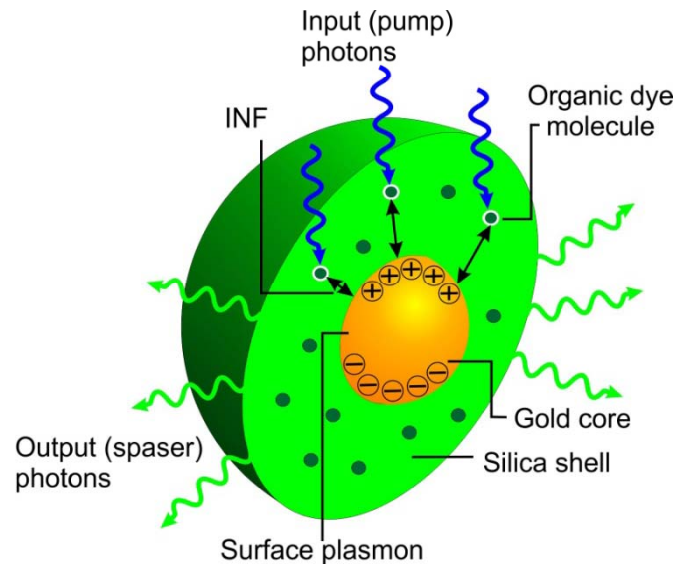
(arXiv:1501.00342;  
Submitted)

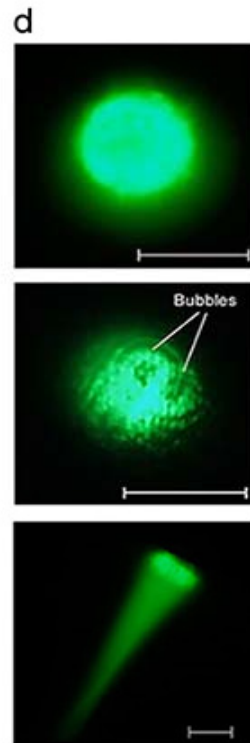
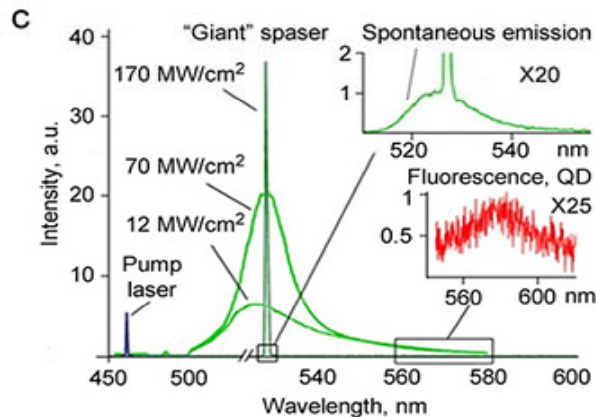
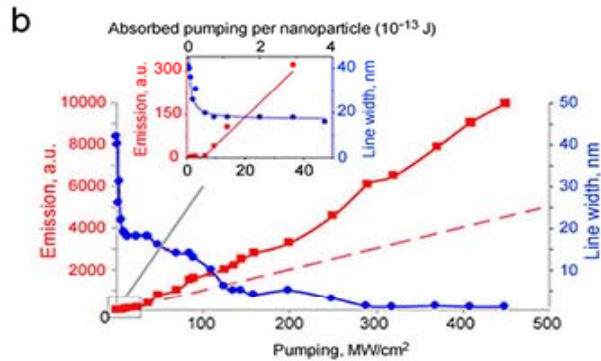
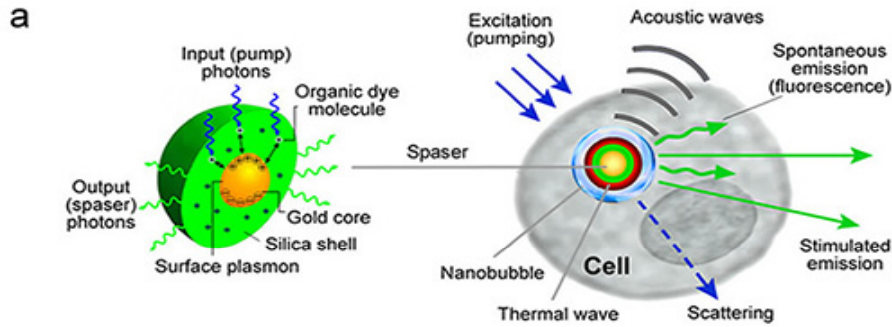
<sup>1</sup>Winthrop P. Rockefeller Cancer Institute, Arkansas Nanomedicine Center, University of  
Arkansas for Medical Sciences, Little Rock, Arkansas 72205

<sup>2</sup>Institute of Automation and Electrometry of the Siberian Branch of the Russian Academy of  
Science, Koptuyug Ave. 1, 630090 Novosibirsk, Russia

<sup>3</sup>Nikolaev Institute of Inorganic Chemistry of the Siberian Branch of the Russian Academy of  
Science, Lavrentiev Ave. 3, 630090 Novosibirsk, Russia

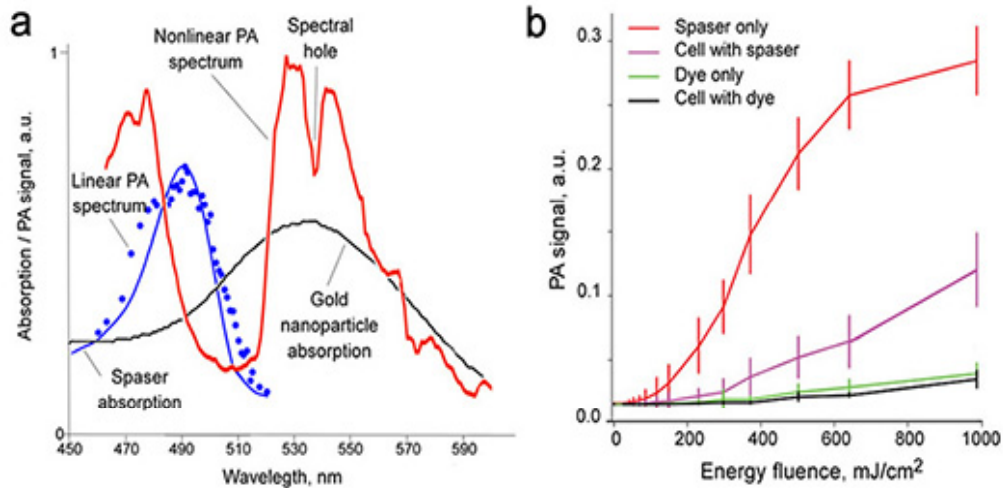
<sup>4</sup>Center for Nano-Optics and Department of Physics and Astronomy, Georgia State University,  
29 Peachtree Center Ave., Atlanta, GA 30302, USA





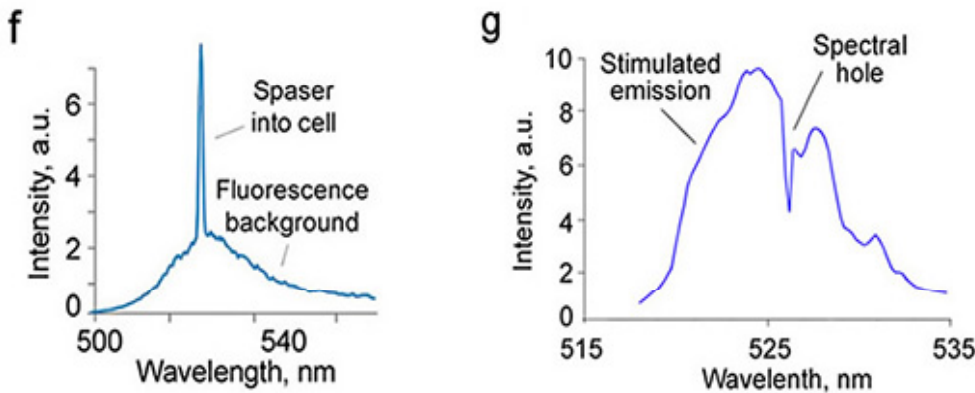
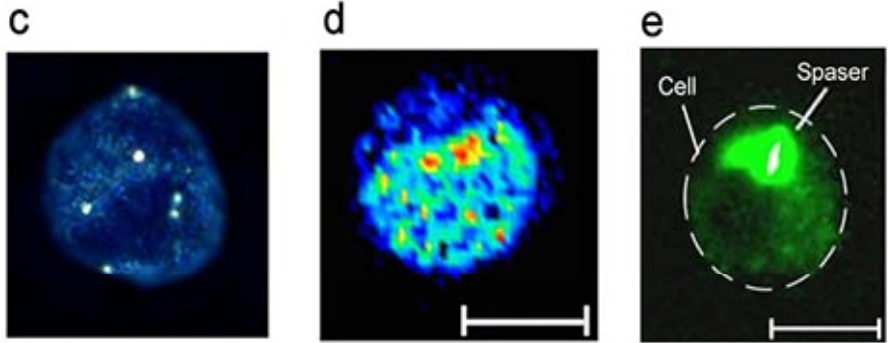
## Spaser for biological applications

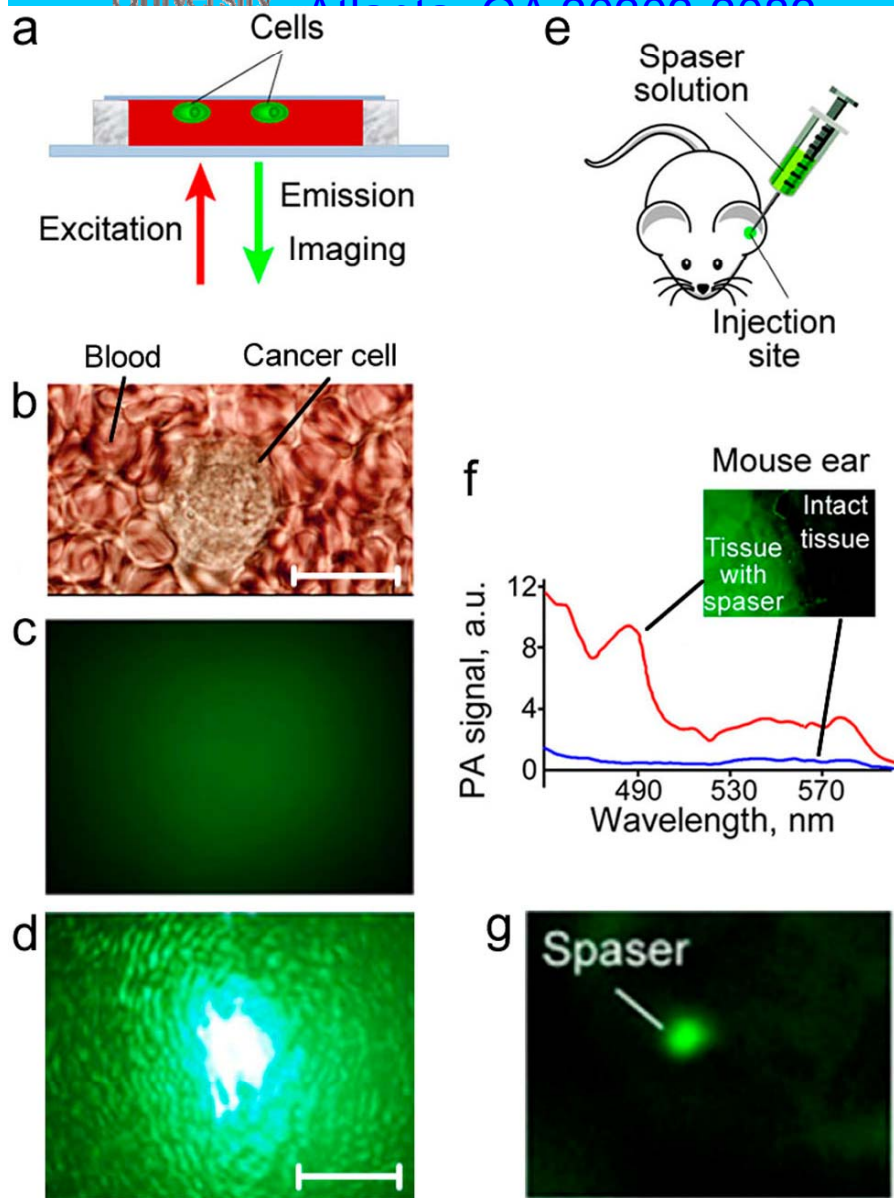
**a**, Schematic of spaser as multifunctional intracellular nanoprobe. **b**, Stimulated emission in spaser suspension. **c**, Radiation spectrum of spaser in suspension at 528 nm at different pump intensities. **d**, Spatially homogenous spaser's emission at a relatively low pump intensity (30 MW/cm<sup>2</sup>, 120-μm thick spaser's suspension); **Middle**: emission during the bubble formation around overheated spasers (150 MW/cm<sup>2</sup>); **Bottom**: "directional" spaser emission in the presence of two large bubbles (200 MW/cm<sup>2</sup>). Scale bars, 10 μm.



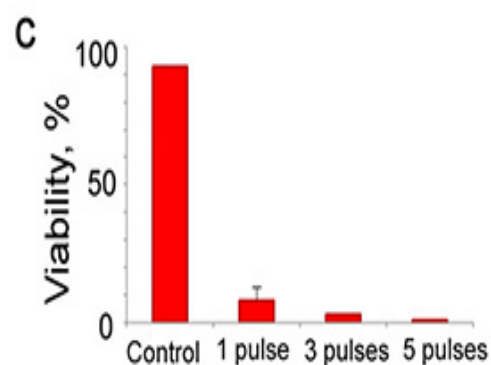
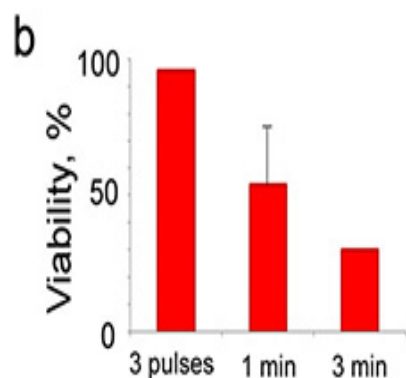
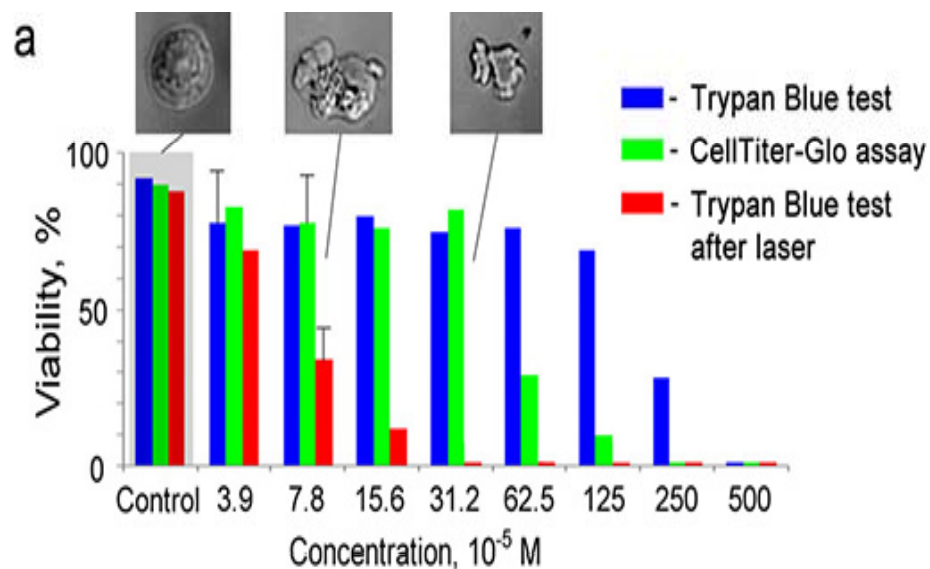
## Nanoplasmonics

**Photoacoustic (PA) and photothermal (PT) spectral microscopy of spasers.** **a**, Absorption spectra, and linear and nonlinear PA spectra of spaser in suspension at laser energy fluence of 20 mJ/cm<sup>2</sup> and 150 mJ/cm<sup>2</sup>, respectively. **b**, PA signal dependence on laser pump energy fluence for dye and spaser in suspension and into cells. **c-e**, Images of single cancer cell with spasers loaded through endocytosis. **(c)**-scattering (dark field), **(d)**-photothermal (PT); **(e)**-stimulated emission for local irradiated cell zone in background of conventional fluorescence image. **f**, Spectral peak from single cancer cell with spasers at relatively low energy fluence (80 mJ/cm<sup>2</sup>). Scale bars, 10 μm. **g**, Spectral peak single cancer cell with spasers showing spectral hole burning in stimulated emission spectra at moderate energy fluence (135 mJ/cm<sup>2</sup>).





**Imaging of spasers in viable cells *in vitro* and in biotissue *in vivo*.** **a**, Schematic *in vitro*. **b**, Optical transmission image. **c, d**, Fluorescence imaging using conventional optical source (lamp) of blood with cancer cells at depth of ~1 mm (**top**) and spaser emission from single cancer cell at depth of 1 mm (**bottom**). **e**, Schematic of intradermal injection of spaser suspension into top layer of mouse ear tissue. **f**, PA identification of spasers in ear tissue using laser spectral scanning (**top**). Laser parameters: beam diameter 15 μm, fluence 20 mJ/cm<sup>2</sup>. **g**, Spaser emission through ~250 μm ear tissue. Pump parameters: beam diameter: 10 μm; intensity, 30 MW/cm<sup>2</sup>.



**Demonstration of spaser as theranostic agent.** **a**, Cell viability tests for different spaser concentration using two various kits without (blue, green) and after (red) laser irradiation ( $100 \text{ mJ/cm}^2$ , 1 Hz, 3min). Inset: intact cell (**left**) and cells labeled with spasers at different concentration (middle and right) after laser irradiation. **b**, Viability test for concentration  $15.6 \times 10^{-5} \text{ M}$  as a function of laser exposure time (3s [3 pulses], 1 min, and 3 min); **c**, Viability test for concentration  $15.6 \times 10^{-5} \text{ M}$  as a function of laser pulse number (1, 3 and 5) showing that even single laser pulse at fluence of  $500 \text{ mJ/cm}^2$  is sufficient for significant damage of cancer cells labeled by spasers. The average SD for each column is 15-20%.

# The most important technological application: Information processing

P. Packan et al., in 2009 IEEE International Electron Devices Meeting (IEDM), *High Performance 32nm Logic Technology Featuring Second Generation High-K + Metal Gate Transistors* (Baltimore, MD, 2009), Vol. IEDM09-662, p. 28.4.1-28.4.4

## Abstract:

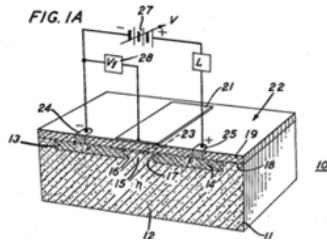
A 32nm logic technology for high performance microprocessors is described. 2nd generation high-k + metal gate transistors provide record drive currents at the tightest gate pitch reported for any 32 nm or 28nm logic technology. NMOS drive currents are 1.62mA/um  $I_{dsat}$  and 0.231mA/um  $I_{dlin}$  at 1.0V and 100nA/um  $I_{off}$ . PMOS drive currents are 1.37mA/um  $I_{dsat}$  and 0.240mA/um  $I_{dlin}$  at 1.0V and 100nA/um  $I_{off}$ . The impact of SRAM cell and array size on  $V_{ccmin}$  is reported.

## MOSFET US Patent

Aug. 27, 1963 3,102,230

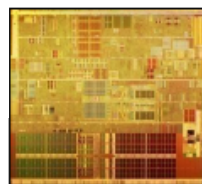
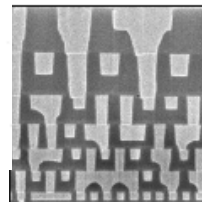
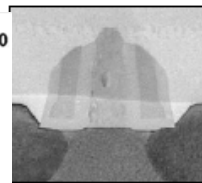
DAWON KAHNG

ELECTRIC FIELD CONTROLLED SEMICONDUCTOR DEVICE  
Filed May 31, 1960

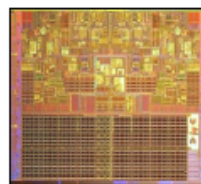
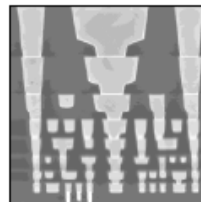
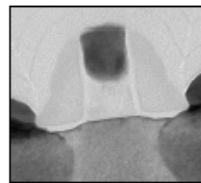


Speed ~ 100-300 GHz  
Low resistance to ionizing radiation

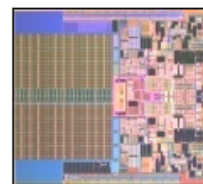
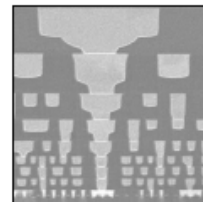
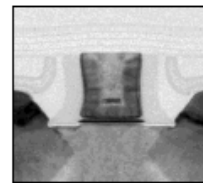
90 nm  
2003



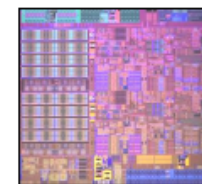
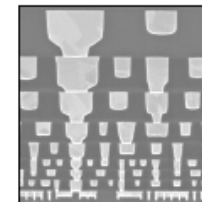
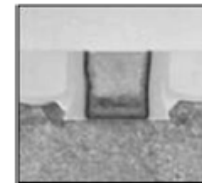
65 nm  
2005



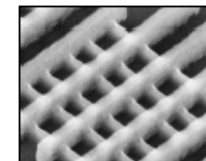
45 nm  
2007



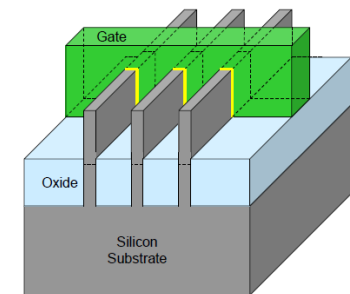
32 nm  
2009



22 nm  
2011



22 nm Tri-Gate Transistor



Tri-Gate transistors can have multiple fins connected together to increase total drive strength for higher performance

## Processor speed :

$$f_{\max} = I_{\text{drive}} / (C_{\text{Intercon}} \Delta U) \sim 3 \text{ GHz}$$

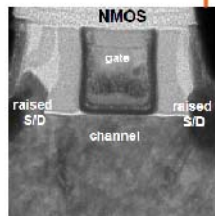
**Transistor speed is not a limiting factor!**

**Charging the interconnects is.**

Concept of ~300 GHz processor unit with ~1% energy cost per flop

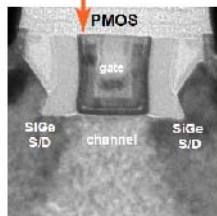
Today C-MOS Technology

Electric interconnect (Copper wire)



$$\tau = RC \sim \epsilon\sigma \frac{L^2}{r^2}$$

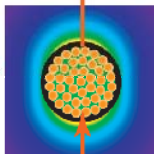
Charging time does not depend on scale



Near-future C-MOS Technology with on-chip plasmonic interconnects

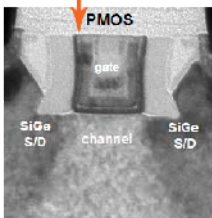
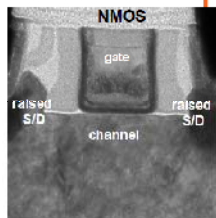
Nanoplasmonic on-chip interconnect (Copper wire)

Spaser pumped by transistor

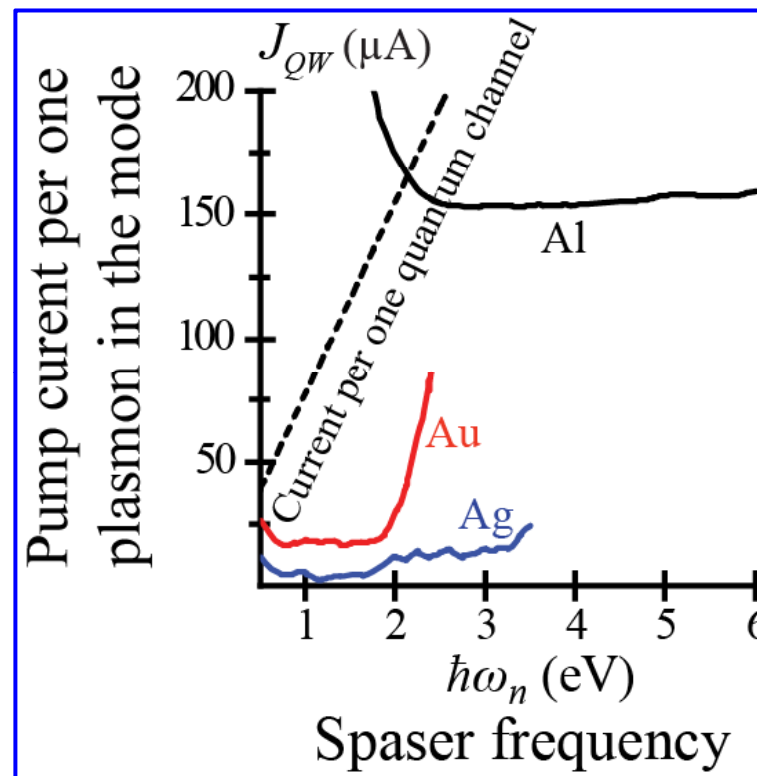


No electric charging of interconnects!

C-MOS Transistors are not connected electrically



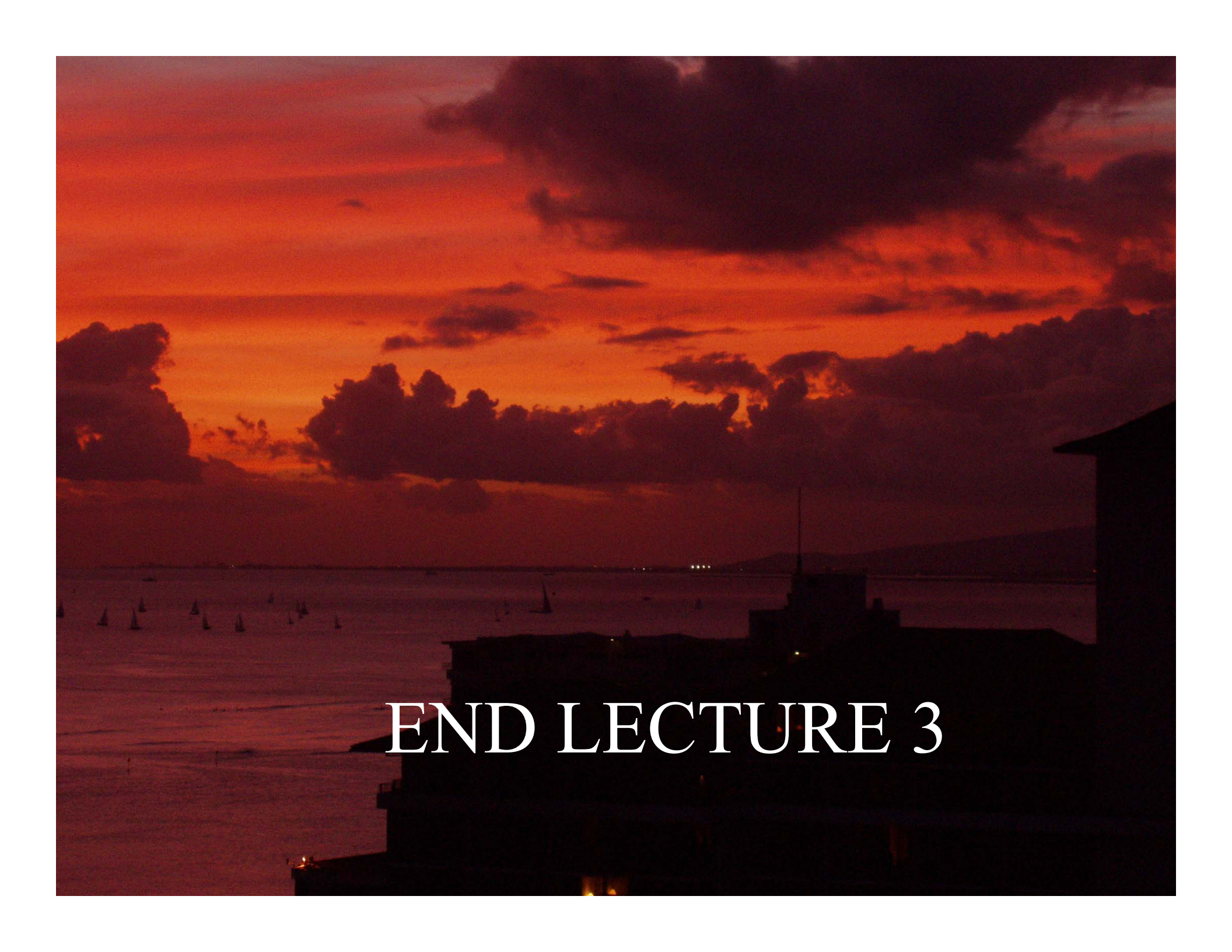
Nanospaser with electric excitation (“pumping”) does not exist as of today yet, but fundamentally it is entirely possible



D. Li and M. I. Stockman, *Electric Spaser in the Extreme Quantum Limit*, Phys. Rev. Lett. **110**, 106803-1-5 (2013)

# BRIEF CONCLUSIONS

1. SPASER is a nanoscopic quantum generator of coherent and intense local optical fields
2. SPASER can also serve as a nanoscale ultrafast quantum amplifier with a switch time  $\sim 100$  fs for silver and  $\sim 10$  fs for gold. It has the same size as MOSFET and can perform the same functions but is  $\sim 1000$  times faster.
3. SPASERs have been experimentally observed. The experiments are in an excellent qualitative agreement with theory
4. Numerous plasmon-polariton spasers (nanolasers) have been designed. In contrast to spaser, their length is on micron order (transverse mode size is nanometric). Their emission is multimode.
5. The most promising applications of the SPASER are a ultrafast nanoamplifier, local optical energy source, and active non-saturable nano-label.

A dramatic sunset over a body of water. The sky is filled with dark, heavy clouds, with a bright orange and red glow from the setting sun breaking through. In the foreground, the dark silhouettes of buildings are visible. The water is dark, and numerous small sailboats are scattered across the horizon. The overall mood is serene and atmospheric.

END LECTURE 3